SPACE RESEARCH IN SLOVAKIA

2022 – 2023

SLOVAK ACADEMY OF SCIENCES

COSPAR

SLOVAK NATIONAL COMMITTEE
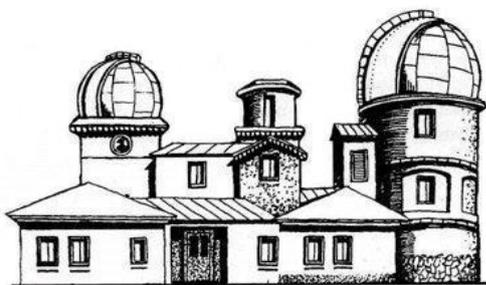
Slovak Central Observatory Hurbanovo

APRIL 2024

CONTENTS

1. EXPERIMENTS FOR MEASUREMENTS IN SPACE

J. Baláž, I. Strhárský, N. Werner

Experiment SERENA/PICAM on board of ESA-BepiColombo mission

IEP SAS contributed to ESA-BepiColombo mission to planet Mercury in the frame of scientific-technical cooperation with Space Technology Ireland (STIL) and Institute for Space Research of Austrian Academy of Sciences (IWF-ÖAW). The delivery involved participation on the mechanical structures of the PICAM (*Planetary Ion CAMera*) instrument that were manufactured in Slovakia (mechanical stress simulations, mechanical components manufacture on 5-axis milling center and laser technologies of Q-Products, Bratislava, space-qualified processing, integration and testing at IEP-SAS, Košice).
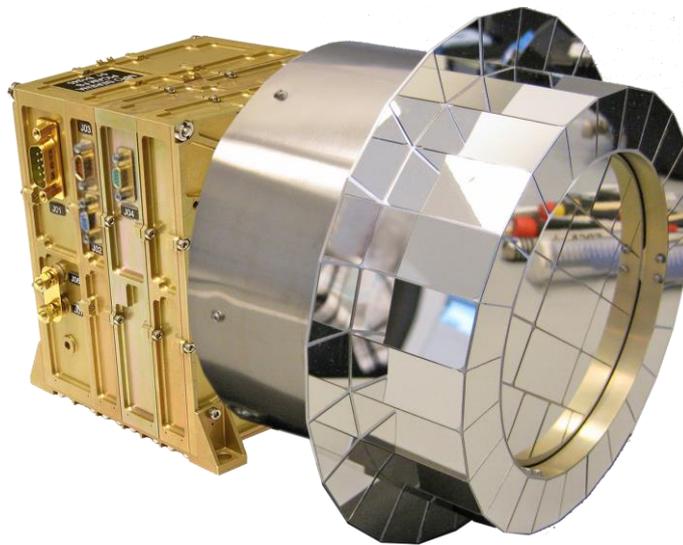
Figure 1.1. *SERENA / PICAM device*

PICAM is a part of a complex space science suite SERENA (*Search for Exospheric Refilling and Emitted Natural Abundances*) for particle detection at environment of the planet Mercury. The launch of the mission was on 20th October 2018 on board of the Ariane-5 launcher, from European spaceport Kourou in French Guiana. The cruise flight of the BepiColombo spacecraft to Mercury requires one flyby of Earth, two flybys of Venus and six flybys of Mercury. To date (February 2024), the science suite SERENA operates nominally and was active during several flybys of Venus and Mercury. Already during the first flyby of Mercury on 1st October 2021, two SERENA devices, PICAM and MIPA recorded unique data from the Mercury southern magnetosphere. The records and their science interpretation is in details depicted in [1]. Surprisingly, some spacecraft outgassing signs were also recorded after four years in deep space, having some consequences to space science and technology as well as design and operations of future missions [2].

The detailed descriptions of the SERENA devices and science objectives are provided in [3] and [4]. The arrival of the BepiColombo spacecraft to Mercury and its injection into orbit is scheduled for December 2025.
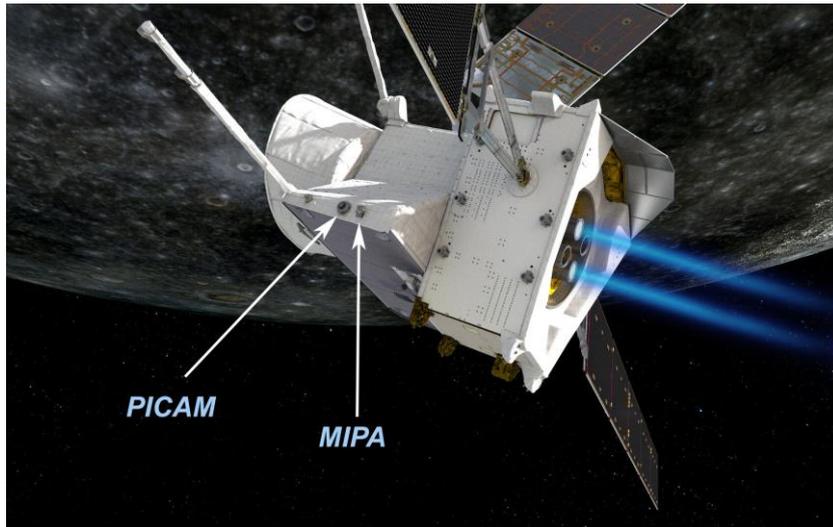
Figure 1.2. Some of science sensors have their field of view blocked by the Mercury transfer module (MTM), however, two devices from the SERENA suite, PICAM and MIPA, have a clear field of view, so they can record valuable data already during flybys around Mercury.
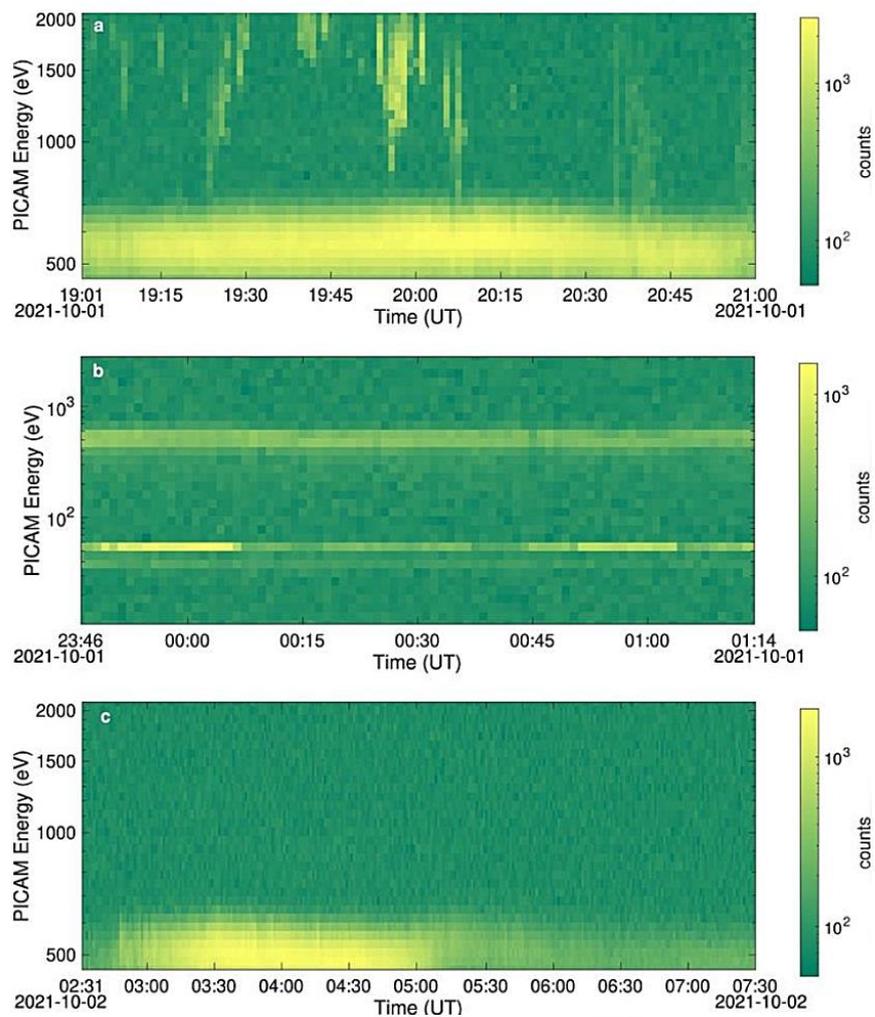
Figure 1.3. PICAM spectrograms outside of Mercury magnetosphere recorded during the Mercury flyby on 1st October 2021 [1].

6

Experiment PEP/JDC for mission ESA-JUICE

Experiment PEP (Particle Environment Package) will provide comprehensive detection and analysis of the plasma and particle environment in the system of planet Jupiter and its Galilean moons Europa, Calisto and Ganymede. PEP will measure density and flux of positive and negative ions, electrons, exospheric neutral gas, thermal plasma and energetic neutral atoms in the energy range from <0.001 eV to >1 MeV with full angular coverage. The PEP suite includes six sensors (JDC, JEI, JoEE, NIM, JNA and JENI) that were developed at several EU and US institutions led by Swedish Institute for Space Physics (IRF, P.I. prof. S. Barabash). Based on invitation from IRF, the IEP-SAS contributes to development and construction of anti-coincidence particle detection system for JDC sensor (*Jovian plasma Dynamics and Composition*) of the PEP suite. The purpose of the anti-coincidence module (ACM) is to provide improvement of the plasma particles detection efficiency on the background of penetrating electron radiation from the Jovian radiation belts. The ACM module consists from silicon solid state detector (SSD) located in the axis of the JDC sensor and from processing electronic unit (ANU) that provides amplification, charge/voltage conversion, shaping and discrimination of the SSD signal.
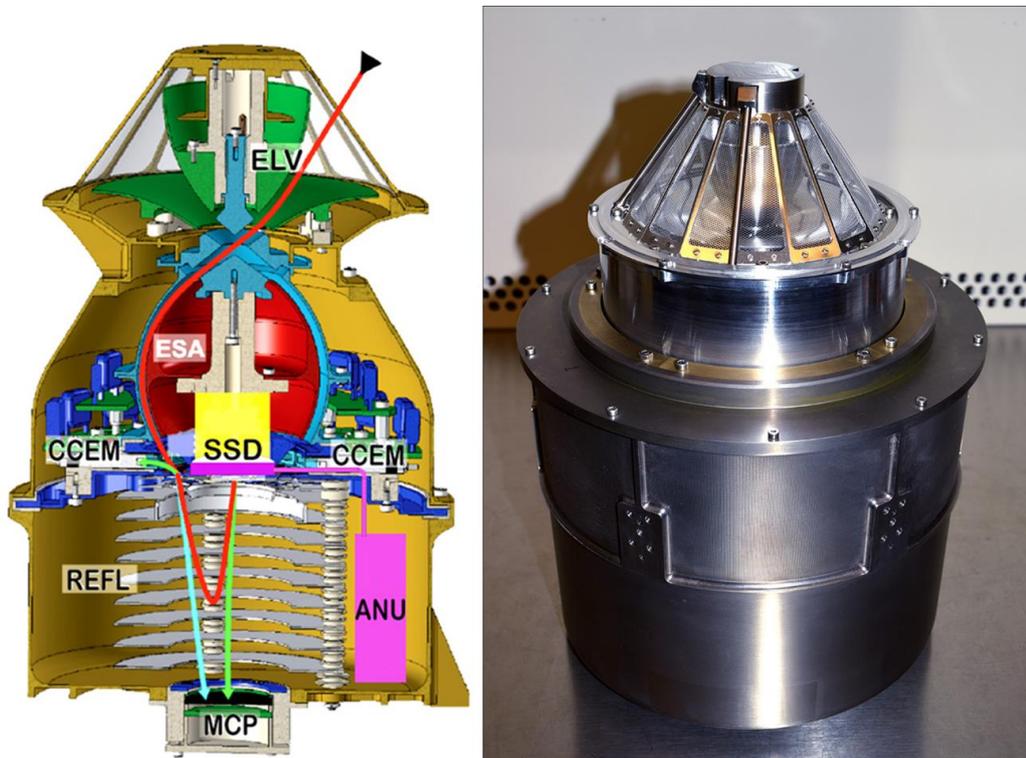
Figure 1.4. Functional cross section of the PEP/JDC sensor and its real photo before delivery for integration to JUICE spacecraft.

The solid state detector is custom-design semiconductor detector with area 300 mm^2 and sensitive thickness of 300μm, the operation bias voltage is 130V. The detector chip was manufactured by Canberra Belgium Ltd. Company. The detector is connected with coaxial cable with the space qualified, radiation tolerant front-end electronics, starting with charge sensitive amplifier A250F, shaping amplifier A275FN and fast discriminator RHR801K1. The threshold control circuitry is under control from JDC computer.
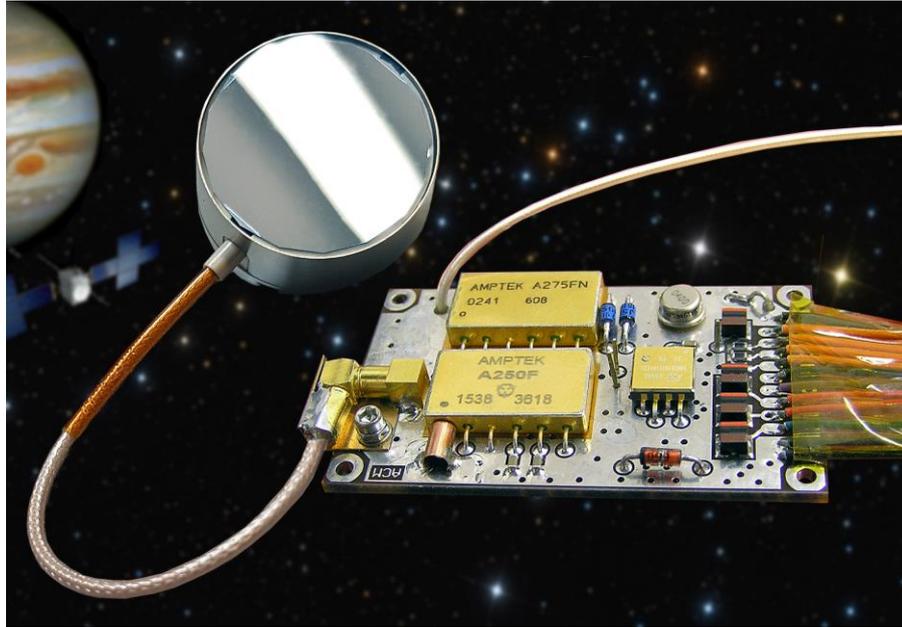
Figure 1.5. *Anticoincidence module ACM for PEP/JDC sensor of JUICE mission.*

The ACM module was physically calibrated with mono-energetic electrons from ^{109}Cd radionuclide and with gamma radiation from ^{241}Am radionuclide at IEP SAS laboratories, where also thermal-vacuum tests were provided before delivery to the Swedish Institute of Space Physics in Kiruna for integration to PEP/JDC sensor.

Figure 1.6. *PEP/JDC installed on board of the JUICE spacecraft and successful launch of the JUICE mission on 14th April 2023.*

The JUICE mission was successfully launched on 14th April 2023 on board of the Ariane-5 launcher from European spaceport Kourou in French Guiana. The PEP science payload was successfully commissioned in June 2023 and operates nominally on board of the JUICE spacecraft. The PEP payload will be also activated during upcoming Moon-Earth flyby in August 2024. The arrival to Jupiter and insertion to the orbit is planned for June 2031. The

JUICE mission including the PEP science suite description is described in [5], the JDC sensor is in details described e.g. in [6].

The participation of IEP SAS to JUICE mission was supported by ESA-PECS (*Plan for European Cooperating States*) project named: *"Slovak contribution to ESA-JUICE mission: Development of Anti-Coincidence Module ACM for Particle Environment Package PEP"*.

Information regarding the CubeSat gamma-ray measurements

GRBAlpha is a 1U CubeSat launched in March 2021 to a sun-synchronous LEO at an altitude of 550 km to perform an in-orbit demonstration of a novel gamma-ray burst detector developed for CubeSats [7]. This instrument detecting gamma-rays in the range of 30-900 keV consist of a 56 cm^2 5 mm thin CsI(Tl) scintillator read-out on a side by a set of 8 SiPM detectors, multi-pixel photon counters by Hamamatsu. The mission allows the characterisation of the degradation of SiPMs due to particles encountered in polar orbit.

The scientific motivation is to detect gamma-ray bursts (GRBs) and other high-energy transient events and serve as a pathfinder for a larger constellation of nanosatellites that could localise these events via triangulation. By the end of February 2024, GRBAlpha detected over 110 such transients confirmed by larger GRB missions. Over 70 of them are identified as gamma-ray bursts, including "brightest-of-all-times" GRB 221009a, where the smaller size of our detectors allowed us to determine the peak emission of the burst when other monitors were saturated [8].

References:

[1] ORSINI, S. – MILILLO, A. – LICHTENEGGER, H., … , BALÁŽ, J., et al. Inner southern magnetosphere observation of Mercury via SERENA ion sensors in BepiColombo mission. Nature Communications 13, 7390 (2022). https://doi.org/10.1038/s41467-022-34988-x

[2] FRÄNZ, M. – ROJO, M. – CORNET, T. – HADID, L. Z. – SAITO, Y. – ANDRÉ, N., et al. (2024). Spacecraft outgassing observed by the BepiColombo ion spectrometers. Journal of Geophysical Research: Space Physics, 129, e2023JA032044. https://doi.org/10.1029/2023JA032044

[3] ORSINI, S. – LIVI, S., ... , BALÁŽ, J., et al. SERENA: A suite of four instruments (ELENA, STROFIO, PICAM and MIPA) on board BepiColombo-MPO for particle detection in the Hermean environment. Planetary and Space Science 58 (2010), pp 166-181. https://doi.org/10.1016/j.pss.2008.09.012

[4] ORSINI, S. – LIVI, S., LICHTENEGGER, H., … , BALÁŽ, J., et al. (2021). SERENA: Particle instrument suite for determining the Sun-Mercury interaction from BepiColombo. Space Science Reviews, 217(1), 11. https://doi.org/10.1007/s11214-020-00787-3

[5] http://sci.esa.int/juice/54993-juice-definition-study-report-red-book/

[6] STUDE, J. Advanced Plasma Analyzer for Measurements in the Magnetosphere of Jupiter. Doctoral Thesis. Swedish Institute of Space Physics and Umeå University, 2016. https://www.diva-portal.org/smash/get/diva2:926416/FULLTEXT01.pdf

[7] PÁL, A. – OHNO, M. – MÉSZÁROS, L. – WERNER, N. – ŘÍPA, J. – CSÁK B. – DAFČÍKOVÁ M. – FRAJT, M. – FUKAZAWA Y. – HANÁK P. – HUDEC, J. – HUSÁRIKOVÁ N. – KAPUŠ, J. – KASAL M. – KOLÁŘ M. – KOLEDA M. – LASZLO R. – LIPOVSKÝ P. – MIZUNO T. – MÜNZ F. – NAKAZAWA K. – REZENOV M. – ŠMELKO

M. – TAKAHASHI H. – TOPINKA M. – URBANEC T. – BREUER J.-P. – BOZÓKI T. – DÁLYA G. – ENOTO T. – FREI Z. – FRISS G. – GALGÓCZI, G. – HROCH F. – ICHINOKE Y. – KAPÁS K. – KISS L. L. – MATAKE H. – ODAKA H. – POON H. – POVALAČ A. – TAKÁTSY J. – TORIGOE, K. – UCHIDA N. – UCHIDA Y., 2023, Astronomy & Astrophysics, 677, id.A40: "GRBAlpha: the smallest astrophysical space observatory - Part 1: Detector design, system description and satellite operations"

[8] ŘÍPA, J. – TAKAHASHI H. – FUKAZAWA Y. – WERNER, N. – MÜNZ F. – PÁL, A. – OHNO, M. – DAFČÍKOVÁ M. – MÉSZÁROS, L. – CSÁK B. – HUSÁRIKOVÁ N. – KOLÁŘ M. – GALGÓCZI, G. – BREUER J.-P. – HROCH F. – HUDEC, J. – KAPUŠ, J. – FRAJT – M. REZENOV M. – LASZLO R. – KOLEDA M. – ŠMELKO M. – HANÁK P. – LIPOVSKÝ P. – URBANEC T. – KASAL M. – POVALAČ A. – UCHIDA Y. – POON H. – MATAKE H. – NAKAZAWA K. – UCHIDA N. – BOZÓKI T. – DALYA G. – ENOTO T. – FREI Z. – FRISS G. – ICHINOHE Y. – KAPÁS K. – KISS L. L. – MIZUNO T. – ODAKA H. – TAKATSY J.– TOPINKA M. – TORIGOE K., 2023, Astronomy & Astrophysics, 677, id.L2: "The peak-flux of GRB 221009A measured with GRBAlpha"

2. SPACE PHYSICS, GEOPHYSICS AND ASTRONOMY

J. Baláž, P. Bobík, I. Dorotovič, A. Galád, L. Kornoš, J. Kubančák,
P. Matlovič, R. Nagy, M. Revallo, J. Rybák, J. Šilha, J. Tóth

The Department of Space Physics, ***Institute of Experimental Physics, SAS, Košice*** (http://space.saske.sk) in collaboration with the laboratories in abroad continued studies of the dynamics of low energy cosmic rays (CR) and of suprathermal cosmic particles, as well as high energy cosmic rays based on measurements in space and on the ground.

Long term continual measurements by Neutron Monitor at High Altitude Laboratory of IEP SAS Lomnický štít (LŠ, data in real time available at http://neutronmonitor.ta3.sk) along with other neutron monitors were used in studies of radiation protection from cosmic rays. The ESA SIREN (Space Ionizing Radiation Project Nursery) project, results of which are currently part of curricula of the Faculty of Sciences of the Pavol Jozef Šafárik University in Košice, has been finished in the reported period. Information about the project, focusing on development of a university course for undergraduate students focused on cosmic ionizing radiation, dosimetry, metrology, radiation protection and radiation risks connected with high-altitude flights and spaceflights, and the resulting course (Detection and Dosimetry of Cosmic Rays) is published here: http://siren.space.saske.sk. Active cooperation continued with the Institute of Atmospheric Physics of the Czech Academy of Sciences. One of the results of the cooperation was published in [1]. An agreement on cooperation has been signed with the Polish University of Defense for the purpose of future cooperation on installation of the first Polish neutron monitor.

Geliosphere [2], a numerical model of the modulation of cosmic rays in the heliosphere implements the stochastic differential equation method to solve Parker's equation with GPU-accelerated and multithread CPU implementations. To verify the Geliosphere 2D model results at different heliospheric latitudes and radii, the article [2] shows that the Geliosphere 2D model, with implemented heliospheric polar field modification, fits well with measurements provided by the Kiel Electron Telescope (KET), which is part of the Ulysses COsmic ray and Solar Particle INvestigation (COSPIN) experiment. Geliosphere is open source and its code is available on https://github.com/msolanik/Geliosphere.

References:

[1] CHUM J. – LANGER R. – KOLMAŠOVÁ I. – LHOTKA O. – RUSZ J. – STRHÁRSKÝ I.: 2023, Solar cycle signatures in lightning activity, EGUsprere preprint 2023-2124 (https://doi.org/10.5194/egusphere-2023-2124).

[2] SOLANIK M. – BOBÍK P. – GENČI J.: 2023, Geliosphere - parallel CPU and GPU based models of cosmic ray modulation in the heliosphere, Computer Physics Communications, Vol. 291, 108847, ISSN 0010-4655 (https://doi.org/10.1016/j.cpc.2023.108847)

The **Faculty of Mathematics, Physics and Informatics, Comenius University, Bratislava** was involved in the following directions of research as listed below.

Meteor observations and analyses by AMOS global meteor network

In 2022-2023 continued the monitoring of meteor activity above the Central Europe in Slovakia, Canary Islands, Atacama Desert in Chile, Hawaii, Australia and South Africa by All-sky Meteor Orbit System (AMOS) and AMOS-Spec systems (Fig. 2.1.). AMOS systems work as autonomous intensified video observatory for detection of meteors and other transient events on the sky. Hardware and software of AMOS have been developed and constructed at Faculty of Mathematics, Physics and Informatics of Comenius University in Bratislava.
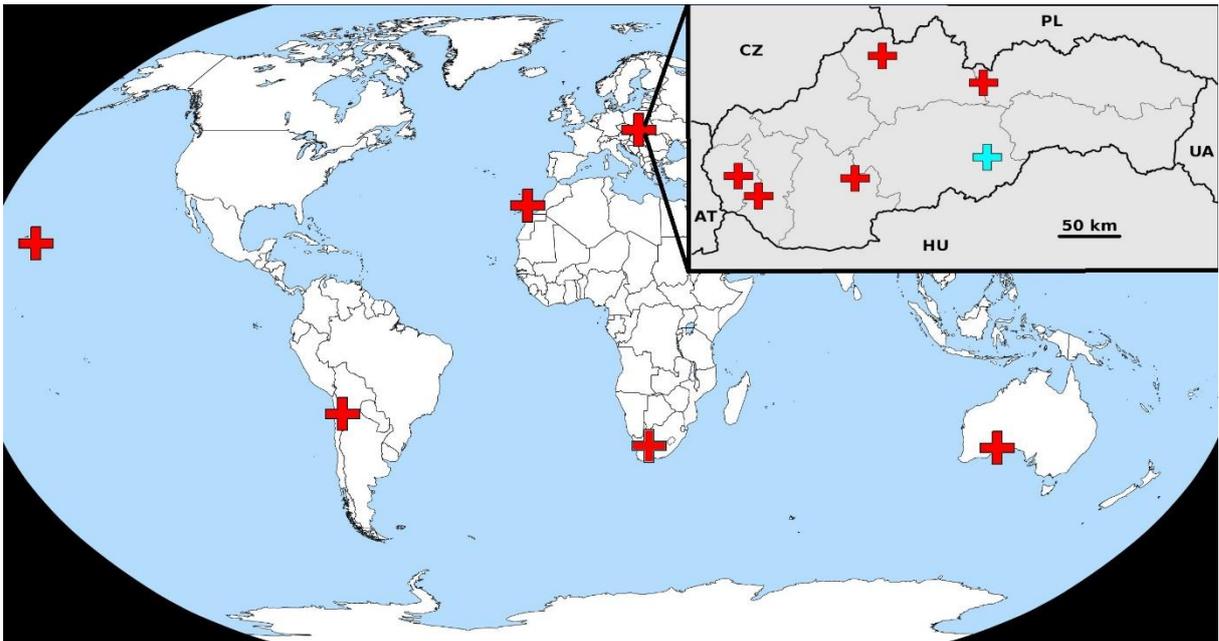
Figure 2.1. *AMOS global meteor network. Red crosses are active location (2-3 AMOS systems), and blue cross is planned location in Slovakia.*

We have demonstrated the capability of the updated All-Sky Meteor Orbit System (AMOS and AMOS-Spec) to provide photometric calibration of the unique Alberta fireball [1] observed from the ground and by the Geostationary Lightning Mapper (GLM) satellite. This case allowed us to better constrain early Solar System models with preference towards the Grand Tack theory with Jupiter migration to the terrestrial region. Moreover, we have characterized several hundreds of meteor showers [2] from the EDMOND database [3] and compared to the IAU Meteor Data Center database using our searching methods [4]. We also led an international ESA project MetSpec focused on simulated ablation of meteorites in plasma wind tunnel of IRS University of Stuttgart, aimed to improve our methods for studying meteoroid composition from meteor spectra observations. From this experiment, we have published the collection of papers in Icarus [5].

In 2023, we were awarded a follow-up ESA project focused the research of H and CN emission in meteorite and meteor spectra. This ongoing project aims to improve our abilities to identify the contents of hydrated minerals and organic compounds in meteoroids. First results from the AMOS spectral program pointed out that the presence of water and organics can be traced by studying the H emission from meteors and revealed the variations of H content in

meteoroids from various dynamical regions [6]. Furthermore, we have demonstrated the first detection of CN in spectra of simulated meteors and pointed out its correlation with the intensity of the H emission and the presence of organic compounds [7].
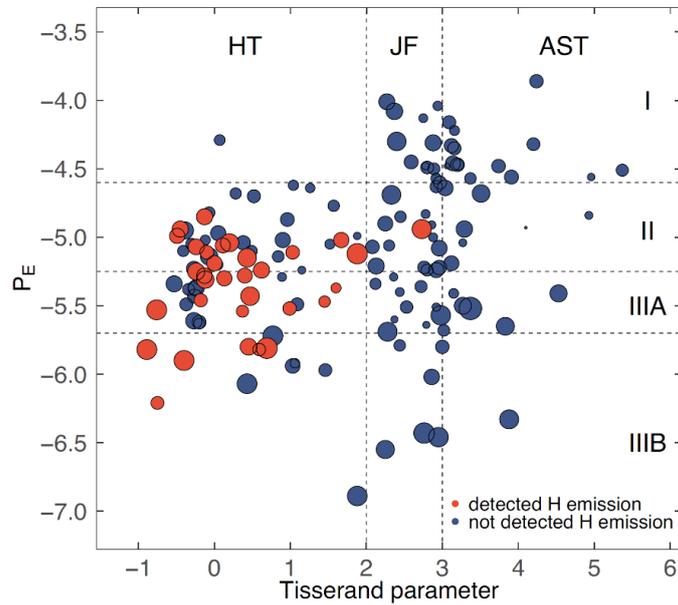
Figure 2.2. *The detected presence of H emission in meteors captured by the AMOS-Spec system displayed on a map containing the orbital classification of meteoroids based on the Jovian Tisserand parameter and material strength classification based on the P_E criterion. The size of the meteoroid symbols reflects the relative meteor magnitude.*
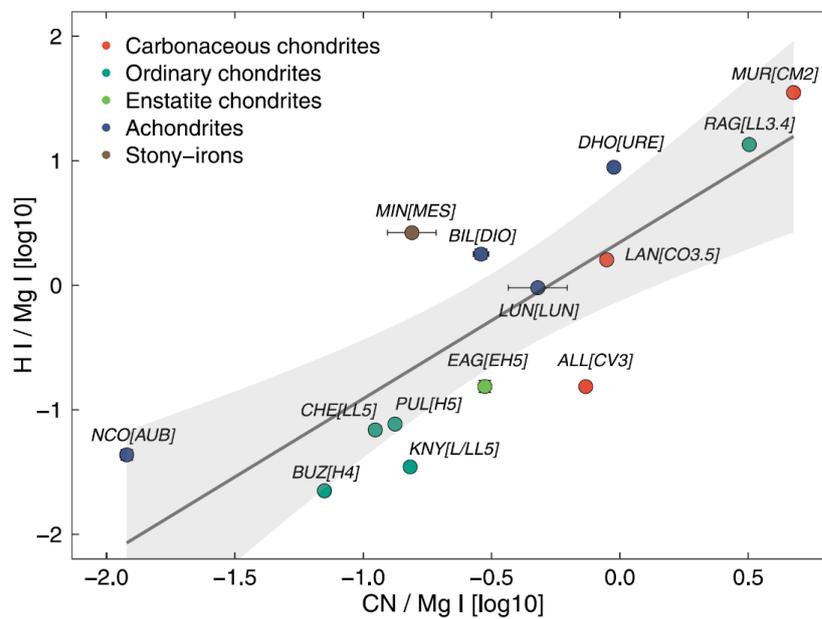
Figure 2.3. *The correlation between the Hα/Mg I-2 and CN/Mg I-2 intensity ratios measured in ablated meteorites of various compositional types marked by name abbreviation and type. The linear fit to the running average with standard error of the mean is shown by the gray line and area.*

13

Space debris photometry and spectroscopy research

The Faculty of Mathematics, Physics and Informatics of Comenius University in Bratislava, Slovakia (FMPI) operates its own 0.7-m Newtonian telescope (AGO70) dedicated to the space surveillance tracking and research, with an emphasis on space debris [8]. The observation planning focuses on objects on geosynchronous (GEO) and eccentric (GTO and Molniya) orbits. Light curve acquisition programme conducted over the years 2017-2022 led to buildup of an extensive space debris catalogue containing almost 2'000 photometric measurements of 759 individual objects. The light curve catalogue of space debris is freely available to the scientific community (www.sdlcd.space-debris.sk) [9] and can be used for further scientific applications such as support of active debris removal missions, rotation axis determination, BVRI photometry, object's shape and albedo estimation, etc.

Each material has reflective signatures, which enable us to distinguish different features on the object's surface and provide information about the object's attitude or utilize the categorization into the population or material groups. We conducted study focused on acquisition of color indices of rocket upper stage Long March 3B [10] where we present a detailed description of methods that must be utilized to be able to extract the standard color indices of space debris objects, as well as our implementation and understanding of these methods. We defined what features of the rotating objects can be seen by the BVR_cI_c photometry, furthermore, we discuss the materials that are the main drivers of reflection. Finally, we describe ways how to interpret these data for space debris characterization. Fig. 2.4, left shows the reconstructed rotation phase function (left) in each passband for selected series to illustrate the complexity of the recorded signal and to mark the local extremes of the reflection (black and purple crosses). Obtained the color index rotation phase curves are shown in Fig. 2.4, right.
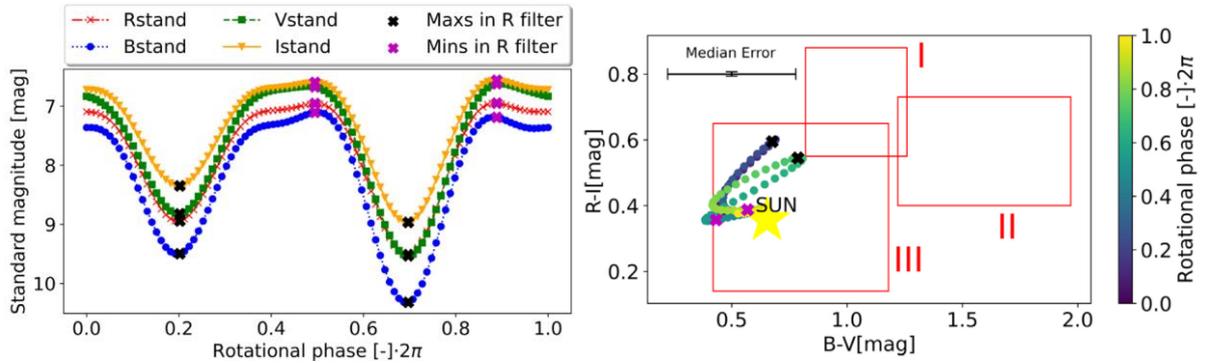
Figure 2.4. *The color photometry results for the 2022–08–02 series of observations for the target CZ-3B (NORAD 39158, COSPAR 2013-020B) was observed near its apogee with AGO70 telescope. Left: The color index rotation phase curves. Right: BVR_cI_c diagrams. The turning points (the crosses) in both diagrams represent the color indices calculated for the positions of the extremes in the R_c filter.*

During spectroscopic observations from 2016 to 2021, AMOS-Spec–HR harnessed numerous debris recordings and by data mining of its archives, dozens of spectra of flares and glints were retrieved. We developed spectroscopic reduction for this specific type of data and reported extracted 44 reflectance spectra of object on Low Earth Orbit (LEO) [11]. Three distinct types of spectra were distinguished among AMOS data: Category I – convex spectra with concave up shape, Category II – spectra with slope increasing towards red wavelength region and Category III – flat, straight-lined spectra. Spectra within the three categories were compared with the published laboratory reflectance spectra to link them with materials

commonly used in space design. Fig. 2.5, left shows three distinct categories into which can be assigned obtained AMOS spectra. Fig. 2.5, right demonstrates the percentage Spearman correlations in monotonicity of the SPOT 3 (22823) normalized reflectance spectra with laboratory measurements of different materials.
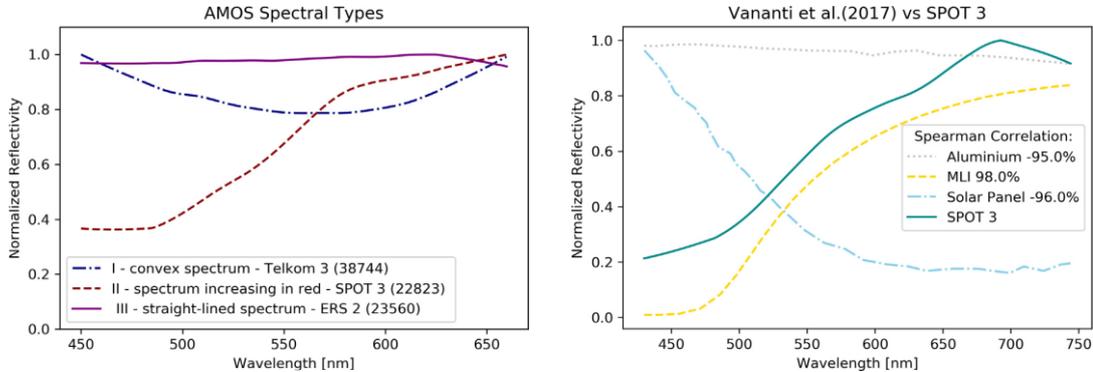
Figure 2.5. *Left: Three categories of reflectance spectra recorded by AMOS-Spec–HR cameras: I – blue dot-dashed line – convex spectrum of Telkom 3 (38744) satellite debris, II – red dashed line – increasing in red wavelengths, spectrum of SPOT 3 (22823) defunct satellite, III – purple straight-lined spectrum of ERS-2 (23560) defunct satellite. Right: Comparison between the spectral function of SPOT 3 (22823) obtained from AMOS data and laboratory spectra reported in the literature. The highest percentage correlation of 98.0% is with the laboratory spectrum of golden Multi-Layer Insulation Kapton foil.*

Photometric observations and research of asteroids using a 60-cm telescope

Our long-term photometric survey of V-type asteroids continued in 2022-23. In the paper [12], all our data up to 2022 were summarized and processed so that part of them could be modeled. Using data from other observatories, we determined the shapes and sense of rotation for about 100 asteroids. All available models (new and old) for V-type asteroids located in the inner part of the main belt, including those outside the Vesta family, show that they mostly originate from the asteroid Vesta. In other words, if there are any other sources out there, their total number is likely to be very small.

Study of the Milky Way galaxy using astrometric data from Gaia mission

The department of astronomy and astrophysics at FMPI CU is actively engaged in investigating the structure of the Milky Way galaxy. In collaboration with the Instituto de Astrofísica de Canarias (IAC), Spain, with University College London, UK, and with Centro Ricerche Enrico Fermi, Rome, Italy, we have delved into structural and kinematical characteristics of the remote regions of the Galaxy. Utilizing the Gaia data DR3, we have gained valuable insights into the Galactic disc at extended distances, allowing us to explore structural features at the outskirts of the Milky Way. By employing a deconvolution technique to address parallax errors, we have calculated the stellar density using Gaia DR3, extending our reach to Galactocentric distances of approximately 20 kpc. Our focus has been on constraining the warp (bending of the Galaxy's plane) and flare (thickening of the Galactic disc, leading to changes in the disc's scale height with increasing Galactocentric distance) while differentiating between distinct stellar populations, with a particular emphasis on supergiants [13]. We found that supergiants exhibit a distinctive asymmetry in their warp, with a maximum amplitude of zw =

15

0.658 kpc and a minimum amplitude of zw = −0.717 kpc at a Galactocentric distance of R = [19.5, 20] kpc, which is almost twice as high as the amplitude of the whole population of the disc. We find a significant flare of the whole population, especially in the thick disc, while the supergiant population has only a small flare, see Fig. 2.6.

We have also constructed three-dimensional kinematic maps of the Galactic disc utilizing Gaia DR3's three-dimensional velocity components spanning Galactocentric distances R between 8 and 30 kpc [14]. These maps reveal that the Milky Way exhibits asymmetrical motions with sizable gradients in all velocity components. Additionally, we have determined the Galactic rotation curve Vc(R) up to approximately 27.5 kpc employing the cylindrical Jeans equation while assuming an axisymmetric gravitational potential. Our findings indicate that Vc(R) experiences a noticeable decline up to the outermost radius examined. Finally, we have also assessed Vc(R) at different vertical heights, demonstrating that for R < 15 kpc, there exists a distinct dependency on Z, while this dependence diminishes at larger R.
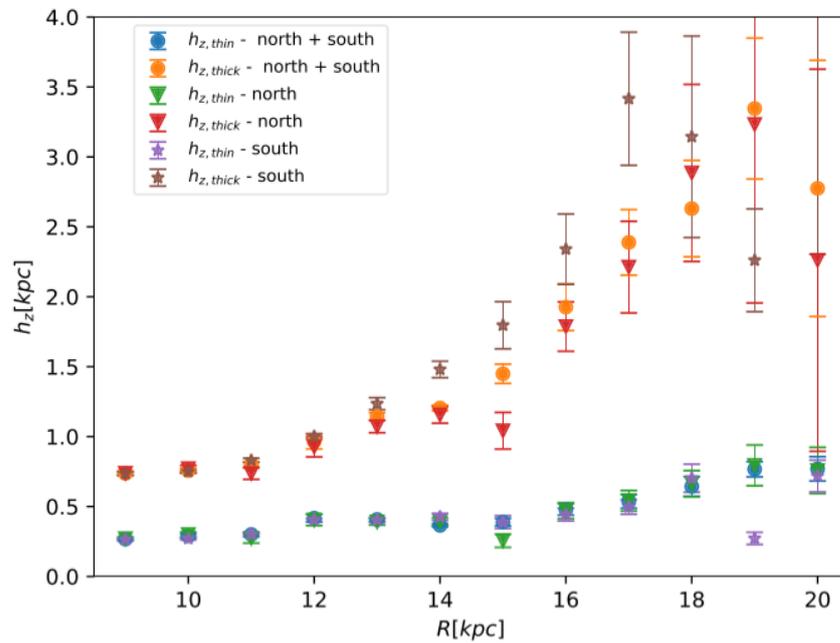
Figure 2.6. Dependence of the scale height of the thick and thin discs on the Galactocentric distance. The Galactic azimuth is φ ∈ [330°,30°]. The northern, southern, and northern+southern flares are compared.

References:

[1] VIDA, D. – BROWN, P. G. – DEVILLEPOIX, H. A. R. – WIEGERT, P. – MOSER, D.E. – MATLOVIČ, P. – HERD, CH. D. K. – HILL, P. J. A. – SANSOM, E. K. – TOWNER, M. C. – TÓTH, J. – COOKE, W. J. – HLADIUK, D. W.: Direct measurement of decimetre-sized rocky material in the Oort cloud, Nature Astronomy, vol. 7, pp. 318–329, (2023), https://doi.org/10.1038/s41550-022-01844-3

[2] ĎURIŠOVÁ, S. – TÓTH, J. – HAJDUKOVÁ, M.: Independent identification of meteor showers from the EDMOND and the search for their parent bodies", Planetary and Space Science, vol. 236, (2023), https://doi.org/10.1016/j.pss.2023.105752

[3] KORNOŠ, L. – KOUKAL, J. – PIFFL, R. – TÓTH, J.: EDMOND Meteor Database, in: Gyssens, M., Roggemans, P., Zoladek, P. (Eds.), Proceedings of the International Meteor Conference, Poznan, Poland, 22-25 August 2013, pp. 23–25, (2014)

[4] RUDAWSKA, R. – MATLOVIČ, P. – TÓTH, J. – KORNOŠ, L.: Independent identification of meteor showers in EDMOND database. Planetary and Space Science 118, 38–47, (2015), https://doi.org/10.1016/j.pss.2015.07.011

[5] TÓTH, J. – MATLOVIČ, P. – LOEHLE, S. – VAUBAILLON, J. – PISARČÍKOVÁ, A. – LEISER, D. – GRIGAT, F. – EBERHART, M. – HUFGARD, F. RAVICHANDRAN, R. – POLONI, E. – HOERNER, I. – DUERNHOFER, CH. – DELAHAIE, S. – FERRIÈRE, L. – ROMMELUERE, S. – RAMBAUX, S.: Overview of the MetSpec project - Artificial meteors in ground testing, Icarus, vol. 407, 115791, (2024), https://doi.org/10.1016/j.icarus.2023.115791

[6] MATLOVIČ P. – PISARČÍKOVÁ A. – TÓTH J. – MACH P. – ČERMÁK P. – LOEHLE S. – KORNOŠ L., et al.: Hydrogen emission from meteors and meteorites: Mapping traces of H2O molecules and organic compounds in small Solar system bodies, Monthly Notices of the Royal Astronomical Society, 513 (3), 3982–3992, (2022), https://doi.org/10.1093/mnras/stac927

[7] PISARČÍKOVÁ A. – MATLOVIČ P. – TÓTH J. – LOEHLE S. – FERRIÈRE L. – LEISER D. – GRIGAT F., et al: Analysis of CN emission as a marker of organic compounds in meteoroids using laboratory simulated meteors, Icarus, 404, 115682, (2023), https://doi.org/10.1016/j.icarus.2023.115682

[8] KRAJČOVIČ, S. – ŠILHA, J. – ZIGO, M., et al. The Image Processing System for Ultra-Fast Moving Space Debris Objects. Arab J Sci Eng 48, 10589–10604, (2023), https://doi.org/10.1007/s13369-023-07669-0

[9] ŠILHA, J. et al., Space debris observations with the Slovak AGO70 telescope: Astrometry and light curves, Advances in Space Research, Volume 65, Issue 8, Pages 2018-2035, ISSN 0273-1177, (2020), https://doi.org/10.1016/j.asr.2020.01.038

[10] ZIGO, M. – ŠILHA, J. – HROBÁR, T. – JEVČÁK, P., Space debris surface characterization through BVRcIc photometry, Advances in Space Research, Volume 72, Issue 9, Pages 3802-3817, ISSN 0273-1177, (2023), https://doi.org/10.1016/j.asr.2023.07.029

[11] ŽILKOVÁ, D. – ŠILHA, J. – MATLOVIČ, P. – TÓTH, J.: Space debris spectroscopy: Specular reflections at LEO egime, Advances in Space Research, Volume 71, Issue 8, Pages 3249-3261, ISSN 0273-1177, (2023), https://doi.org/10.1016/j.asr.2022.12.001

[12] OSZKIEWICZ, D. – TROIANSKYI, V. – GALÁD, A. – HANUŠ, J. – ĎURECH, J. – WILAWER, E. – MARCINIAK, A. – KWIATKOWSKI, T. – KOLEŃCZUK, P. – SKIFF, B. A. – POLAKIS, T. – MOSKOVITZ, N. A. – GEIER, S. – FÖHRING, D. – HUNG, D. – GAJDOŠ, Š. – VILÁGI, J. – POLČIC, L. – KASHUBA, V. – UDOVICHENKO, S. – KEIR, L. – BENISHEK, V. – PRAY, D. P. – SHEVCHENKO, V. – KRUGLY, Y. – KANKIEWICZ, P. – HASEGAWA, S. – BEHREND, R. – BERNASCONI, L. – LEROY, A. – ROY, R. – IVANOVA, O. – HUSÁRIK, M. – SIMON, A.: Spins and shapes of basaltic asteroids and the missing mantle problem. Icarus, Volume 397, article id. 115520, (2023), https://doi.org/10.1016/j.icarus.2023.115520

[13] CHROBÁKOVÁ, Ž. – NAGY, R. – LÓPEZ-CORREDOIRA, M.: Warp and flare of the Galactic disc revealed with supergiants by Gaia EDR3, AA, 664, A58, (2022), https://doi.org/10.1051/0004-6361/202243296

[14] WANG, H.-F. – CHROBÁKOVÁ, Ž. – LÓPEZ-CORREDOIRA, M. – SYLOS LABINI, F.: Mapping the Milky Way Disk with Gaia DR3: 3D Extended Kinematic Maps and Rotation Curve to ≈30 kpc. ApJ, 942, 12, (2023), https://doi.org/10.3847/1538-4357/aca27c

In the **Earth Science Institute of the Slovak Academy of Sciences, Bratislava and Hurbanovo**, a number of issues concerning space weather modeling and forecasting were investigated and ground magnetic field measurements were performed.

Theoretical research in [2,5] was particularly focused on data from historical geomagnetic measurements. On the basis of a unique collection of printed yearbooks with geomagnetic records from the 19th century from the Clementinum observatory in Prague, the magnetograms were reconstructed by converting the measured values into physical units. The published results concern some technical details about the observation instruments and observation records that were crucial for the beginnings of geomagnetic field measurement at the Clementinum observatory in Prague. The early years of geomagnetic registration and the first geomagnetic survey in Bohemia were associated with the name of Karl Kreil. Attention was drawn to the fact that systematic regular observations of the magnitude of the geomagnetic field had commenced in Prague as early as in 1839; in fact, this happened 2 years after Gauss invented the bifilar device and 5 years after Gauss introduced the physical unit for the magnetic field. This ranks Clementinum among the world's leading workplaces that have significantly contributed to the development of geomagnetism. Details concerning the principles and calibration of the bifilar magnetometer, the main instrument for observing magnetic storms at the time, were also discussed. The bifilar apparatus that was in operation at Clementinum at the beginning of geomagnetic observations made it possible to record several interesting magnetic storms, for example the event of 3–4 September 1839, as shown in Fig. 2.7.
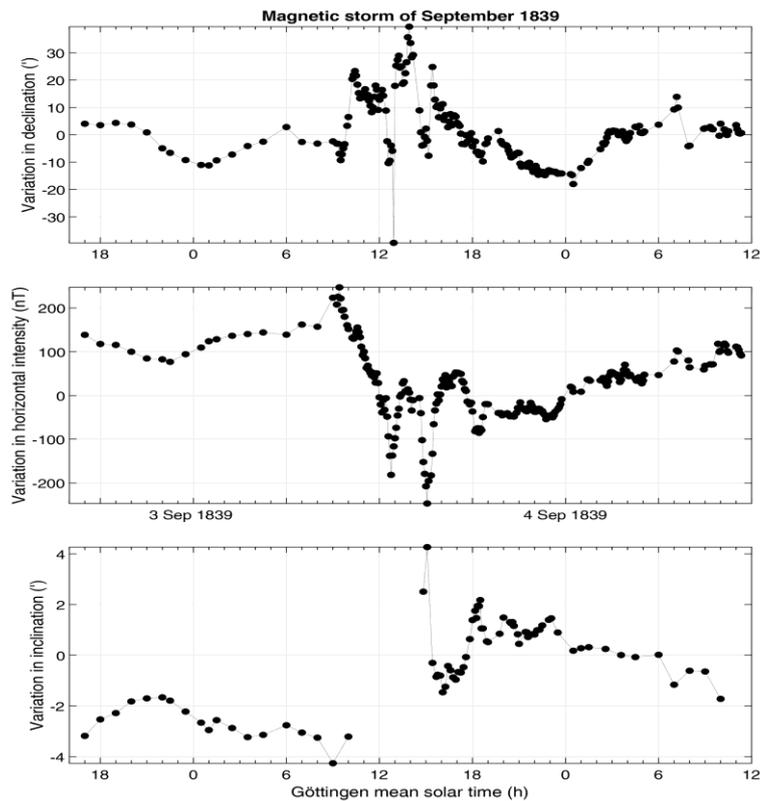
Figure 2.7. *The first magnetic storm recorded at the Clementinum observatory in Prague on 3–4 September 1839, [5]. The course of magnetic declination, horizontal intensity and magnetic inclination is shown. For the records of declination and inclination, conversion from divisions of the instrument scale obtained from the yearbook to angular units was performed. Despite the visible gap in the inclination record, it is indicated here that a slight change in inclination during the main phase of a magnetic storm was feasible at that time.*

Collecting historical geomagnetic records can be beneficial for the study of adverse space weather conditions in the past. Also, important insights into possible interplanetary conditions for intense magnetic storms and probable frequency of their occurrence can be deduced. Historical geomagnetic data can be also useful in improving models of the global geomagnetic field. It is expected that the detailed methodology for researching old geomagnetic records will stimulate future collaborative research in the collection and analysis of previously unknown historical geomagnetic data from observatories around the world. Mapping the distribution of the geomagnetic field, on the other hand, represents another aspect of research on the Earth's body, in which regular geomagnetic surveys continue to these days.

Using data from the observatory in Stará Ďala, at present Hurbanovo, a strong magnetic storm from of May 1921 was examined in [3,6]. This geomagnetic disturbance is called 'New York Railroad Storm' and represents the strongest magnetic storm of the 20th century. The previous notion of extreme geomagnetic activity due to enhanced ring current is currently being revised. It turns out that strong magnetic storms can also occur locally as a result of increased auroral activity (intensity of current systems of the auroral oval), and in addition, the auroral oval itself can move up to the level of magnetic mid-latitudes. To assess whether the magnetic disturbance is global or local, it is necessary to examine magnetograms from several observatories. This analysis is also the content of the dissertation topic of the doctoral student Eduard Koči. A method of displaying the time evolution of a magnetic disturbance for a specific location on the Earth represented by magnetic coordinates was proposed. This methodology can help in the classification of magnetic disturbances, whether they were caused by the ring current or were local in nature due to increased auroral activity. However, magnetic registration instruments did not record the horizontal intensity at that time, and the magnetic declination as well as the vertical intensity went out of range on some parts of record, as shown in Fig. 2.8. In addition, the original magnetograms did not have axes and scales described. The records were reconstructed by comparing the registered data with magnetograms and data both before and after the studied event from Stará Ďala observatory and also with data from other observatories. Although the preserved record does not cover the entire event, it still shows extremely large variations of the field: in declination up to almost 1° in less than 1 hour (followed by going out of range), in the vertical component an increase of more than 80 nT in less than 3 hours (after returning to the measuring range).

The magnetospheric magnetic field model has proven useful in the study of various magnetospheric current systems and associated magnetic fields. In particular, such a model can be used for the quantitative expression of geomagnetic field disturbances in response to variable solar wind input. This is an important application of the model for the short-term (1 hour ahead) space weather forecasting. In [1], the role of specific magnetospheric current systems in magnetosphere dynamics was discussed and their possible contribution to the development of strong magnetic storms was evaluated. More extensive data sets will be needed to validate the model and make it suitable for reliable space weather forecasting. It is expected that newly admitted doctoral students will take up this research topic.

The latter period falls within the ascending phase of the solar cycle with only weak solar activity and without extreme geomagnetic disturbances. A gradual growth of geomagnetic activity is expected in the near future. In this context, a new recording device was tested at the observatory in Hurbanovo. The results of testing the set of the datalogger LB-480 connected to the older Bobrov type magnetometer PSM-8711 in quiet and disturbed geomagnetic conditions are presented in [4]. An important intermediate result of the study is the sensitivities of the variometer sensors. The testing under both quiet and disturbed conditions has shown the satisfactory accuracy of our instrument set. There was also pointed to a weakness of the set, which is a limited measuring range. The results of the registrations were compared with
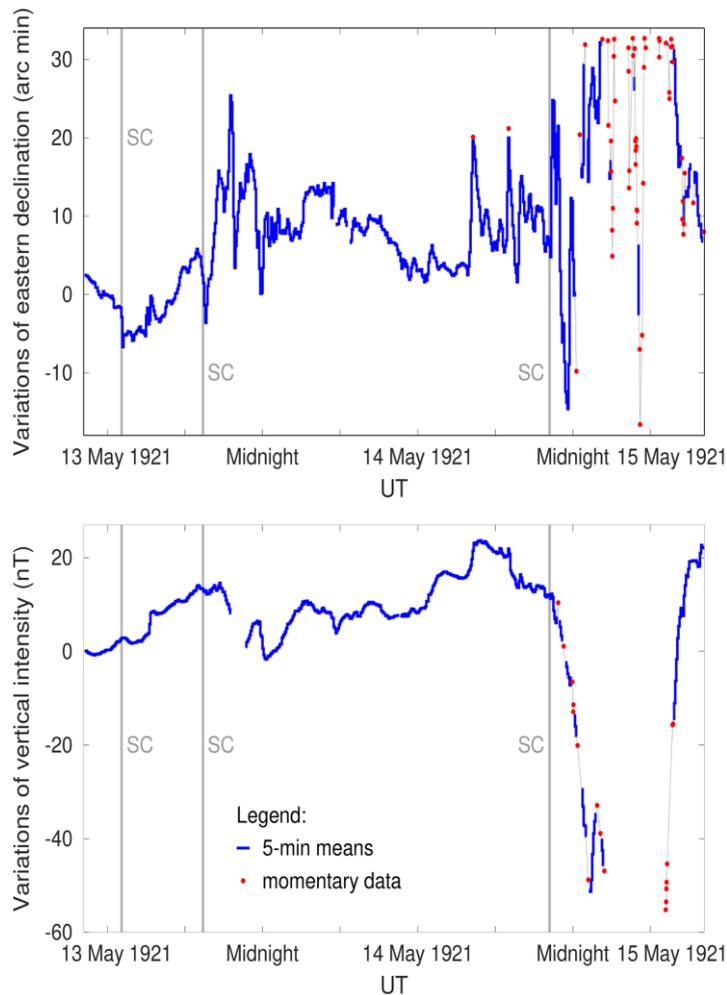
Figure 2.8. *The records of magnetic declination and vertical intensity in Stará Ďala for the storm of 15 May 1921, [6]. The 5 min means, as well as some important momentary values, are displayed. The occurrences of sudden storm commencements (SSCs) on 13 May at 13:06 and 19:24 UT and on 14 May at 22:12 UT are also indicated.*

reference values within the database of the program of the international network of geomagnetic observatories INTERMAGNET.

In addition to the theoretical focus of the research work, there are regular observatory measurements of the geomagnetic field performed at the Hurbanovo Geomagnetic Observatory of the Earth Science Institute of the SAS. The Hurbanovo Observatory is located at geographical latitude 47.87° and geographical longitude 18.18°. It performs continuous monitoring and registration of the geomagnetic field components. The one-minute mean values of all geomagnetic field components as well as the records acquired with the one-second sampling interval are available. K-indexes characterizing the geomagnetic activity in the middle latitudes are computed regularly. Main equipment of the observatory includes the digital variometer station TPM made in Poland (1996) and magnetoregistration device DI-fluxgate Magson gained on the co-operation bases with Geo Forschung Zentrum Potsdam and VW Stiftung. For absolute geomagnetic measurements, the DI-fluxgate magnetometer and proton precession magnetometer PMG 1 are employed. The magnetovariational data in the one-minute step are supplied via the internet to the INTERMAGNET centre. The data are sent to World Data Centers in Paris, from where they are available for the whole geomagnetic and space

20

weather community. The data are published also on the CD-ROMs prepared in the frame of INTERMAGNET. That is because the Hurbanovo Geomagnetic Observatory of the Earth Science Institute of the SAS is a member of INTERMAGNET, the international network of world first order magnetic observatories. Information about the geomagnetic activity is also published on the web site of the observatory, www.geomag.sk.

References:

[1] REVALLO, M. – VALACH, F. – HEJDA, P. Magnetospheric magnetic field model applied to strong magnetic storms. In Zborník referátov z 26. celoštátneho slnečného seminára, Piešťany 2022. - Hurbanovo: Slovenská ústredná hvezdáreň, 2022, p. 15. ISBN 978-80-89998-29-6.

[2] VALACH, F. – HEJDA, P. – REVALLO, M. Geomagnetic observations in the mid-19th century and the historical observatory Clementinum in Prague. In Zborník referátov z 26. celoštátneho slnečného seminára, Piešťany 2022. Ed. I. Dorotovič. - Hurbanovo: Slovenská ústredná hvezdáreň, 2022, p. 16. ISBN 978-80-89998-29-6.

[3] KOČI, E. – VALACH, F. New York Railbroad Storm of 1921 recorded on magnetograms at Stará Ďala observatory. In Zborník referátov z 26. celoštátneho slnečného seminára, Piešťany 2022. - Hurbanovo: Slovenská ústredná hvezdáreň, 2022, p. 12. ISBN 978-80-89998-29-6.

[4] KOČI, E. – VALACH, F. – VÁCZYOVÁ, M. Testing the set of the datalogger LB-480 connected to the older Bobrov type magnetometer PSM-8711. In Zborník referátov z 26. celoštátneho slnečného seminára, Piešťany 2022. - Hurbanovo: Slovenská ústredná hvezdáreň, 2022, p. 13. ISBN 978-80-89998-29-6.

[5] HEJDA, P. – VALACH, F. – REVALLO, M. Historical geomagnetic observations from Prague observatory (since 1839) and their contribution to geomagnetic research. In History of Geo- and Space Sciences, 2023, vol. 14, p. 51-60. ISSN 2190-5010. (https://doi.org/10.5194/hgss-14-51-2023)

[6] KOČI, E. – VALACH, F. The record of the magnetic storm on 15 May 1921 in Stará Ďala (present-day Hurbanovo) and its compliance with he global picture of this extreme event. In Annales Geophysicae, 2023, vol. 41, no. 2, p. 355-368. ISSN 0992-7689. (https://doi.org/10.5194/angeo-41-355-2023)

In the ***Slovak Central Observatory* (SCO)** in Hurbanovo (http://www.suh.sk) a number of activities related to space research were performed. We observed sunspots (the Wolf number data were submitted to the SILSO in Brussels, Belgium and to the SONNE Netz in Germany), solar chromosphere and prominences (images are published at https://www.kozmos-online.sk/obs/aktivita/activity.htm). We performed also spectrographic observations of the solar spectrum (variations of selected spectral lines during a solar activity cycle) using a horizontal solar telescope with spectrograph, we registered solar radio bursts using a solar radio spectrometer CALLISTO. The research activities comprise study of the differential rotation of the solar corona.

One researcher from the SCO is the national ISWI (International Space Weather Initiative, http://iswi-secretariat.org) coordinator for the Slovak Republic and since October 2022 he is also delegate of the Slovak Republic in the programme board of ESA for space safety (PB-SSA). He is member of the National Committee of the SCOSTEP and chair and representative to the COSPAR.

We continued to publish at the website of the SCO data on the modified coronal index (MCI) and the modified homogeneous data set (MHDS) of coronal intensities based on satellite EUV measurements as a replacement of ground-based coronagraphic observations at Lomnický Štít. Both the MCI and the MHDS data sets can be used further for studies of the coronal solar activity and its cycle. These data are available at https://www.kozmos-online.sk/slnko.

In the Computer Intelligence Group (CA3) of the CTS/UNINOVA (Caparica, Portugal) has been developed in previous years various software tool for automatic tracking of solar activity features (sunspots and coronal bright points - CBPs) using a hybrid algorithm combining PSO (Particle Swarm Optimization) and Snake algorithms, and an image segmentation algorithm, respectively, for detecting and tracking of a feature, and determining the differential rotation of the Sun. Another segmentation algorithm for automatic detection of CBPs was developed using SunPy and OpenCV in Python. An automatic tool to detect coronal holes (CHs) and to determine solar differential rotation using CBPs inside and outside the CHs, respectively, is being developed in the CTS/UNINOVA-CA3 group.

In the SCO we developed also an alternative software tool to estimate the solar rotational profile based on cross-correlation (CC) method. Analysis of additional SDO data from the years 2022 -2023 is being performed.

One researcher from the SCO is a PhD student at the Geomagnetic Observatory Hurbanovo of the Earth Science Institute of the Slovak Academy of Sciences (Bratislava). His published results are referenced as [3], [4], and [6] in the previous section.

The SCO organised in the year 2022 in Piešťany the 26th National Solar Physics Meeting with participation from abroad. The goal of the Meeting was to present new results of solar physics and from the field of the space weather (Sun-Earth connections), to provide overview of present status in selected fields of solar physics, geophysics, meteorology, and climatology. A separate space was devoted to the presentation of research results of undergraduate and PhD students of university and academic departments and also to results of scientific and popularisation activities of Astronomical Observatories in the Slovak Republic and the Czech Republic. Invited talks, short contributions and posters covered the following fields: physical phenomena in the solar atmosphere, solar activity, total solar eclipses, space weather, geoactivity, meteorological events with solar forcing.

The activities of **the Astronomical Institute of the Slovak Academy of Sciences (AISAS)**, Tatranská Lomnica (http://www.astro.sk), related to COSPAR, were devoted to research in stellar, solar, and interplanetary physics using different satellite observations, mainly in the UV, XUV and X-ray spectral regions. Stellar data of the Swift, XMM-Newton, TESS, CHEOPS, and Kepler satellites, were used for research of various variable stars [1,3,4,5,8,10,18], stars hosting exoplanets and the exoplanets themselves [2,9,11,12,13,14,15,16,17]. Data of the current SDO, IRIS, STEREO, Hinode, and other satellites were used for solar research. In common, these data were used with the simultaneously acquired data by the ground-based solar telescopes [6,19,20,21,22,23]. Different topics of the solar system bodies have been addressed, in many articles from the laboratory physics side [7,24,25,26,27,28,29,30]. Hereby we present some examples of the results obtained by the AISAS staff.

Accretion of mass onto a white dwarf (WD) in a binary system can lead to stellar explosions. If a WD accretes from stellar wind of a distant evolved giant in a symbiotic binary, it can undergo occasional outbursts in which it brightens by several magnitudes, produces a low- and high-velocity mass outflow, and, in some cases, ejects bipolar jets. In paper [1] the current picture of these outbursts is complemented by the transient emergence of a neutral region in the orbital plane of symbiotic binaries consisting of wind from the giant. Its presence was proved by determining H^0 column densities (N_H) in the direction of the WD and at any orbital phase of the binary by modelling the continuum depression around the Lyα line caused by Rayleigh scattering on atomic hydrogen for all suitable objects, i.e., eclipsing symbiotic binaries, for which a well-defined ultraviolet spectrum from an outburst is available. The N_H values follow a common course along the orbit with a minimum and maximum of a few times
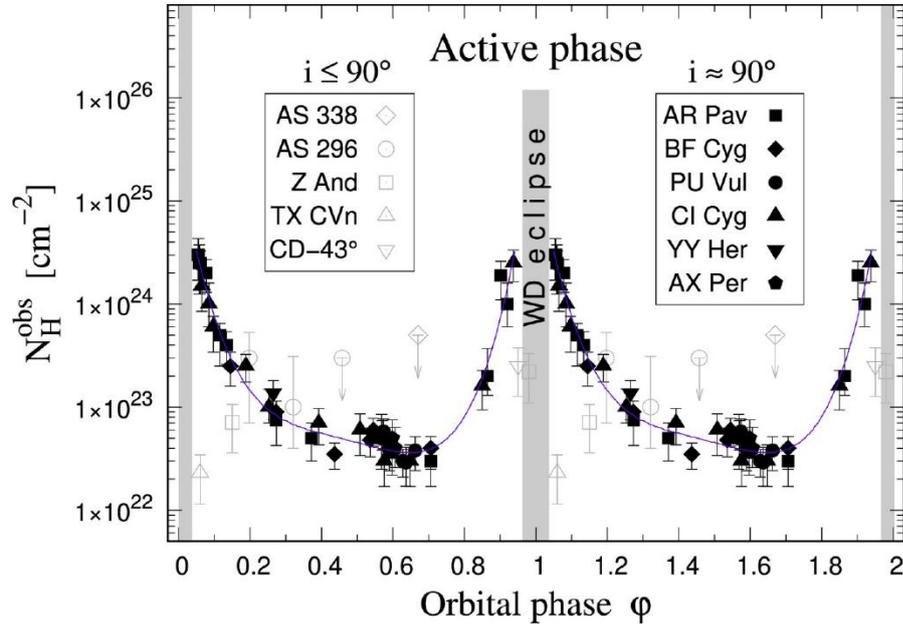
Figure 2.9. *Column densities of atomic hydrogen, $N_H{}^{obs}$, between the observer and the WD, measured for our targets during active phases as a function of the orbital phase φ. For better visualization, the values are plotted over two orbital cycles. Eclipsing objects (black filled symbols) follow a common course. The blue line indicates their fit with a fourth-degree polynomial. Open gray symbols denote values for objects with poorly defined UV spectra (AS 338, AS 296) or not eclipsing, but with a high orbital inclination (Z And, TX CVn, CD −43°14304 (CD−43° in the legend)).*

23

10^{22} and 10^{24} cm^{-2} around the superior and inferior conjunction of the giant, respectively. Its asymmetry implies an asymmetric density distribution of the wind from the giant in the orbital plane with respect to the binary axis. The neutral wind is observable in the orbital plane owing to the formation of a dense disk-like structure around the WD during outbursts, which blocks ionizing radiation from the central burning WD in the orbital plane.

Based on the combined TESS and CHEOPS observations [2], the true orbital period of the planet d of the star HD 22946 (late F-type star) was successfully determined o be 47.42489 ± 0.00011 days, precise radii of the planets in the system were derived, namely 1.362 ± 0.040 $R_\oplus$, 2.328 ± 0.039 $R_\oplus$, and 2.607 ± 0.060 $R_\oplus$ for planets b, c, and d, respectively. Due to the low number of radial velocities, it was possible to determine only 3σ upper limits for these respective planet masses, which are 13.71 $M_\oplus$, 9.72 $M_\oplus$, and 26.57 $M_\oplus$. The stellar parameters for the host star were also derived. Planet c around the HD 22946 star appears to be a promising target for future atmospheric characterisation via transmission spectroscopy. We can also conclude that planet d, as a warm sub-Neptune, is very interesting because there are only a few similar confirmed exoplanets to date. Such objects are worth investigating in the near future, for example in terms of their composition and internal structure.
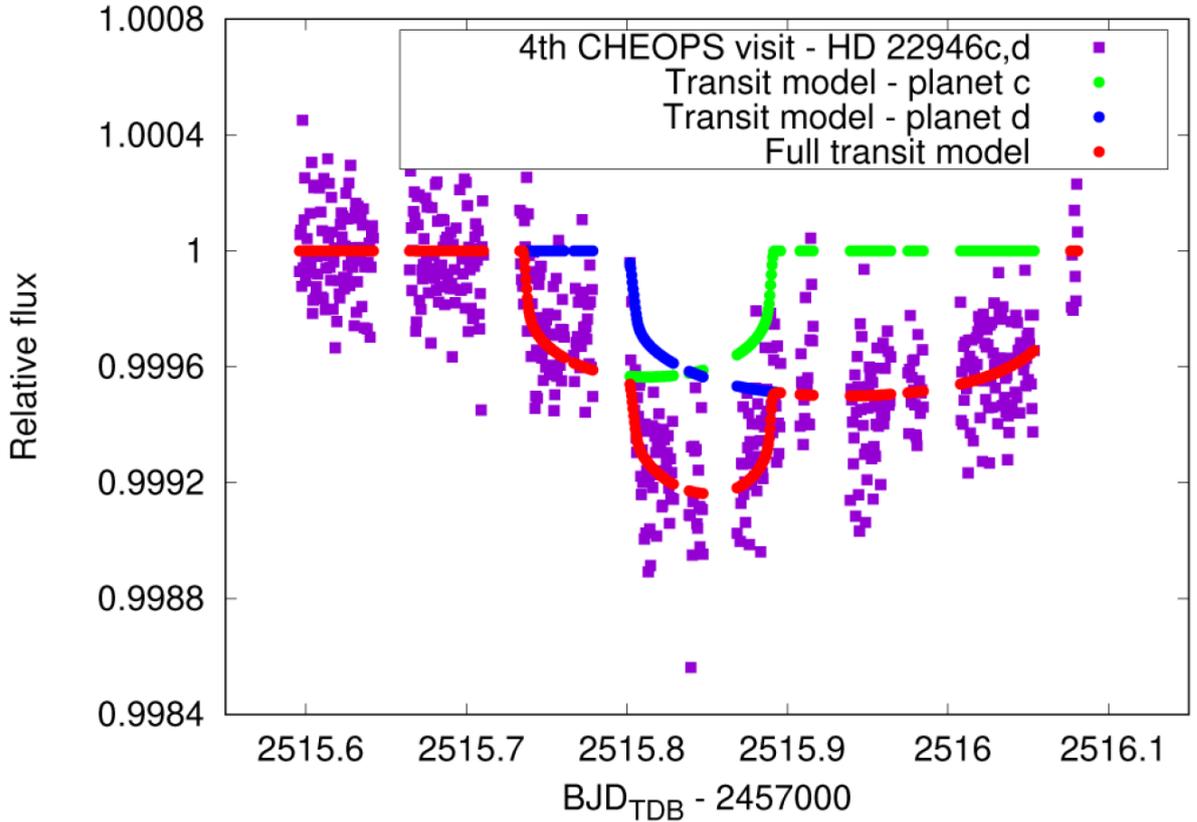
Figure 2.10. *CHEOPS observations of the star HD 22946 on October 28, 2021. The observed light curve wad overplotted with the best fit model. Besides the summed model also the individual models of the planets c and d are displayed.*

On 2021 February 12, two subsequent eruptions occurred above the western limb of the Sun, as seen along the Sun-Earth line. The first event was a typical slow coronal mass ejection (CME), followed ~7 h later by a smaller and collimated prominence eruption, originating south of the CME, followed by a plasma blob. These events were observed not only by the SOHO

and STEREO-A missions, but also by the suite of remote-sensing instruments on board Solar Orbiter [19]. It was shown how data acquired by the Full Sun Imager (FSI), the Metis coronagraph, and the Heliospheric Imager (HI) from the Solar Orbiter perspective can be combined to study the eruptions and different source regions. Images acquired by the two Metis channels in the visible light (VL) and H I Ly-α line (UV) were combined to derive physical information about the expanding plasma. The polarization ratio technique was also
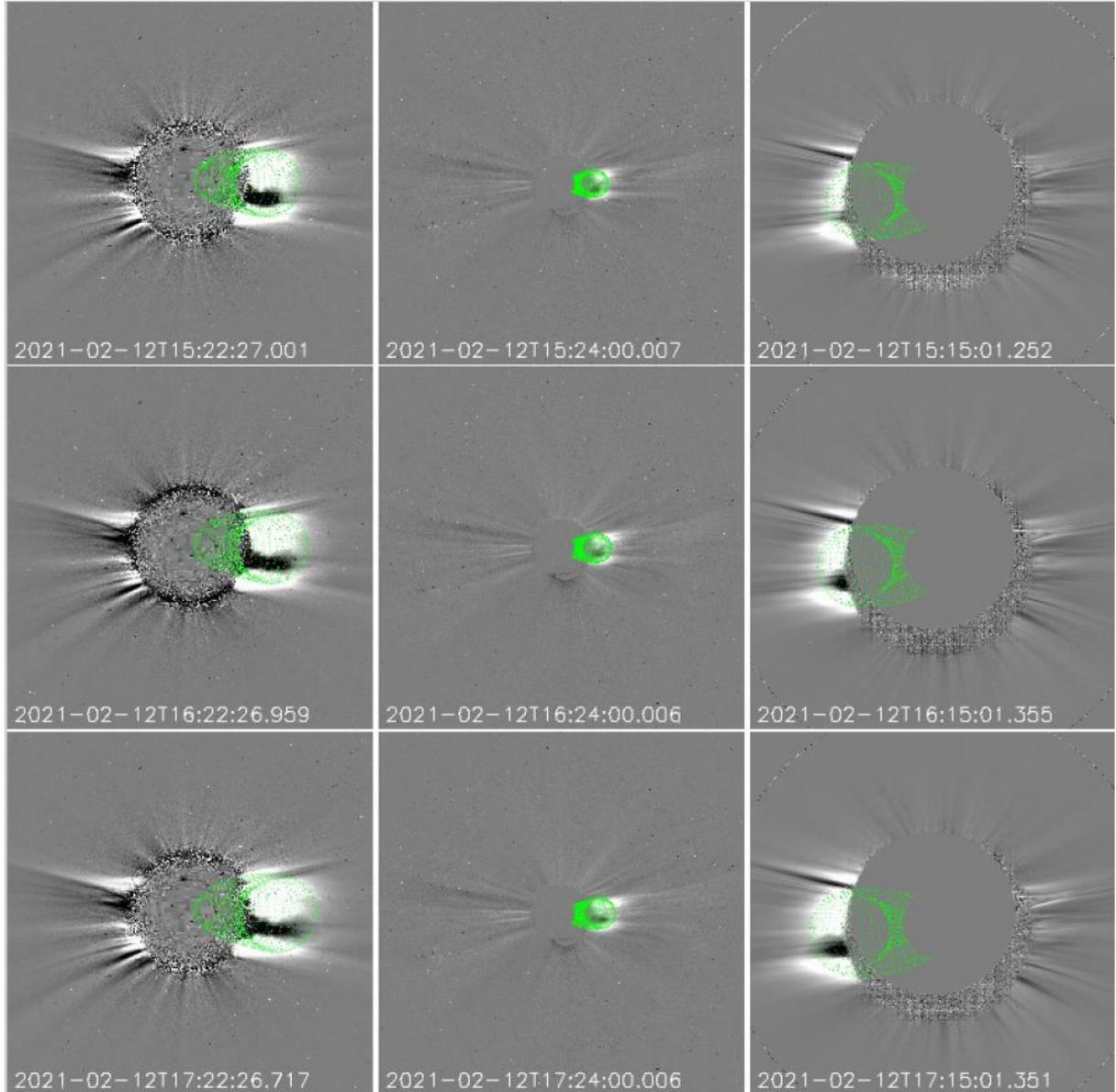
Figure 2.11. *The February 12 CME as observed by coronagraphs on board different spacecraft at different times. Upper row: GCS reconstruction of the CME on February 12 observed by LASCO-C2 at 15:22–07:58 UT (left panel), by COR2-A at 15:24–08:24 UT (middle panel), and by Metis at 15:15–12:15 UT (right panel). Middle row: GCS reconstruction of the CME on February 12 observed by LASCO-C2 at 16:22–07:58 UT (left panel), by COR2-A at 16:24–08:24 UT (middle panel), and by Metis at 16:15–12:15 UT (right panel). Lower row: GCS reconstruction of the CME on February 12 observed by LASCO-C2 at 17:22–07:58 UT (left panel), by COR2-A at 17:24–08:24 UT (middle panel), and by Metis at 17:15–12:15 UT (right panel).*

25

applied for the first time to Metis images acquired in the VL channel. The two eruptions were followed in 3D from their source region to their expansion in the intermediate corona. By combining VL and UV Metis data, the formation of a post-CME current sheet (CS) was followed for the first time in the intermediate corona. The plasma temperature gradient across a post-CME blob propagating along the CS was also measured for the first time.

Water (H_2O) ice is a ubiquitous component of the universe, having been detected in a variety of interstellar and Solar System environments where radiation plays an important role in its physico-chemical transformations. Although the radiation chemistry of H_2O astrophysical ice analogues has been well studied, direct and systematic comparisons of different solid phases are scarce and are typically limited to just two phases. In the article [25] there are described the results of an in-depth study of the 2 keV electron irradiation of amorphous solid water (ASW), restrained amorphous ice (RAI) and the cubic (Ic) and hexagonal (Ih) crystalline phases at 20 K so as to further uncover any potential dependence of the radiation physics and chemistry on the solid phase of the ice. Mid-infrared spectroscopic analysis of the four investigated H_2O ice phases revealed that electron irradiation of the RAI, Ic, and Ih phases resulted in their amorphization (with the latter undergoing the process more slowly) while ASW underwent compaction. The abundance of hydrogen peroxide (H_2O_2) produced as a result of the irradiation was also found to vary between phases, with yields being highest in irradiated ASW. This observation is the cumulative result of several factors including the increased porosity and quantity of lattice defects in ASW, as well as its less extensive hydrogen-bonding network. Our results have astrophysical implications, particularly with regards to H_2O-rich icy interstellar and Solar System bodies exposed to both radiation fields and temperature gradients.

References:

[1] SKOPAL, A. The emergence of a neutral wind region in the orbital plane of symbiotic binaries during their outbursts. In The Astronomical Journal, 2023, vol. 165, no. 6, article no. 258, p. 1-19.

[2] GARAI, Z. – OSBORN, H. P. – GANDOLFI, D. – BRANDEKER, A. – SOUSA, S. G. – LENDL, M. – BEKKELIEN, A. – BROEG, C. – COLLIER CAMERON, A. – EGGER, J. A. – HOOTON, M. J. – ALIBERT, Y. – DELREZ, L. – FOSSATI, L. – SALMON, S. – WILSON, T. G. – BONFANTI, A. – TUSON, A. – ULMER MOLL, S. – SERRANO, L. M. – BORSATO, L. – ALONSO, R. – ANGLADA, G. – ASQUIER, J. – BARRADO Y NAVASCUES, D. – BARROS, S. C. C. – BÁRCZY, T. – BAUMJOHANN, W. – BECK, M. – BECK, T. – BENZ, W. – BILLOT, N. – BIONDI, F. – BONFILS, X. – BUDER, M. – CABRERA, J. – CESSA, V. – CHARNOZ, S. – CSIZMADIA, S. – CUBILLOS, P. E. – DAVIES, M. B. – DELEUIL, M. – DEMANGEON, O. D. S. – DEMORY, B.-O. – EHRENREICH, D. – ERIKSON, A. – VAN EYLEN, V. – FORTIER, A. – FRIDLUND, M. – GILLON, M. – VAN GROOTEL, V. – GUEDEL, M. – GUENTHER, M. N. – HOYER, S. – ISAAK, K. G. – KISS, L. L. – KRISTIANSEN, M. H. – LASKAR, J. – LECAVELIER DES ETANGS, A. – LOVIS, Christophe – LUNTZER, A. – MAGRIN, D. – MAXTED, P. F. L. – MORDASINI, C. – NASCIMBENI, V. – OLOFSSON, G. – OTTENSAMER, R. – PAGANO, I. – PALLÉ, E. – PETER, G. – PIOTTO, G. – POLLACCO, D. – QUELOZ, D. – RAGAZZONI, R. – RANDO, N. – RAUER, H. – RIBAS, I. – SANTOS, N. C. – SCANDARIATO, G. – SÉGRANSAN, D. – SIMON, A. E. – SMITH, A. M. S. – STELLER, M. – SZABÓ, Gy. M. – THOMAS, N. – UDRY, S. – VENTURINI, J. – WALTON, N. Refined parameters of the HD 22946 planetary system and the true orbital period of planet d. In Astronomy and Astrophysics, 2023, vol. 674, article no. A44, p. 1-14

[3] SHAGATOVA, N. – SKOPAL, A. – KUNDRA, E. – KOMŽÍK, R. – SHUGAROV, S. – PRIBULLA, T. – KRUSHEVSKA, V. Density asymmetry and wind velocities in the orbital plane of the symbiotic binary EG Andromedae. In Astronomy and Astrophysics, 2023, vol. 676, article no. A98, p. 1-12.

[4] PRIBULLA, T. – BORKOVITS, T. – JAYARAMAN, R. – RAPPAPORT, S. A. – MITNYAN, T. – ZASCHE, P. – KOMŽÍK, R. – ANDRÁS, P. – UHLÁŘ, R. – MAŠEK, M. – HENZL, Z. – BARNA BIRÓ, I. – CSÁNYI, I. – STUIK, R. – KRISTIANSEN, M. H. – SCHWENGELER, H. M. – GAGLIANO, R. – JACOBS, T.. – OMOHUNDRO, M. – KOSTOV, V. B. – POWELL, B. P. – TERENTEV, I. A. – VANDERBURG, A. – LACOURSE, D. M. – RODRIGUEZ, J. E.– BAKOS, G. – CSUBRY, Z. – HARTMAN, J. BU Canis Minoris - the most compact known flat doubly eclipsing quadruple system. In Monthly Notices of the Royal Astronomical Society, 2023, vol. 524, no. 3, p. 4220-4238.

[5] RAPPAPORT, S. A. – BORKOVITS, T. – GAGLIANO, R. – JACOBS, T. L. – TOKOVININ, A. – MITNYAN, T. – KOMŽÍK, R. – KOSTOV, V. B. – POWELL, B. P. – TORRES, G. – TERENTEV, I. – OMOHUNDRO, M. – PRIBULLA, T. – VANDERBURG, A. – KRISTIANSEN, M. H. – LATHAM, D. W. – SCHWENGELER, H. M. – LACOURSE, D. – BIRÓ, I. B. – CSÁNYI, I. – CZAVALINGA, D. – GARAI, Z. – PÁL, A. – RODRIGUEZ, J. E. – STEVENS, D. J. A study of nine compact triply eclipsing triples. In Monthly Notices of the Royal Astronomical Society, 2023, vol. 521, no. 1, p. 558-584.

[6] KARLICKÝ, M. – RYBÁK, J. Multi-periodicity of high-frequency type III bursts as a signature of the fragmented magnetic reconnection. In Universe, 2023, vol. 9, no. 2, article no. 92, p. 1-12.

[7] MIFSUD, D. V. – HERCZKU, P. – RAHUL, K. K. – RAMACHANDRAN, R. – SUNDARARAJAN, P. – KOVÁCS, S. T. S. – SULIK, B. – JUHÁSZ, Z. – RÁCZ, R. – BIRI, S. – KAŇUCHOVÁ, Z. – MCCULLOUGH, R. W. – SIVARAMAN, B. – IOPPOLO, S. – MASON, N. A systematic mid-infrared spectroscopic study of thermally processed SO2 ices. In Physical Chemical Physics, 2023, vol. 25, p. 26278-26288.

[8] SKOPAL, A. Multiwavelength modeling the SED of luminous supersoft X-ray sources in Large Magellanic cloud and Small Magellanic cloud. In The Astronomical Journal, 2022, vol. 164, no. 4, article no. 145, p. 1-18.

[9] BORKOVITS, T. – MITNYAN, T. – RAPPAPORT, S. A. – PRIBULLA, T. – POWELL, B. P. – KOSTOV, V. B. – BIRÓ, I. B. – CSÁNYI, I. – GARAI, Z. – GARY, B. L. – KAYE, T. G. – KOMŽÍK, R. – TERENTEV, I. – OMOHUNDRO, M – GAGLIANO, R. – JACOBS, T. – KRISTIANSEN, M. H. – LACOURSE, D. – SCHWENGELER, H. M. – CZAVALINGA, D. – SELI, B. – HUANG, C. X. – PÁL, A. – VANDERBURG, A. – RODRIGUEZ, E. – STEVENS, D. J. Triply eclipsing triple stars in the northern TESS fields: TICs 193993801, 388459317, and 52041148. In Monthly Notices of the Royal Astronomical Society, 2022, vol. 510, no. 1, p. 1352-1374.

[10] BUDAJ, J. – MALIUK, A. – HUBENY, I. WD 1145+017: Alternative models of the atmosphere, dust clouds, and gas rings. In Astronomy and Astrophysics, 2022, vol. 660, article no. A72, p. 1-14.

[11] GARAI, Z. Grazing, non-transiting disintegrating exoplanets observed with the planned Ariel space observatory. In Experimental Astronomy, 2022, vol. 53, no. 2, p. 729-748.

[12] GARAI, Z. – PRIBULLA, T. – KOVÁCS, J. – SZABÓ, Gy. M. – CLARET, A. – KOMŽÍK, R. – KUNDRA, E. Rapidly rotating stars and their transiting planets: KELT-17b,

KELT-19Ab, and KELT-21b in the CHEOPS and TESS era. In Monthly Notices of the Royal Astronomical Society, 2022, vol. 513, no. 2, p. 2822-2840.

[13] MANNADAY, V. K. – THAKUR, P. – SOUTHWORTH, J. – JIANG, I.-G. – SAHU, D.K. – MANCINI, L. – VAŇKO, M. – KUNDRA, E. – GAJDOŠ, P. – A-THANO, N. – SARIYA, D. P. – YEH, L.-C. – GRIV, E. – MKRTICHIAN, D. – SHLYAPNIKOV, A.. Revisiting the transit timing variations in the TrES-3 and Qatar-1 systems with TESS data. In The Astronomical Journal, 2022, vol. 164, no. 5, article no. 198, p. 1-20

[14] POWELL, B. P. – RAPPAPORT, S. A. – BORKOVITS, T. – KOSTOV, V. B. – TORRES, G. – JAYARAMAN, R. – LATHAM, D. W. – KUČÁKOVÁ, H. – GARAI, Z. – PRIBULLA, T. – VANDERBURG, A. – KRUSE, E. – BARCLAY, T. – OLMSCHENK, G. – KRISTIANSEN, M. H. K. – GAGLIANO, R. – JACOBS, T. L. – LACOURSE, D. M. – OMOHUNDRO, M. – SCHWENGELER, H. M. – TERENTEV, I. A. – SCHMITT, A. R. TIC 114936199: A quadruple star system with a 12 day outer-orbit eclipse. In The Astrophysical Journal, 2022, vol. 938, no. 2, article no. 133, p. 1-15.

[15] RAPPAPORT, S. A. – BORKOVITS, T. – GAGLIANO, R. – JACOBS, T. L. – KOSTOV, V. B. – POWELL, B. P. – TERENTEV, I. – OMOHUNDRO, M. – TORRES, G. – VANDERBURG, A. – MITNYAN, T. – KRISTIANSEN, M. H. – LACOURSE, D. – SCHWENGELER, H. M. – KAYE, T. G. – PÁL, A. – PRIBULLA, T. – BIRÓ, I. B. – CSÁNYI, I. – GARAI, Z. – ZASCHE, P. – MAXTED, P. F. L. – RODRIGUEZ, J. E. – STEVENS, D. J. Six new compact triply eclipsing triples found with TESS. In Monthly Notices of the Royal Astronomical Society, 2022, vol. 513, no. 3, p. 4341-4360.

[16] SZABÓ, Gy. M. – GARAI, Z. – BRANDEKER, A. et al., Transit timing variations of AU Microscopii b and c. In Astronomy and Astrophysics, 2022, vol. 659, article no. L7, p. 1-9.

[17] SZABÓ, Gy. M. – KÁLMÁN, Sz. – PRIBULLA, T. – CLARET, A. – MUGNAI, L. V. – PASCALE, E. – WALTHAM, D. – BORSATO, L. – GARAI, Z. – SZABÓ, R. High-precision photometry with Ariel. In Experimental Astronomy, 2022, vol. 53, no. 2, p. 607-634.

[18] VAŇKO, M. – PRIBULLA, T. – GAJDOŠ, P. – BUDAJ, J. – ZVERKO, J. – PAUNZEN, E. – GARAI, Z. – HAMBÁLEK, Ľ. – KOMŽÍK, R. – KUNDRA, E. HD 183986: A high-contrast SB2 system with a pulsating component. In The Astronomical Journal, 2022, vol. 163, no. 6, article no. 245, p. 1-14.

[19] BEMPORAD, A. – ANDRETTA, V. – SUSINO, R. – MANCUSO, S. – SPADARO, D. – MIERLA, M. – BERGHMANS, D. – D' HUYS, E. – ZHUKOV, A. N. – TALPEANU, D.-C. – COLANINNO, R. – HESS, P. – KOZA, J. – JEJČIČ, S. – HEINZEL, P. – ANTONUCCI, E. – DA DEPPO, V. – FINESCHI, S. – FRASSATI, F. – JERSE, G. – LANDINI, F. – NALETTO, G. – NICOLINI, G. – PANCRAZZI, M. – ROMOLI, M. – SASSO, C. – SLEMER, A. – STANGALINI, M. – TERIACA, L. Coronal mass ejection followed by a prominence eruption and a plasma blob as observed by Solar Orbiter. In Astronomy and Astrophysics, 2022, vol. 665, article no. A7, p. 1-15.

[20] BERRIOS SAAVEDRA, G. – UTZ, D. – VARGAS DOMINGUEZ, S. – CAMPOS ROZO, J. I. – GONZÁLEZ MANRIQUE, S. J. – GÖMÖRY, P. – KUCKEIN, Ch. – BALTHASAR, H. – ZELINA, P. Observational evidence for two-component distributions describing solar magnetic bright points. In Astronomy and Astrophysics, 2022, vol. 657, article no. A79, p. 12.

[21] GUNÁR, S. – HEINZEL, P. – KOZA, J. – SCHWARTZ, P. Large impact of the Mg II h and k incident radiation change on results of radiative transfer models and the importance of dynamics. In The Astrophysical Journal, 2022, vol. 934, no. 2, article no. 133, p. 1-7.

[22] KOZA, J. – GUNÁR, S. – SCHWARTZ, P. – HEINZEL, P. – LIU, W. Data-driven model of temporal evolution of solar Mg II h and k profiles over the solar cycle. In The Astrophysical Journal Supplement Series, 2022, vol. 261, no. 2, article no. 17, p. 1-18.

[23] VASHALOMIDZE, Z. – ZAQARASHVILI, T. V. – KUKHIANIDZE, V. – RAMISHVILI, G. – HANSLMEIER, A. – GÖMÖRY, P. Prominence instability and CMEs triggered by massive coronal rain in the solar atmosphere. In Astronomy and Astrophysics, 2022, vol. 658, article no. A18, p. 1-10.

[24] MIFSUD, D. V. – HERCZKU, P. – RÁCZ, R. – RAHUL, K. K. – KOVÁCS, S. T. S. – JUHÁSZ, Z. – SULIK, B. – BIRI, S. – MCCULLOUGH, R. W. – KAŇUCHOVÁ, Z. – IOPPOLO, S. – HAILEY, P. A. – MASON, N. Energetic electron irradiations of amorphous and crystalline sulphur-bearing astrochemical ices. In Frontiers in Chemistry, 2022, vol. 10, article no. 1003163, p. 1-12.

[25] MIFSUD, D. V. – HAILEY, P. A. – HERCZKU, P. – JUHÁSZ, Z. – KOVÁCS, S. T. S. – SULIK, B. – IOPPOLO, S. – KAŇUCHOVÁ, Z. – MCCULLOUGH, R. W. – PARIPÁS, B. – MASON, N. Laboratory experiments on the radiation astrochemistry of water ice phases. In European Physical Journal D, 2022, vol. 76, no. 5, article no. 87, p. 1-15

[26] MIFSUD, D. V. – KAŇUCHOVÁ, Z. – IOPPOLO, S. – HERCZKU, P. – TRASPAS MUIŇA, A. – FIELD, T. A. – HAILEY, P. A. – JUHÁSZ, Z. – KOVÁCS, S. T. S. – MASON, N. – MCCULLOUGH, R. W. – PAVITHRAA, S. – RAHUL, K. K. – PARIPÁS, B. – SULIK, B. – CHOU, S.-L. – LO, J.-I. – DAS, A. – CHENG, B.-M. – RAJASEKHAR, B. N. – BHARDWAJ, A. – SIVARAMAN, B. Mid-IR and VUV spectroscopic characterisation of thermally processed and electron irradiated CO_2 astrophysical ice analogues. In Journal of Molecular Spectroscopy, 2022, vol. 385, article no. 111599, p. 1-12.

[27] MIFSUD, D. V. – HAILEY, P. A. – HERCZKU, P. – SULIK, B. – JUHÁSZ, Z. – KOVÁCS, S. T. S. – KAŇUCHOVÁ, Z. – IOPPOLO, S. – MCCULLOUGH, R. W. – PARIPÁS, B. – MASON, N. Comparative electron irradiations of amorphous and crystalline astrophysical ice analogues. In Physical Chemistry Chemical Physics, 2022, vol. 24, no. 18, p. 10974-10984.

[28] MIFSUD, D. V. – KAŇUCHOVÁ, Z. – IOPPOLO, S. – HERCZKU, P. – TRASPAS MUIŇA, A. – SULIK, B. – RAHUL, K. K. – KOVÁCS, S. T. S. – HAILEY, P. A. – MCCULLOUGH, R. W. – MASON, N. – JUHÁSZ, Z. Ozone production in electron irradiated CO_2: O_2 ices. In Physical Chemistry Chemical Physics, 2022, vol. 24, no. 30, p. 18169-18178.

[29] MIGLIORINI, A. – KAŇUCHOVÁ, Z. – IOPPOLO, S. – BARBIERI, M. – JONES, N. C. – HOFFMANN, S. V. – STRAZZULLA, G. – TOSI, F. – PICCIONI, G. On the origin of molecular oxygen on the surface of Ganymede. In Icarus, 2022, vol. 383, article no. 115074, p. 1-11.2

[30] NESLUŠAN, L. – TOMKO, D. The impact hazard of near-Sun comets. In Monthly Notices of the Royal Astronomical Society, 2022, vol. 512, no. 3, p. 3414-3421.

3. LIFE SCIENCES

M. Musilová

Life sciences research in Slovakia, related to the space sector, is primarily performed through a non-profit organization called Michaela Musilová, o.z. The non-profit is focused on astrobiology and human space exploration research and educational activities in collaboration with multiple Slovak and international partners. The Slovak collaborating organizations include the Faculty of Electrical Engineering and Information Technology of the Slovak University of Technology in Bratislava (FEI STU) and the Comenius University. Teams from the NASA Goddard Space Flight Center, NASA Headquarters, University of Maryland, Georgetown University, University of Zurich, Honeybee Robotics and others are among the international partners of the non-profit's projects.

The Michaela Musilová, o.z.'s team's research can be subdivided into two main areas. First of all, it is concerned with studying the limits of life in extreme environments to define the possibilities of where to search for life beyond Earth for astrobiology purposes. The second area involves studying human behaviour in isolated and extreme or confined conditions with the goal of preparing humans for long duration space exploration missions.

The astrobiology-focused research projects have taken place in Hawaii, for instance, in unique lava caves on the volcano Mauna Loa. Michaela Musilová, o.z.'s lead scientist collected biochemical, microbiological and geological samples in collaboration with NASA to understand what lifeforms can survive in these cave systems and whether similar extreme lifeforms could potentially survive in the similar caves on Mars. Data suggests that lava caves most likely exist on Mars and they are considered some of the most promising places to look for Martian extra-terrestrial life. The teams have presented their results at multiple space conferences worldwide and they are currently preparing several peer-reviewed publications from the results of their research.

Michaela Musilová, o.z.'s most recent project, Astro Seven Summits, is a continuation of this research in collaboration with NASA. The project involves a series of scientific and educational expeditions to the summits of the tallest mountain on each continent (the Seven Summits), with a focus on astrobiology and climate change. In terms of astrobiology and planetary science, the Michaela Musilová, o.z. team has been collecting samples of extremophiles (extreme lifeforms), geobiochemical samples and sensor measurements to evaluate the changing environmental conditions in some of the most extreme environments on the planet.

With regards to the human space exploration research by Michaela Musilová, o.z., it is being performed during the Astro Seven Summits expeditions in collaboration with the University of Zurich, as well as at the Hawaii - Space Exploration Analog and Simulation (HI-SEAS). The HI-SEAS facility used to be directed by the aforementioned Michaela Musilová, o.z.'s lead scientist. They organized over 40 simulated missions to the Moon and Mars at HI-SEAS since 2018. They were performed in collaboration with NASA, ESA and numerous other space organizations and companies from around the world.

HI-SEAS is an analog space research facility located at 2,500 meters in elevation on the active volcano Mauna Loa, on the Big Island of Hawaii. It is used for a variety of research projects, which include astrobiology, geology, engineering, psychology, physiology, botany, education, in situ resource utilization and other experiments. The goal of the analog space missions is to field-test scientific and technological initiatives aimed to help humans return to the Moon and explore Mars one day. The missions can last from several weeks up to a whole year, depending on the research goals of the mission.

A mission involves a crew of six people living as if they were on the Moon or Mars, while performing various scientific and engineering projects. This means that they are subject to time delays when communicating with the Mission Control Centre on "Earth", they eat freeze-dried astronaut-like food and they have to survive on their own with very limited supplies of all the materials they bring with them. They are also isolated from the rest of the world, as if they were truly on another planet. Moreover, the Michaela Musilová, o.z.'s lead scientist has also brought several Slovak technologies to HI-SEAS to be tested during simulated lunar and martian missions. These include environmental sensors from the company HB Reavis and several high school student experiments.

Michaela Musilová, o.z.'s representatives regularly present about these varied research projects worldwide at multiple international conferences, including the International Astronautical Congress (IAC) run by the International Astronautical Federation (IAF), American Geophysical Union (AGU), European Geophysical Union (EGU), Europlanet Science Congress (EPSC), Lunar and Planetary Science Conference (LPSC), various NASA workshops and forums, COSPAR Scientific Assembly and others. Michaela Musilová, o.z.'s lead scientist is also a reviewer for the NASA Planetary Protection Research Program and many other grant programs and research journals in space life sciences, such as Astrobiology and the National Science Foundation. They are a Global Faculty of the International Space University as well, where they lecture and organise workshops in astrobiology, and the robotic and human exploration of the Moon and Mars.

Figure 3.1. The Astro Seven Summits project lead is performing geobiochemical sampling for astrobiology research on Aconcagua – the tallest mountain in South America. (Photo credit: Michaela Musilova).

Figure 3.2. *Michaela Musilová, o.z.'s lead scientist is examining extreme lifeforms that can survive at high elevations, in dry conditions and with a limited availability of nutrients for astrobiology research on Kilimanjaro – the tallest mountain in Africa. (Photo credit: Michaela Musilova)*

Figure 3.3. *A sensor from the Slovak company HB Reavis was used during simulated lunar and martian missions at HI-SEAS. (Photo credit: Michaela Musilova)*

References:

[1] FISHMAN, C.B. – BEVILACQUA, J. G. – HAHN, A. S. – MORGAN-LANG, C. – WAGNER, N. – GADSON, O. – McADAM, A. C. – BLEACHER, J. – ACHILLES, C. – KNUDSON, C. – MILLAN, M. M. – BOWER, D. M. – MUSILOVÁ, M. – JOHNSON, S. S. (2023) Extreme Niche Partitioning and Microbial Dark Matter in a Mauna Loa Lava Tube. Journal of Geophysical Research: Planets, 128:6, e2022JE007283, https://doi.org/10.1029/2022JE007283

[2] POUWELS, C. – NUNES, A. P. C. P. – MUSILOVÁ, M. – TOOP-ROSE, J. – POLI, E. C. – FOING, B. (2022) An Endorsement to Utilize Terrestrial Analogs as Support for the Upcoming Artemis Missions. *Proceedings of the 53rd Lunar and Planetary Science Conference,* March 7-11, 2022, The Woodlands, Texas, USA. LPI Contribution No. 2678, 2022, id.1902

[3] TACHERA, D. K. (2022) A Hydrogeochemical Examination of West HAWAIʻI's Water Cycle. University of Hawai'i at Manoa ProQuest Dissertations Publishing, 29067565

4. MATERIALS RESEARCH IN SPACE

M. Gebura, N. Beronská, E. Hodúlová, T. Dvorák, L. Karaffa

Since its last project concluded in 2018, the "Novel magnesium composites for ultralight structural components (MagUltra)," the ***Institute of Materials and Machine Mechanics of the Slovak Academy of Sciences (IMSAS)*** has embarked on a visionary path within the space sector. The MagUltra project, a cornerstone in materials science, paved the way for groundbreaking advancements in lightweight materials, producing one of the world's lightest construction materials. This magnesium-fibre-reinforced composite, enhanced through the addition of alloying elements such as Zr, Cr, Ti, and Y, achieved strengths above 600 MPa and a Young's modulus above 300 GPa, at a density of 1.8 g.cm^{-3}. The innovation lies not just in the exceptional strength and stiffness-to-weight ratio but also in its machinability, damping properties, thermal conductivity, and dimensional stability, marking a significant leap towards reducing fuel costs and rocket exhaust gases in aerospace missions.

In 2022, IMSAS embarked on a **transformative journey towards the emergent domains of in-orbit servicing, manufacturing, and recycling, aligning with the European Space Agency's (ESA) vision for a sustainable circular economy in space by 2050.** This strategic redirection underscores the institute's commitment to pioneering the next frontier of space technology, emphasizing the critical role of collaboration in achieving these ambitious goals. A pivotal partnership was forged with Space scAvengers, a dynamic Slovak-based startup. This collaboration is emblematic of a shared vision for a sustainable cyclic economy in space, leveraging advanced multi-agent systems. Space scAvengers brings to the table their expertise in Guidance, Navigation, and Control (GNC) technologies, including the development of sophisticated simulation software. This software is essential for the training of GNC systems, designed to manage complex missions that necessitate precise contact and account for various energetic interactions between spacecraft. This collaboration sets the stage for groundbreaking advancements in autonomous space operations. Additionally, IMSAS has partnered with Telespazio, a company boasting over 40 years of experience in satellite operations for ESA and various governmental entities. Telespazio's evolving focus towards managing complex missions, especially those utilizing the technologies currently under development at IMSAS, enriches the institute's ventures into space. This collaboration ensures that the innovative solutions emerging from IMSAS are seamlessly integrated into practical applications, setting new standards for mission complexity and execution in the space sector. The collaboration landscape is further enriched by the inclusion of First Welding Company, a Slovakian entity with several years of experience in the development of power electronics and electron beam devices for the nuclear industry. This partnership plays a critical role in the advancement of IMSAS's welding and electron beam technologies, bringing invaluable expertise and capabilities to the institute's projects. First Welding Company's contributions are pivotal in enhancing the institute's research and development efforts, particularly in the context of space manufacturing and assembly technologies.

Through these strategic collaborations, **IMSAS is poised to lead the way in developing the next generation of space technologies.** By harnessing the synergies between advanced GNC systems, satellite operations expertise, and cutting-edge welding and electron beam technologies, the institute is actively contributing to the realization of a sustainable circular economy in space. The partnerships with Space scAvengers, Telespazio, and First Welding Company underscore a collective commitment to innovation, sustainability, and the advancement of space technology. This collaborative approach promises to revolutionize the way we approach in-orbit servicing, manufacturing, and recycling for future space missions.

Leveraging its rich legacy in materials science and mechanical engineering, IMSAS is now pioneering research tailored for the unique challenges of low gravity and vacuum environments. This strategic direction underscores the institute's commitment to pushing the boundaries of space research, focusing on the development of materials and mechanical systems that can withstand the rigours of space, enabling more sustainable and efficient exploration and utilisation of space resources.

Currently, IMSAS is spearheading the ESA contract 4000141916/23/NL/MH/rp project, titled "**Feasibility Study of Contact Capacitor Discharge Welding Gear for In-orbit and Lunar Applications.**" This project embodies the institute's commitment to addressing the technical challenges of space manufacturing and assembly, providing innovative solutions for in-orbit construction and repair. This project has seen considerable progress toward its milestones, thanks to the collaborative efforts of IMSAS, Space scAvengers, and First Welding Company. The project has successfully established system concepts and technical requirements for CCDS Welding technology applications in space, developing conceptual models for critical technologies like the Capacitor Bank System, Welding End-Effector, and Welding Stud.

As we approach the Milestone 1 (Requirements and Concept Review, scheduled at March 2024) sub-contracted at Space scAvengers, this report provides an updated overview of our project's progress in developing welding technologies for space applications. The preliminary welding trials have laid a solid foundation for the innovative approaches to welding both conductive and non-conductive surfaces in space.

This report outlines the progress of developing a laboratory model designed to advance the research and application of Contact Capacitor Discharge Stud Welding (CCDSW), particularly in space environments. The model integrates with an existing vacuum chamber to accurately simulate space-like conditions, facilitating comprehensive tests on CCDSW processes.

Laboratory Model Concept

The laboratory model incorporates a **Dual Pulse Capacitor Bank System**, comprising Low Voltage (LV) and High Voltage (HV) modules. This system is engineered to store and discharge energy precisely, accommodating both tip ignition and short-cycle drawn arc welding processes. The versatility of this system allows for a wide range of welding scenarios, ensuring the model's applicability to diverse research objectives.

The **Welding End-Effector** is conceptualized with precision alignment and controlled impact force, capable of adapting to various stud types. A notable feature is its ability to direct welding fumes towards non-conductive layers, aiding in their removal and enhancing the welding efficiency. This innovative approach leverages the natural by-products of the welding process to streamline operations.

A **composite (hybrid) stud** has been proposed, optimized for penetrating non-conductive layers. It features an extended, sharpened tip coated with a hard, electrically conductive material, without altering the stud's base material. This hybrid stud amalgamates the benefits of both tip ignition and short-cycle drawn arc methods, offering improved performance across a range of welding scenarios.

The laboratory model is conceptualized to be seamlessly integrated with the existing vacuum chamber to emulate the vacuum conditions of space. The model supports a variety of tests, including welding on metallic surfaces with and without non-conductive layers, using commercial studs and the optimized hybrid stud. It facilitates the evaluation of different stud geometries and welding processes, providing insights into joint quality, penetration efficiency, and the feasibility of using welding fumes to remove non-conductive layers.

Preliminary tests have **demonstrated the feasibility of achieving effective welds through non-conductive layers using both conventional studs.** These findings underscore the potential of the laboratory model to significantly contribute to the field of space welding technology. Ongoing studies will focus on refining stud designs and welding parameters to enhance performance further.

Figure 4.1. This figure illustrates AlMg3 threaded studs joined to an aluminium alloy workpiece with an anodized surface on the left, and a polyimide (Kapton) surface on the right. The surface was pre-penetrated by the impact of a 100 N central hole puncher, simulating the novel impact welding procedure.
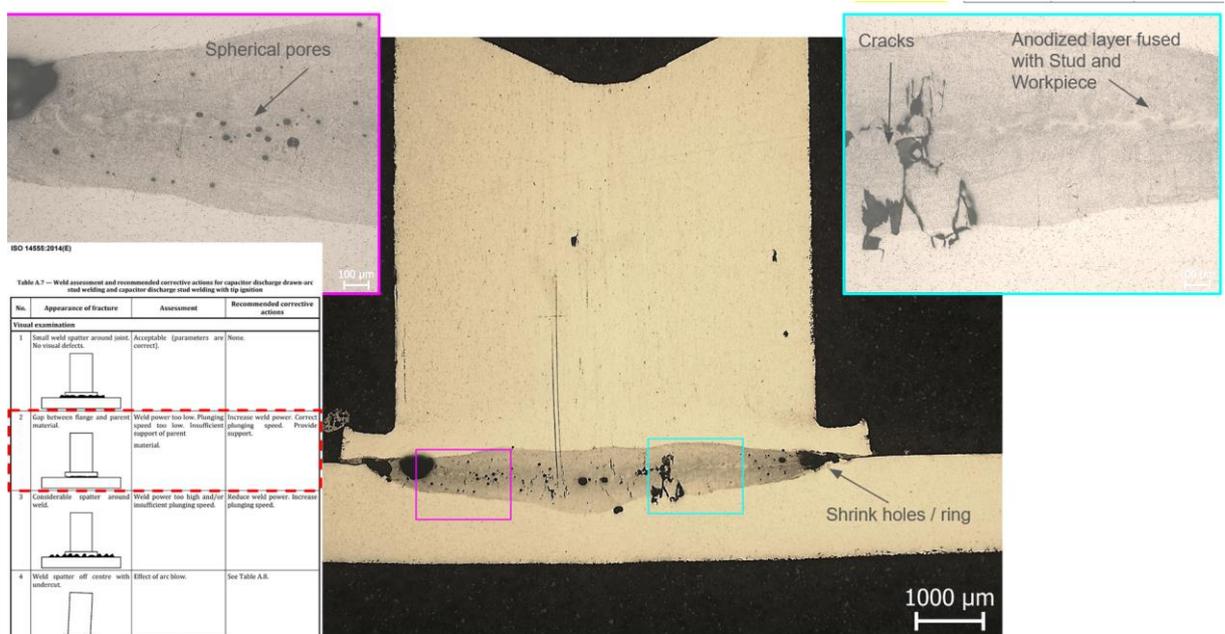
Figure 4.2. Cross section and details on microstructure of the welded COTS stud on the aluminium alloy sheet with anodized surface (from preliminary welding trials focusing on feasibility of the proposed solutions).

The development of the laboratory model represents a significant step forward in the study and application of CCDS welding techniques for space applications. The integration of the model with an existing vacuum chamber and the initial testing results highlight the project's success in simulating space-like conditions and studying welding processes. Future phases will concentrate on optimizing the model based on initial findings, with the ultimate goal of enhancing the reliability and efficiency of welding technologies for space exploration and construction.

As the project moves towards Milestone 2, the Design Review, and eventually to the Final Milestone, the assessment and analysis of the CCDS Welding procedure in a vacuum chamber will be crucial. The achievements so far signify a major step forward in the feasibility study of CCDS Welding Gear for space applications, overcoming significant technical challenges and setting the stage for a new era of in-orbit and lunar manufacturing and assembly technologies.

Additionally, the institute has showcased its forward-thinking approach by proposing a novel solution for space debris management on the ESA OSIP platform. This proposal, **focusing on the utilization of Electron Beam Technology to process space debris into manageable pieces for recycling**, underscores IMSAS's dedication to environmental sustainability in space operations.

As IMSAS looks towards the next two years, the institute is poised to actively develop and refine these technologies, both in the realms of materials and metallurgy and machine mechanics. The aim is not only to advance the state of the art in technology but also to contribute significantly to the sustainability and efficiency of future space missions. Through its pioneering research and collaborative projects, **IMSAS is setting the stage for innovative solutions that will enable the exploration, development, and maintenance of space infrastructure, reflecting a profound commitment to the advancement of the space industry and the sustainability of space activities.**

5. REMOTE SENSING

I. Barka, T. Bucha, J. Feranec, Z. Fulmeková, M. Gallay, T. Goga, A. Halabuk,
J. Hofierka, M. Kopecká, J. Nováček, K. Onačillová, Š. Opravil, R. Pazúr,
M. Rusnák, I. Sačkov, M. Sedliak, M. Sviček, D. Szatmári, A. Zverková

Selected activities of five institutions are included in this report (2022-2023):

Institute of Geography, Slovak Academy of Sciences in Bratislava

Methodical approach to identifying illegal activities in landscape through land cover changes

The result was obtained within the solution of the ESA RPA project: ***Land Cover Change Monitoring for Identification of Potential Illegal Activities in Slovakia (LAPIA)***, No. 4000141176/23/NL/SC/rp (2023-2024): Institute of Geography, Slovak Academy of Sciences, Bratislava (prime contractor); National Agricultural and Food Centre, Soil Science and Conservation Research Institute, Bratislava; Slovak University of Technology, Faculty of Civil Engineering, Department of Theoretical Geodesy and Geoinformatics, Bratislava (subcontractors)

In the first phase of the project, attention was paid to defining illegal human activities in the landscape, such as illegal operation on closed and rehabilitated dump sites, illegal ploughing of protected meadows, and illegal cutting of non-forest woody vegetation in agricultural landscapes (especially those with the highest degree of protection), as well as to testing the identification of land cover (LC) changes (Fig. 5.1) caused by these activities based on remote sensing data. To identify potential illegal activities, values of the NDVI vegetation index were tested on the PlanetScope optical satellite imagery with 3 m spatial resolution on six experimental sites selected in cooperation with the Slovak Environmental Inspectorate (SIŽP). The results of the analysis confirmed that in the case of areas disturbed by illegal activities
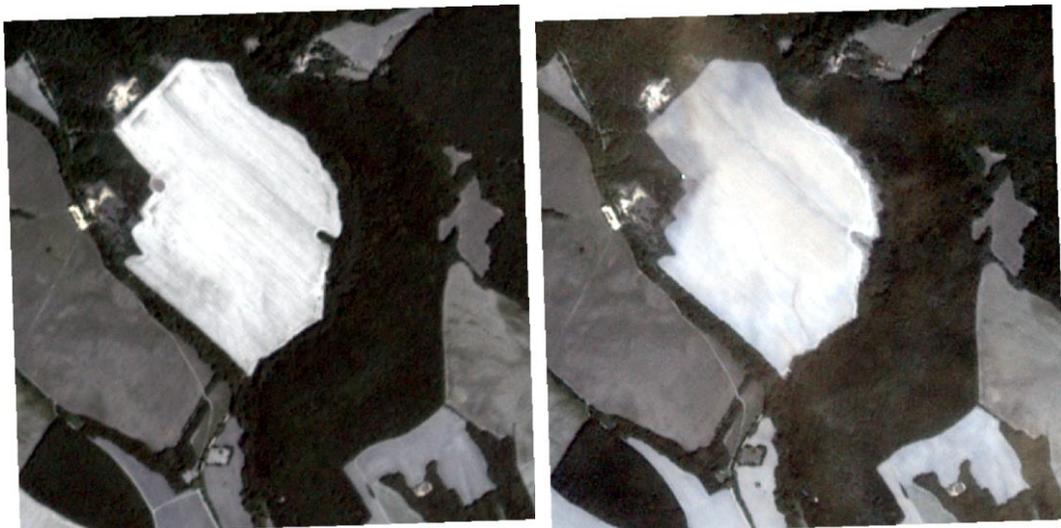
Figure 5.1. *Land cover change (removal of woody non-forest vegetation) in the experimental area Naháč between 20 July 2017 (left) and 24 August 2017 (right) on a PlanetScope satellite imagery. Source: Planet Team (2022). Planet Application Program Interface: In Space for Life on Earth. San Francisco, CA.* https://api.planet.com

related to the removal of aboveground biomass, the value of the NDVI index is significantly lower than its value in the vicinity of these areas, thus confirming their identifiability on PlanetScope optical images. Illegal activities were also analysed using changes in intensity and coherence on Sentinel-1 radar images (Synthetic Aperture Radar – SAR). The analysis of these data confirmed that using radar imagery with greater spatial resolution than the 10 m provided by Sentinel-1 to identify LC changes caused by illegal activities is necessary.

***Figure 5.2.** One day of Low cloud cover data over Europe, with NOWCASTSAT grid in orange color. The data provided are ERA5 hourly data scenes on single levels downloaded from the Climate Data Store. These data consist of 17544 hourly observations from the low cloud cover and medium cloud cover scenes, for the years 2020 and 2021 at a spatial resolution of 0.25° x 0.25°, stored in NetCDF format.*

Solar energy forecasting is one of the key drivers of growth and improved integration of photovoltaics into energy grids. Short term forecasting (also called nowcasting) is used for the edition of solar power generation in a time horizon of a few minutes to 3-4 hours ahead. This project aims at improving the existing solar radiation nowcast solution operated by Solargis by the development of more accurate cloud motion vectors algorithms by (i) implementing additional data inputs (more spectral channels and data from numerical weather models), (ii) increasing spatial and temporal resolutions, and (iii) integrating a priori geographical data describing effects of geographical barriers.

Project: ***G4B – Grasslands for biodiversity: supporting the protection of the biodiversity-rich grasslands and related management practices in the Alps and Carpathians.*** Part of the Biodiversa+ project scheme (funded by the European Commission) supporting excellent research in the field of biodiversity.

The G4B project aims to assess the richness of mountain grasslands across Europe, specifically in the Alps and the Carpathians, identifying natural conditions and management activities affecting their biodiversity. The project focuses on understanding local and regional grassland biodiversity drivers, utilizing location-specific information on management regimes, stakeholder interactions, collecting in-situ samples, involvement of stakeholders and acquisition of multitemporal remote sensing (RS) data, especially satellite and aerial images, maps, information about climate, soil and terrain. Given the significant increase in data availability, the project aims to explore the possibilities of identifying biodiversity-rich grasslands and their management regimes using RS data and model grassland management systems, including mowing, fertilization, grazing, silage and hay production.
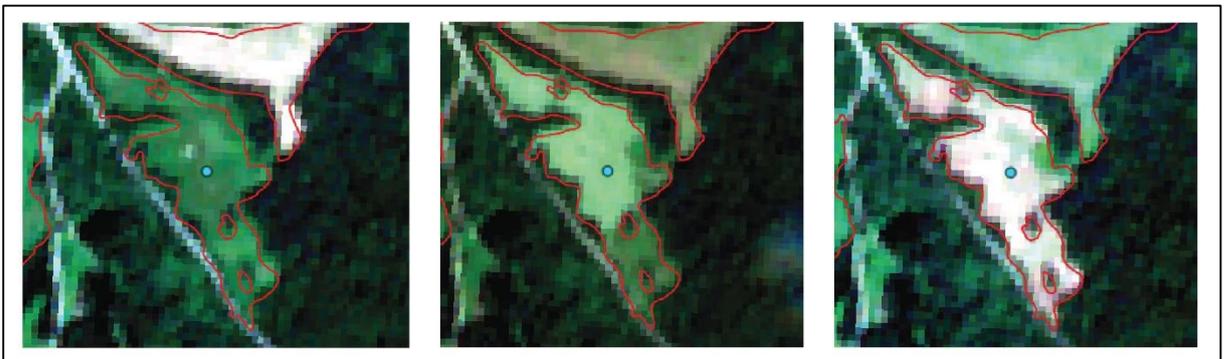
Figure 5.3. An example of mowing based on Sentinel-2 images.
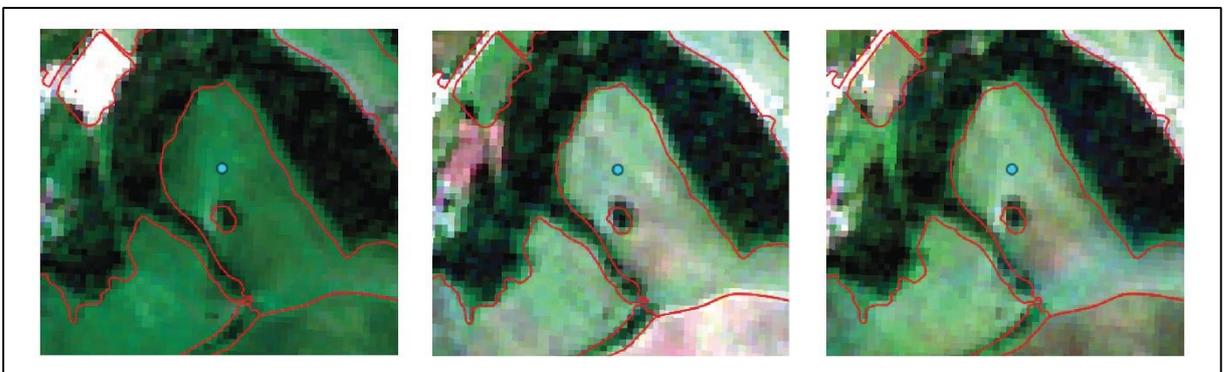
Figure 5.4. An example of grazing based on Sentinel-2 images.

Institute of Geography, Faculty of Science, Pavol Jozef Šafárik University in Košice

Project: *ENEUM: Enhancing Earth Observation Curriculum with a Focus on ESA Sensors (4000140187/23/NL/SC/rp)*

The ENEUM is an 18-month educational project (2023-24) funded by ESA focusing on Bachelor level and Master level university students of Geography and Geoinformatics. The aim was to develop and introduce two new university courses: "Earth Observation Applications" and "Applied Radar Remote Sensing," to improve students' knowledge and skills in Earth Observation (EO) and its applications promoting awareness of ESA activities in Slovakia.

The first course included lectures on the evolution of EO missions, access to ESA EO data, principles of remote sensing, and practical applications in fields like agriculture, deforestation, wildfire mapping, air quality, and marine studies. Practical sessions complement the lectures, offering hands-on experience with ESA EO data, including data processing and analysis using software tools like SNAP, demonstrating real-world applications of EO data in environmental monitoring and management. The second course delves into the basics of radar remote sensing and ESA SAR space missions, SAR applications in land, forestry, agriculture, and disaster management including floods, fires, and earthquakes. Practical complement lectures by providing hands-on experience with ESA EO data, utilizing software like SNAP for data processing and analysis across various applications like land cover mapping, precision agriculture, and post-disaster assessment. The project provided an opportunity for inviting 5 guest lecturers for University in Cagliari, University in Wroclaw, and from Slovak Technical University in Bratislava emphasizing the importance of international collaboration and EO in various fields such as disaster management and environmental monitoring.

For a detailed overview, visit the project's website: https://www.uge.science.upjs.sk/esa-eneum?lang=en
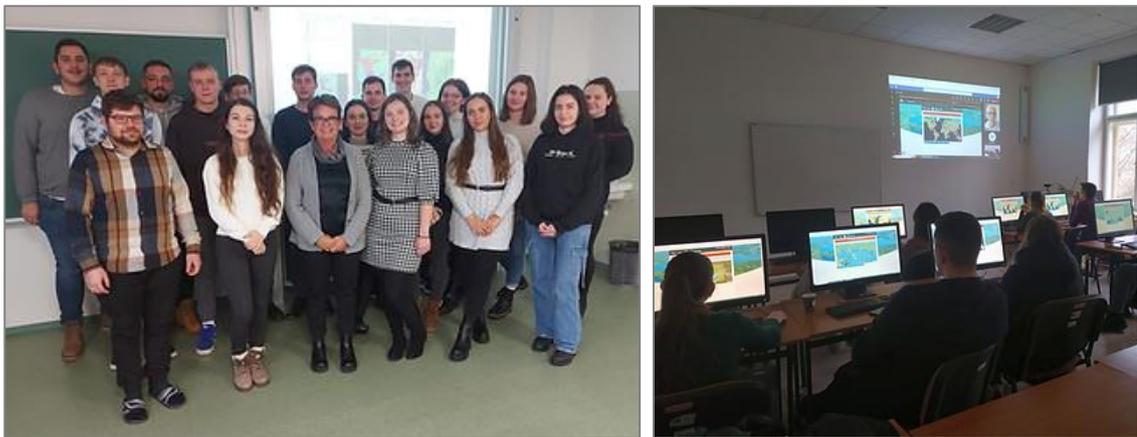
Figure 5.5. Our students of Applications of ESA sensors course with the invited lecturer prof. Maria Teresa Melis, University of Cagliari (left). Practical teaching of professor Tomasz Niedzielsky and Michal Halicky on Sentinel 3 application for river level monitoring with Sentinel 3 (right).

Events: International Remote Sensing Summer School, Experiencing Remote Sensing on Sardinia inland site: Advanced summer school on instruments and methodology for a CAL/VAL site for Optical data, 17-21 July, 2023, San Vero Milis, Italy

Four academic staff members of our institute demonstrated and taught laser scanning and hyperspectral mapping with unpiloted aerial systems (UAS) during the summer school in Sardinia. The dry bed of a unique salt lake became the main object of hand-on training and research between 15 – 20 July 2023 aim of which was the mutual sharing of knowledge and skills in the processing of hyperspectral and lidar data from ground, aerial, and satellite measurements for the purposes calibration and validation of hyperspectral satellite data. The event was organized by the Department of Chemical and Geological Sciences of the University of Cagliari and other institutions also participated: Italian National Institute of Geophysics and Volcanology (INGV), the Italian Association for Remote Sensing of the Earth (AIT) and the Italian Space Agency (ASI). Over the course of five days, 30 doctoral students from around the globe engaged in data collection under challenging conditions, amassing over 300 GB of geospatial data. This intense workshop not only provided practical experience in environmental monitoring using cutting-edge EO technologies but also showcased the collaborative effort in pushing the boundaries of remote sensing education.

For further details, you can visit the UPJŠ website. https://www.upjs.sk/prirodovedecka-fakulta/en/actual-news/odbornici-z-ustavu-geografie-ucili-mapovat-za-pomocou-bezpilotnych-leteckych-systemov-v-letnej-skole-international-remote-sensing-summer-school-na-sardinii/
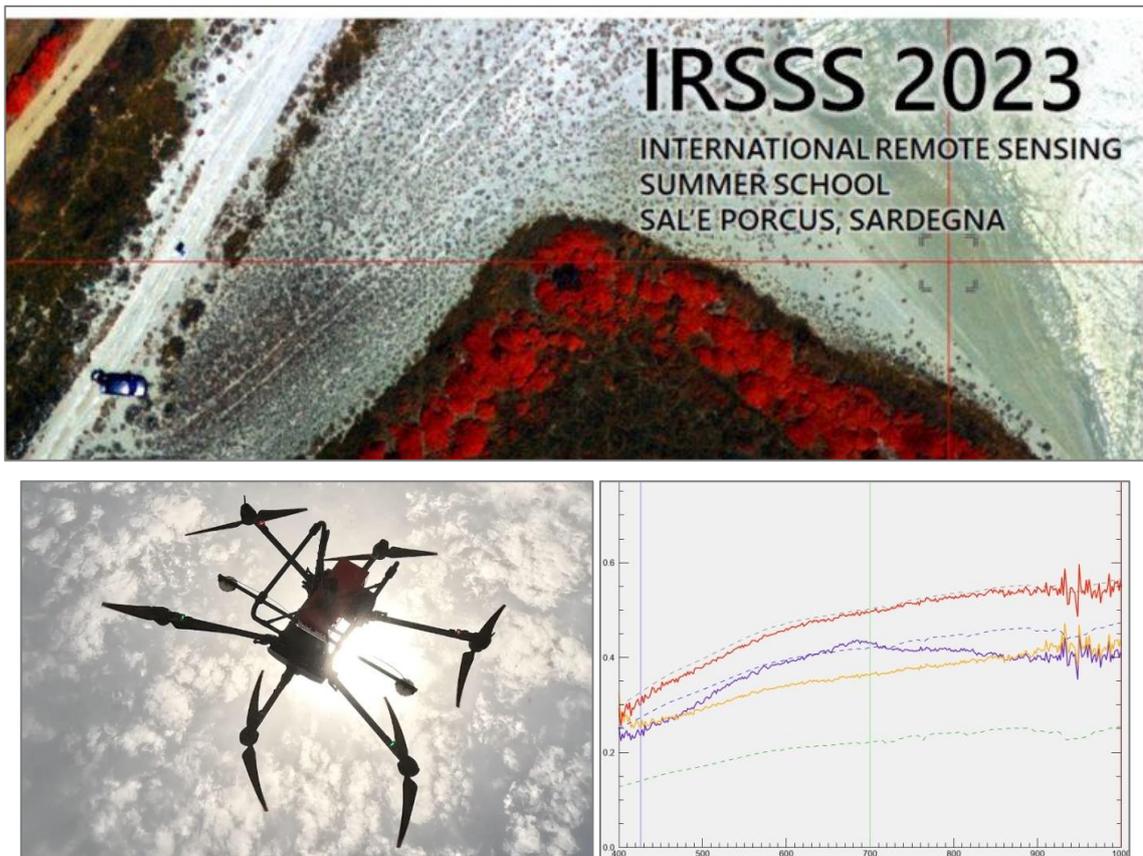
Figure 5.6. False-colour composite of the Sale'e Porcus salt lake hyperspectral data acquired during the IRSSS 2023 by our UAS system and its profile of spectral reflectance (bottom images).

National Forest Centre Zvolen

Remote Sensing activities of the National Forest Centre in Zvolen were aimed at two basic topics:
- Satellite-based observation of forest ecosystem's response to global environmental changes,
- Research of the applications of airborne laser scanner technology in the forest management.

1) Satellite-based observation of forest decline – STALES web service.

The operational activities are ongoing in a continuous manner. Recently, satellite data and layers of forest damage classification from both 2022 and 2023 have been integrated into the STALES web service, accessible at https://www.nlcsk.org/stales/. This system is designed to provide timely information to forest owners and the forest state administration, offering insights into the current condition of forest stands and any observable changes.

To establish a comprehensive historical perspective, individual satellite images spanning from 1990, 1996, 1998, 2000, 2003, and 2006-2023 have been meticulously combined into a nationwide mosaic. This mosaic serves as the foundation for assessing forest damage throughout these years. The services primarily utilize Landsat satellite images with a spatial resolution of 30×30 meters and Sentinel data with a resolution of 10×10 meters since 2016. Mosaics are crafted by blending Landsat (Sentinel) bands in false colours, specifically Near-infrared, Mid-infrared, and Red bands.

Mapping applications have been developed to showcase forest district boundaries at a scale of 1:100,000 and forest compartment boundaries at a scale of 1:20,000. The STALES service encompasses four distinct map applications:
1. Map Application 1 (currently not updated) – offering visualization of satellite scenes and forest health condition.
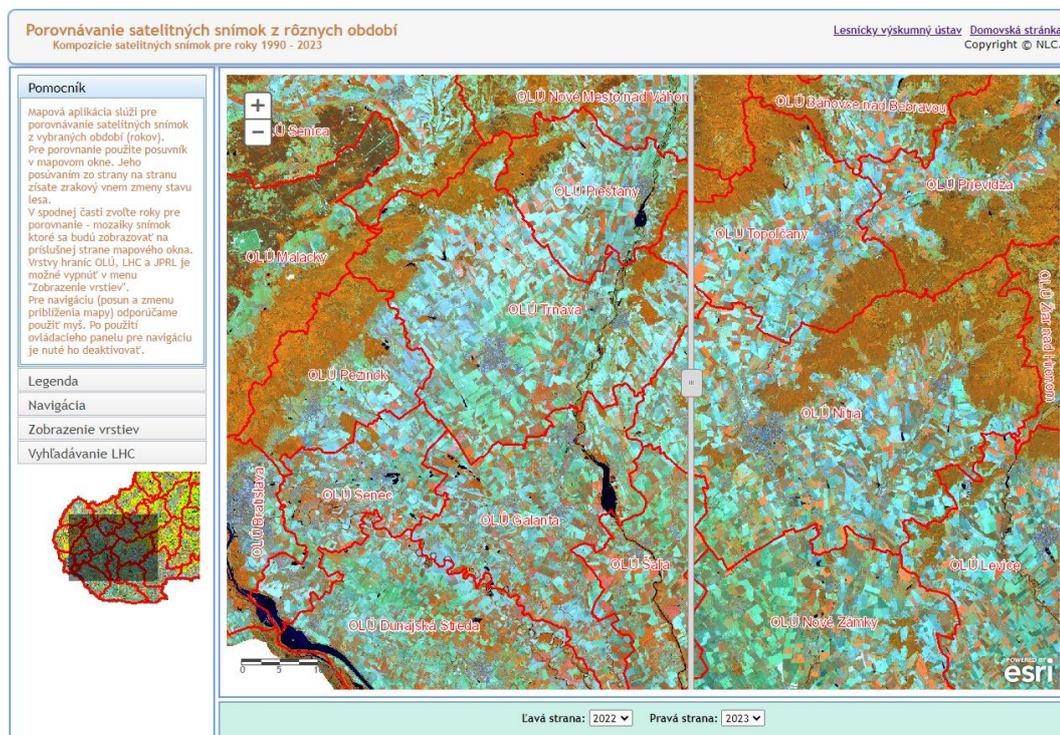
Figure 5.7. Web service www.nlcsk.sk/stales/stales_swipe_tool.html – *map application for comparison of satellite scenes from two different years according to selection.*

2. Map Application 2 – facilitating the comparison of satellite scenes from two different periods (Fig. 5.7).
3. Map Application 3 – providing dynamic visualization of both current and historical satellite scenes.
4. Map Application 4 – presenting dynamic visualization of forest health condition (Fig. 5.8).
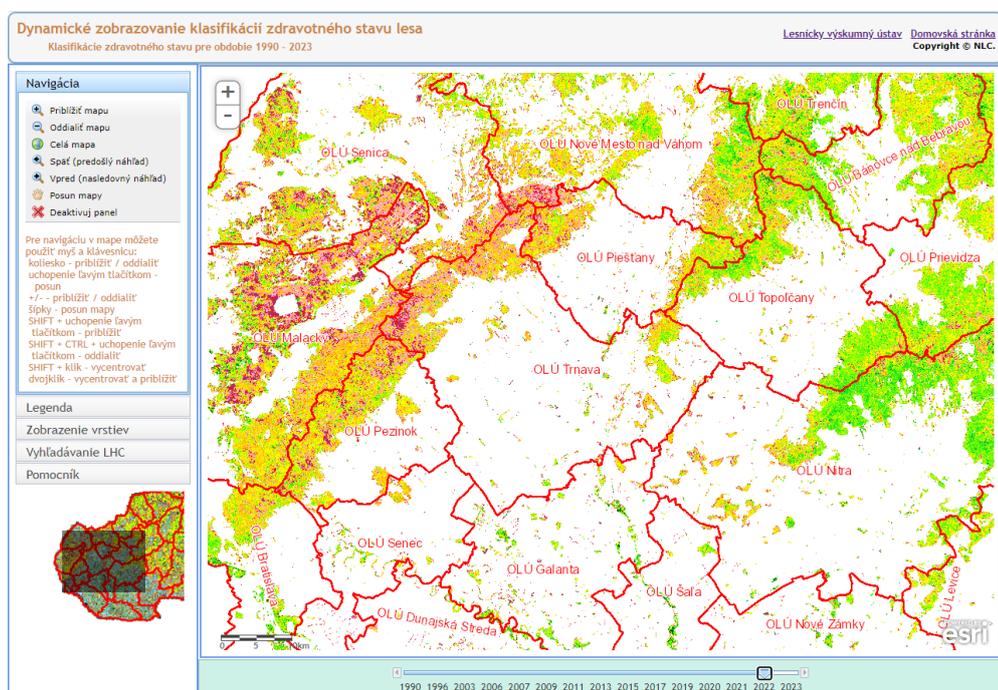
Figure 5.8. *Web service* www.nlcsk.sk/stales/klasdynam.html *– map application for dynamic visualization of forest health condition from 1990 to 2023.*

2) **Satellite-based observation of the effects of drought on the forests health condition in 2022**

An extensive discolouration (yellowing, browning) and leaf fall were noticed in Slovak forests in the summer of 2022 (Fig. 5.9). This phenomenon was related to the lack of atmospheric precipitation in combination with extremely high air temperatures in July and early August. The classification of Sentinel-2 satellite images confirmed the deterioration of forest health. The share of heavily damaged stands with defoliation above 50% doubled compared to the previous years and reached 19.3% (417,000 ha). By comparing two classifications of the forest condition, namely from the years without (2020) and with the occurrence of drought (2022), we found an increase in defoliation by 30% or more on 223 thousand hectares (Fig. 5.10). After deducting harvesting, the estimated area of drought-damaged stands is approximately 193,000 ha. Damage was spatially localised unevenly. The most influenced were regions of the west and south part of the middle and partly south part of eastern Slovakia. The most damaged were forest stands on SW exposures.

44
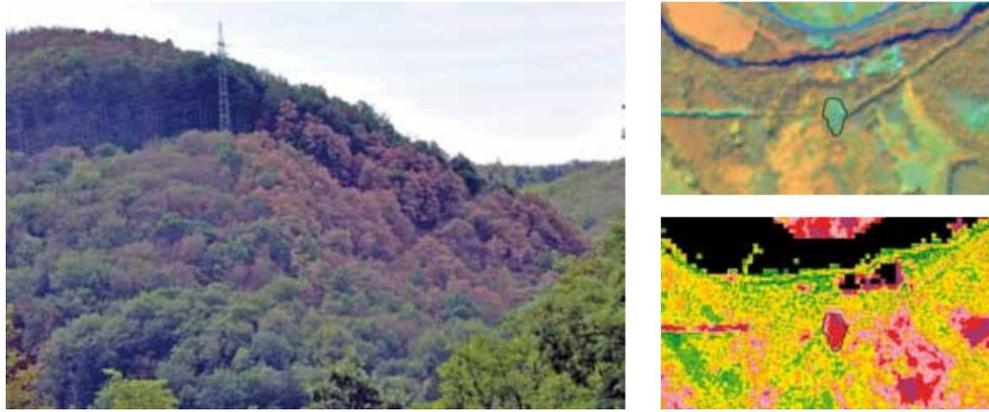
Figure 5.9. *Left: Significant summer browning of leaves due to drought and high air temperatures. Forest district: Zvolen, Forest compartment: 1199a (photo by T. Bucha, August 7, 2022). Top-right: The area of interest from the photo on the Sentinel-2 image in false-colour composition, bands 8-11-4. Turquoise colour indicates damaged forest. The heavily damaged part is bounded by the polygon. Bottom-right: Resulting damage classification. Shades of red colour indicate heavily damaged stands.*
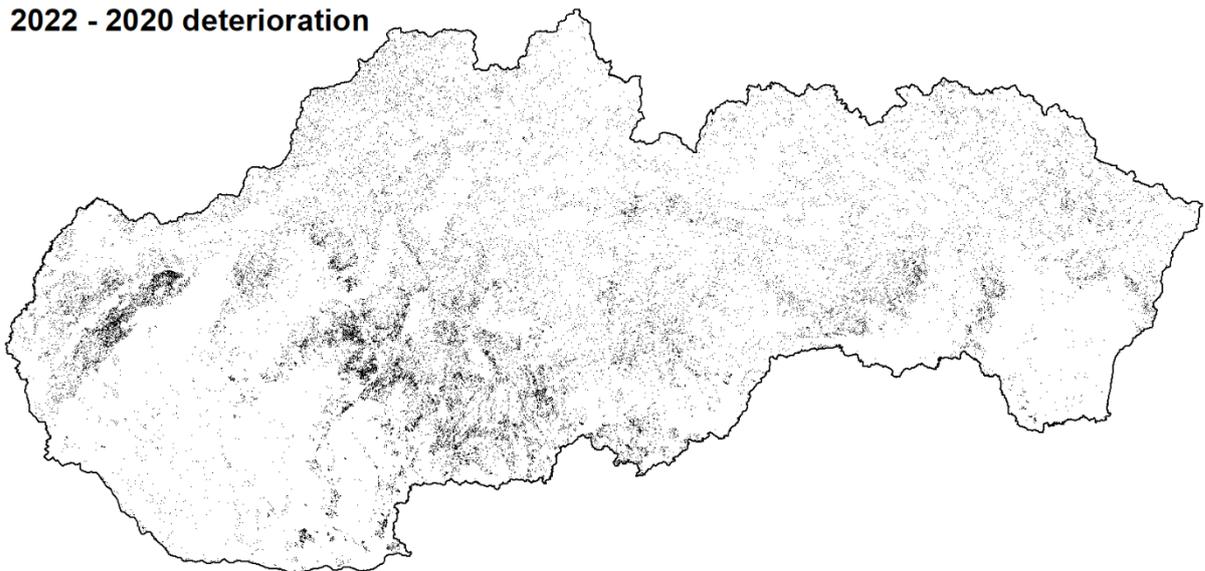
Figure 5.10. *Increase of defoliation higher than 30% between the 2020 and 2022 years. Clusters of pixels indicate drought damage in the year 2022. Scattered individual pixels indicate harvesting carried out between 2020 and 2022.*

3) **Satellite-based observation of forest phenology**

The research concentrated on (i) validation of satellite metrics from Moderate Resolution Imaging Spectroradiometer (MODIS) using ground-based observations and (ii) deriving the trends and identifying driving forces of spring phenology of oak and beech stands in the Western Carpathians from MODIS.

The first study focuses on the validation of the leaf unfolding (LU) onset of oak stands in the Western Carpathians in 2000–2021 derived from MODIS satellite data. LU onset was derived from the annual trajectories of the Normalised Difference Vegetation Index (NDVI) fitted with a double sigmoid logistic function. The satellite metric Growing speed day (GSD) corresponding to the LU onset is represented by the first derivative of the sigmoid function.

45

Ground-based observations from 22 phenological stations of the Slovak Hydrometeorological Institute (SHMI) were used to validate the date of GSD. The results showed a good agreement between the medians of ground- and satellite-based LU onset dates (Fig. 5.11a). In addition to the median, the LU onset at the 5th and 95th percentiles were compared. For both percentiles, we found differences in the onset from MODIS and SHMI. The 5th percentile of the LU onset derived from MODIS was determined later than the one from SHMI data (Fig. 5.11b). With the 95th percentile, it was the opposite (Fig. 5.11c). As a result, the range determining the duration of LU onset from MODIS was significantly shorter than from SHMI observations (Fig. 5.12). The second study focused on trends and driving forces of the LU onset of oak and beech forests in the Slovak Carpathians along elevational gradients in the period 2000-2021. Particular attention was paid to improving the modelling of the LU onset using the MOD/MYD09 MODIS products. The LU onset was derived from the annual NDVI trajectories fitted with a double logistic function. An improved estimate of the onset was obtained by calculating 6 parameters
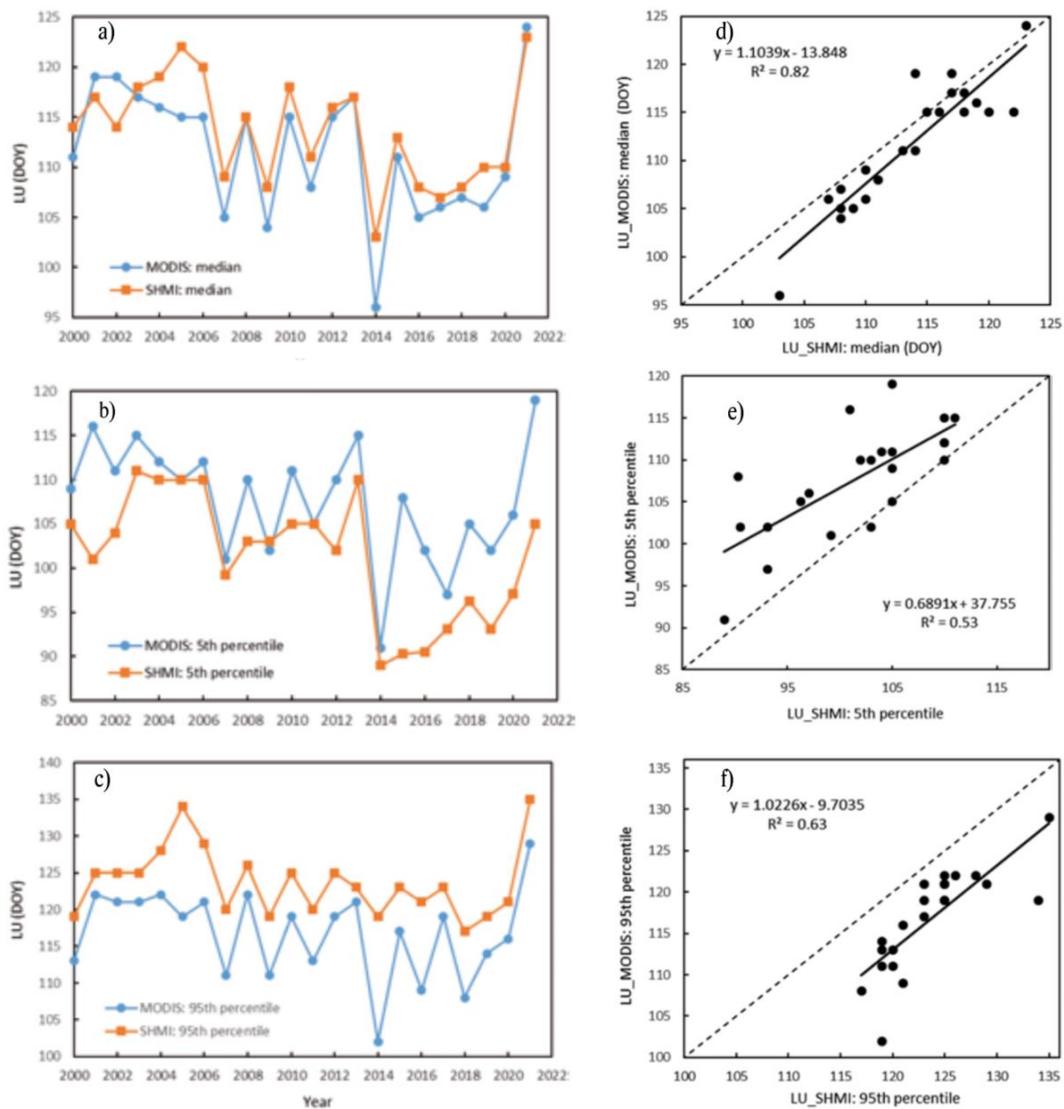
Figure 5.11. *Left: Comparison of the leaf unfolding onset from SHMI and MODIS observations for the period 2000–2021: a) median, b) 5th percentile, c) 95th percentile. X–axis: year; Y–axis: Day of the year (DOY). Right: Dependence between the leaf unfolding onset from SHMI and MODIS observations for d) median, e) 5th percentile, f) 95th percentile. X– and Y–axes: Day of the year (DOY). The dashed line corresponds to the line y = x.*

of the logistic function and by comparing with the LU onset from phenological field observations. Between 2000 and 2021, we found a trend towards an earlier LU onset at the national level by ~0.39 day.year^{-1} for oak stands (p = 0.13) and ~0.08 day.year^{-1} for beech stands (p = 0.48) – see Fig. 5.13.
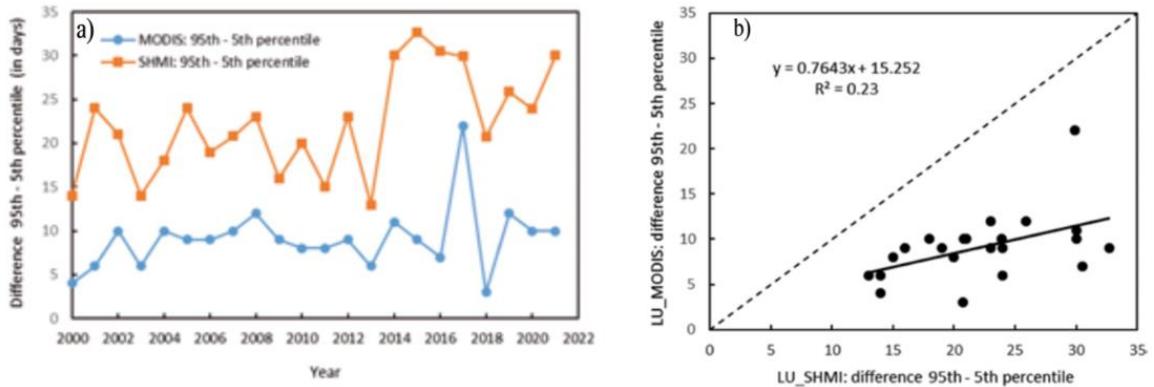
Figure 5.12. Course (a) and dependence (b) between the duration of the LU onset on 22 SHMI phenological stations and 413 MODIS pixels. Duration is expressed in days and is calculated as the difference between the 95th and 5th percentiles for each year of the period 2000–2021.
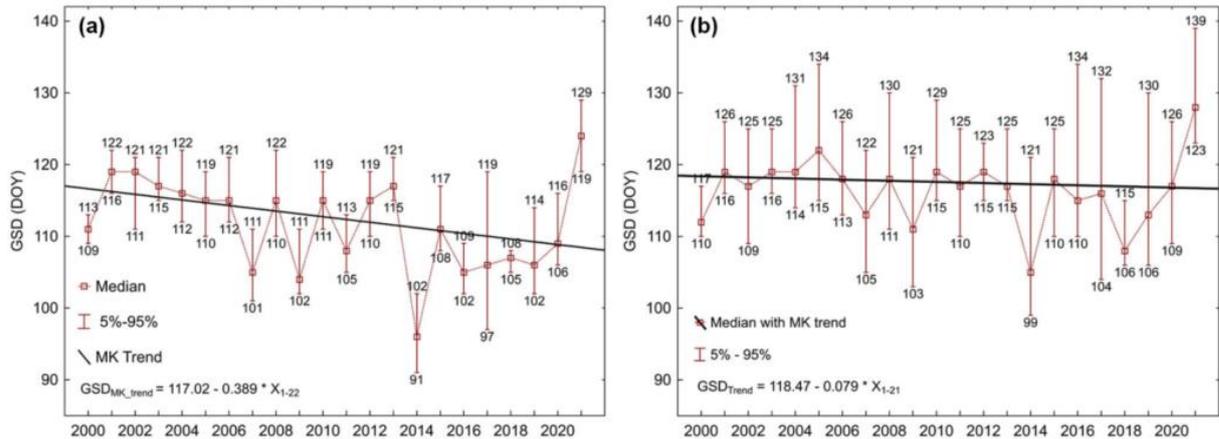
Figure 5.13. Onset of leaf unfolding (median of GSD), its duration (5th and 95th percentiles) and Mann-Kendall trend of GSD for (a) oak and (b) beech stands on the whole territory of Slovakia. (X-axis): year; (Yaxis): day of the year (DOY).

The analysis of trends in three elevation zones showed a difference in the LU onset of oak and beech stands as a function of elevation (Fig. 5.14).

For oak in 100-350 and 350-500 m a.s.l. zones was found a shift towards an earlier onset by ~0.41 day.year^{-1} (p = 0.12). This corresponds to a shift of 8.6 days for the entire observation period 2000-2021. In the elevation zone above 500 m, the trend was milder, ~0.27 day.year^{-1} (p = 0.21), i.e. 5.6 days for the entire analysed period. The shift towards an earlier onset at lower elevations and a later onset at higher elevations for beech was not statistically significant, with p-values between 0.44 and 0.51. The atypical year 2021, with the latest onset of LU during the entire observation period, fundamentally affected the significance of all trends. Nevertheless, the pixel-level analysis revealed a significant trend towards an earlier LU onset (p < 0.05) in 20.3% of oak stands. The same result was found only in 0.8% of beech stands.

Strong negative correlations with R^2 = 0.72 for oak and R^2 = 0.81 for beech (p < 0.001) were found between the LU onset and March and April temperature deviations from the long-term normal (Fig. 5.15). Temperature changes are the main driving force affecting the LU onset in the studied region.
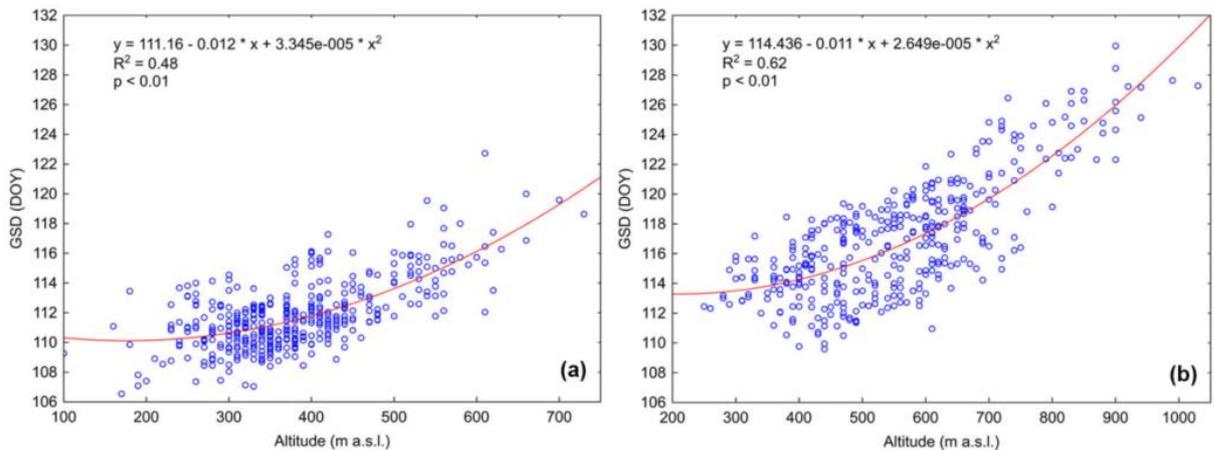
Figure 5.14. *Correlation between elevation and onset of leaf unfolding (GSD) for (a) oak and (b) beech.*
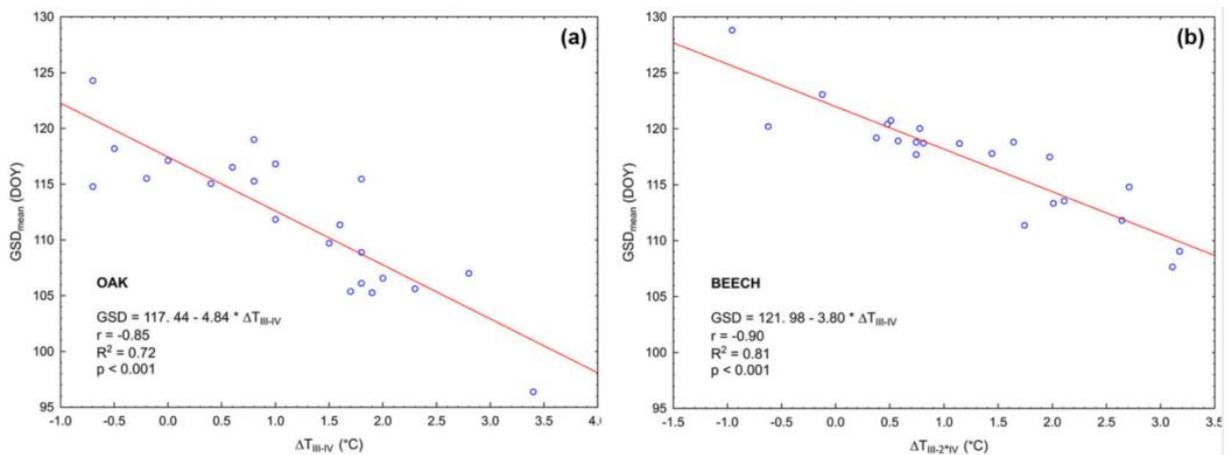
Figure 5.15. *Relationship between air temperature deviation and the GSD for (a) oak and (b) beech. X-axis: ΔT_{III-IV} (°C) – arithmetic mean of air temperature deviations of March and April in 2000-2021 from the long-term normal 1961-1990; Y-axis: $GSD_{mean}(DOY)$ - day of year of LU onset calculated as arithmetic mean of all pixels for each year from 2000-2021.*

4) **Airborne LiDAR-based forest inventory**

Airborne Laser Scanning (ALS) also known as LiDAR has emerged as a remote sensing technology capable of providing data suitable for deriving all types of elevation models. A Canopy Height Model (CHM) derived from ALS data, which represents absolute height of objects above the ground in meters, is the one most commonly used within the forest inventory. Since 2014, National Forest Centre provides every year the CHM for 10% area of Slovakia.

In this context, in 2022-2023, several scientific studies were carried out in order to assess the performance of forest inventory using the CHM. These studies were primarily focused on assessment of accuracy and applicability of freely available data and software. Moreover, related study area included a comprehensive forest unit with an area of 17,583 ha (Fig. 5.16).

48
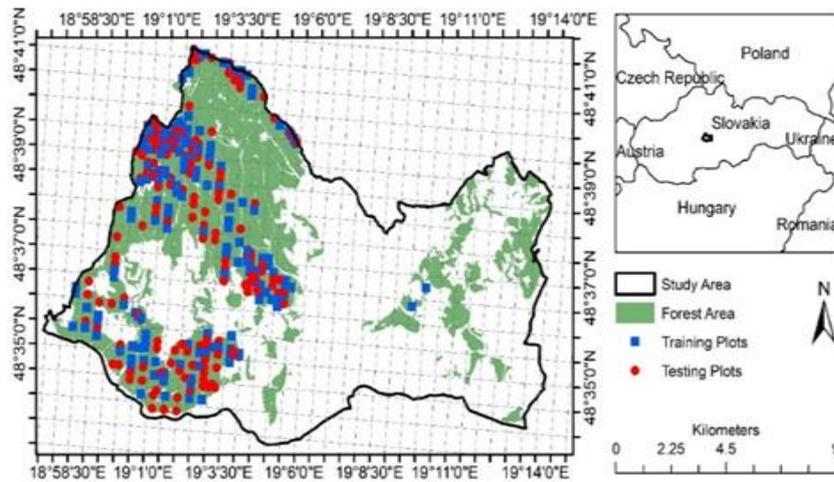
Figure 5.16. *The scientific studies were conducted in the territory of the forest management unit University Forest Enterprise of the Technical University in Zvolen located in central Slovakia (approx. 48°37′N, 19°05′E).*

ALS data acquisition was performed in June 2021 over the entire study area. This area was scanned using a Leica ALS 70 CM scanner. The CHM of 0.5 m resolution was processed with vertical accuracy of ±0.2 m. Ground data were obtained during the leaf-on season in 2021 within 180 training plots and 180 testing plots (11.25 ha). These plots were classified into beech stratum, oak stratum, and fir stratum. A total of 12,176 trees were measured for stem position, species, height, and diameter. The workflow of forest inventory using CHM, QGIS software, and packages for R environment is shown in Fig. 5.17.
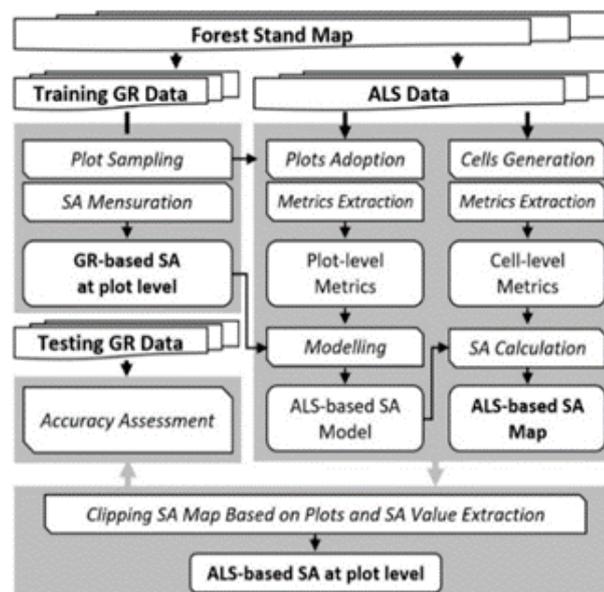
Figure 5.17. *Flowchart for CHM-based forest inventory. Note: GR: ground; ALS: airborne laser scanning; SA: forest stand attribute.*

The differences between CHM-predicted and ground-observed forest stand attributes are shown in Fig. 5.18. The differences reached a relative root mean square error at 10.9%, 23.1%, and 34.5% for the mean height, mean diameter, and volume, respectively. Moreover, all predictions were unbiased (p-value < 0.05) and the strength of the relationships between CHM-predicted and ground-observed forest stand attributes were relative high ($R^2 = 0.7–0.8$).
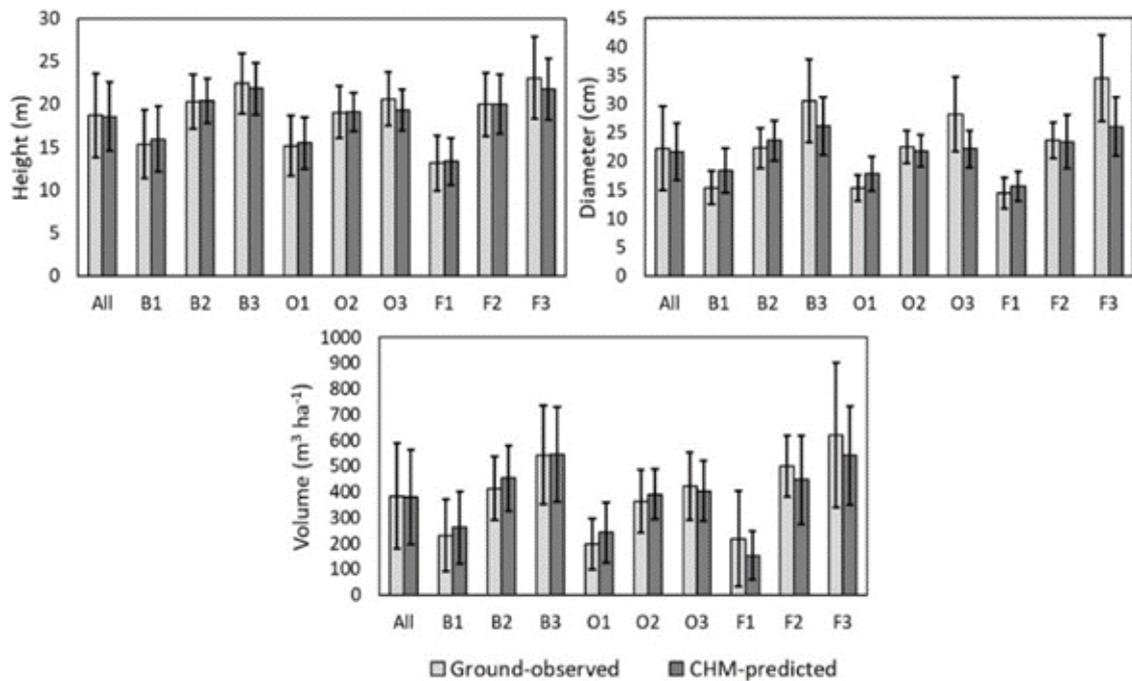
Figure 5.18. Ground-observed and CHM-predicted forest stand attributes including standard deviation (whiskers). Note: All: All testing plots; B1-3: Beech stratum; O1-3: Oak stratum; F1-3: Fir stratum.

The results of scientific studies confirmed that CHM-based forest inventory represents a practical solution that allows make a general overview of natural resources for the whole forest unit (Fig. 5.19). Moreover, this solution can be performed directly and repeatedly by stakeholders without the need for additional investments focused on data, software and hardware. On the other hand, overall accuracy of CHM-based forest inventory in these studies did not meet the requirements of forest management from some countries in Central Europe (e.g., Slovakia). Consequently, continuous research and development of CHM-based forest inventory seems to be valid and necessary.
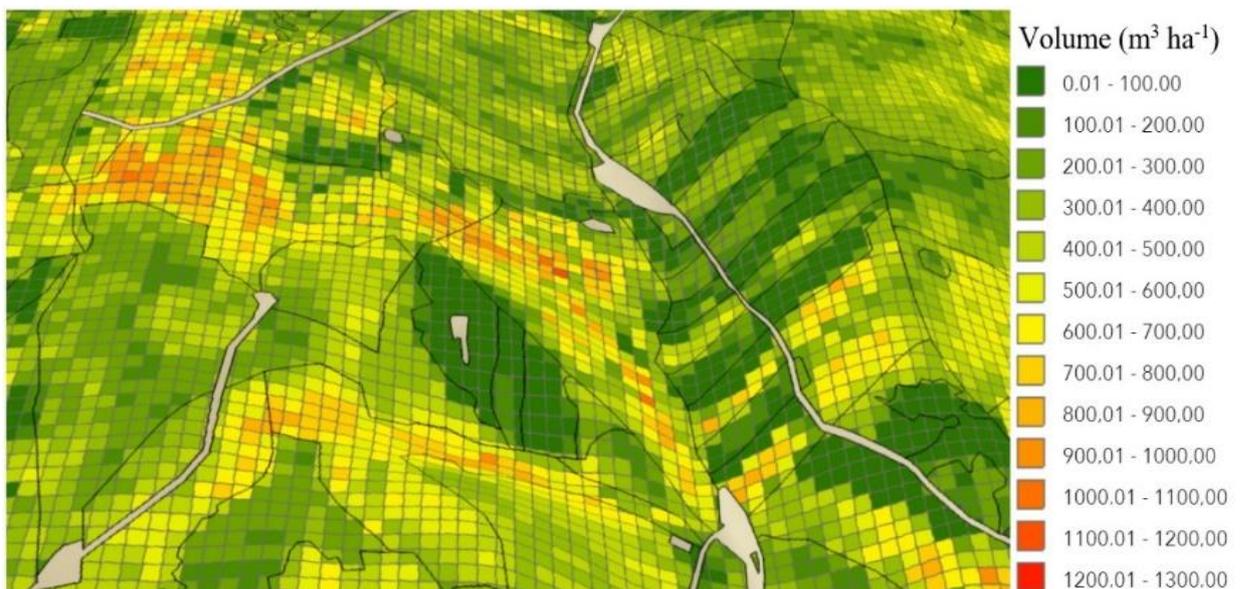
Figure 5.19. Visualization of 3D map representing CHM-predicted forest stand attribute for part of study area over grid cell 20 × 20 m (illustrative example for volume per hectare).

50

National Agricultural and Food Centre - Soil Science and Conservation Research Institute

Remote sensing-oriented projects and activities 2022 - 2023

1. Remote sensing control of area-based subsidies in agriculture

The subsidies play a key role in agriculture sector and contribute to the prosperity of agricultural subjects. The subsidies to agriculture sector represent major part of European budget and that is why there is taken an emphasis to the control.

During the years 2022 and 2023, the control with remote sensing (CwRS) was no longer performed at the NPPC-VÚPOP, unlike previous years / periods.

2. Quality Assessment of Land Parcel Information System – QA LPIS (2022;2023)

Land Parcel Identification System (LPIS) is the main component of Integrated Administration and Control System (IACS) for area based direct support. The purpose of LPIS is to implement the Common agricultural policy of the European Union (CAP EU) measures.

The quality assessment framework of LPIS is an integral part of LPIS management and upkeep processes and is also required by European legislation. EU member states are required to perform QA LPIS annually.

In this framework, the LPIS of a MS/Region is regarded as a system under test, which is composed of two major components: the local application schema and the data records stored in the system. The so-called Executable Test Suite (ETS) targets at the data component by annually assessing conformity according to Article 6 of EU Regulation No 640/2014.

QA implementation is based on current satellite images taken in the year of review. Selected reference parcels by European Commission (EC) for QA LPIS were on SCRI vectorised on the background of current satellite images, provided by EC. Subsequently, they are compared with the valid state of the LPIS layer. The satellite images were overlaid with the digitized vectors showing the position of the parcels which were checked. The land use check was completed by Rapid field visits RFVs; directly in the field in cases of ambiguous situation on satellite images.

QA LPIS is realized through 9 quality elements, grouped into two conformance classes, as defined by the Regulation. Based on the item conformance verdicts issued for the various criteria during the item inspection, verdicts made on each conformance class. There are several reasons for errors. The two most common are operator error and outdated orthophotomaps/ land use changes.

The conformance class 1 means to *"assess the quality of LPIS"* and counts non-conforming items. Furthermore, counting items offers a straightforward entry for the LPIS upkeep processes. This counting of items includes the first three types of the quality elements (QE1, QE2 and QE3).

QE1 assesses the maximum eligible area of the system and evaluates 2 quality elements: QE1a absence of bias (i.e. accuracy) of the land represented in the LPIS as a whole, QE1b parcel level precision of the land represented in the LPIS as a whole – overestimation areas and underestimation areas.

QE2 assesses individual parcels with correctness issues and evaluates 3 quality elements: QE2a proportion of items with incorrectly recorded area or "contaminated" with ineligible features – error type Update – outdated orthophotomaps (Fig. 5.23).

QE2b distribution of items, according to the correctness of the eligible area recorded and QE2c number of non-conforming reference parcels in LPIS with classification error – mistake/ error of operator (Fig. 5.22).

QE3 shows number of reference parcels that have functional issues – "critical defects" (Fig. 5.21).

Conformance class 2 is assessed under the last three elements (QE4, QE5 and QE6). QE4 categorization of the non-conformities, QE5 ratio of total declared area in relation to the total area recorded for the area conforming reference parcels and QE6 rate of non-conforming reference parcels due to undetected and unaccounted land cover change, as observed in ETS, accumulated over the years.

These 3 elements aim to *"identify possible weaknesses" and* this requires a broader system wide analysis, beyond the individual item or reference parcel. This is most obvious for QE4 which analyses the LPIS processes and design as factors for creating quality problems. For instance, a single, large parcel can be contaminated, can have critical defect (for example, multi-parcel), and can have its land wrongly classified. Although this represents a single non-conforming item, it does reflect three different system weaknesses.

QA IACS 2023 was changed from QA LPIS, were added to QA LPIS: QA GSA – Geospatial Application (GSA) quality assessments and QA AMS – quality assessments Area Monitoring System (AMS). The methods of selecting parcels, the satellite providing VHR scenes on the Pleiades as well as the reporting have completely changed. In the article, we will no longer deal with QA AMS and QA GSA 2023, as they are still ongoing at the moment and not final.

Quality assessment of the Slovak LPIS was realized in 3 zones for campaign year 2022 and in 13 zones for campaign year 2023 (Fig. 5.20). VHR satellite imagery for each zone were delivered from JRC EC.

Site LPIS2022-SK-01 covers parts of Skalica district (EC provided World View 3 satellite image from 1st July 2022, pixel size 0.4 m), zone is localised in West Slovakia. Site LPIS2022-SK-02 covers parts of Trnava district (EK provided GEO EYE 1 satellite image from 4th August 2022, pixel size 0.5 m), zone is localised in West Slovakia. Site LPIS2022-SK-03 covers part of Veľký Krtíš district in south part of Slovakia (EK provided World View 2 satellite image from 6th August 2022, pixel size 0.5 m).

Site LPIS2023-SK-01 covers parts of Tvrdošín district (EC provided Pléiades Neo 4 satellite image from 31st May 2023, pixel size 0.3 m), zone is localised in North Slovakia. Site LPIS2023-SK-02 covers parts of Kežmarok and Poprad districts (EC provided Pléiades Neo 3 satellite image from 14th August 2023, pixel size 0.3 m), zone is localised in North Slovakia. Site LPIS2023-SK-03 covers parts of Humenné and Medzilaborce districts in east part of Slovakia (EC provided Pléiades Neo 3 satellite image from 16th July 2023, pixel size 0.3 m). Site LPIS2023-SK-04 covers parts of Prešov district in east part of Slovakia (EC provided Pléiades Neo 3 satellite image from 27th August 2023, pixel size 0.3 m). Site LPIS2023-SK-05 covers parts of Vranov and Topľou district in east part of Slovakia (EC provided Pléiades Neo 3 satellite image from 14th August 2023, pixel size 0.3 m). Site LPIS2023-SK-06 covers parts of Púchov and Ilava districts in west part of Slovakia (EC provided Pléiades Neo 3 satellite image from 22nd April 2023, pixel size 0.3 m). LPIS2023-SK-07 covers parts of Nové Mesto nad Váhom and Trenčín districts in west part of Slovakia (EC provided Pléiades Neo 3 satellite image from 8th May 2023, pixel size 0.3 m). LPIS2023-SK-08 covers parts of Brezno district in the middle part of Slovakia (EC provided Pléiades Neo 3 satellite image from 31st May 2023, pixel size 0.3 m). LPIS2023-SK-09 covers parts of Trenčín and Nové Mesto and Váhom districts in west part of Slovakia (EC provided Pléiades Neo 3 satellite image from 3rd June 2023, pixel size 0.3 m). LPIS2023-SK-10 covers parts of Detva and Zvolen districts in the middle part of Slovakia (EK provided Pléiades Neo 3 satellite image from 27th August 2023, pixel size 0.3 m). LPIS2023-SK-11 covers parts of Levice district in south part of Slovakia (EC provided Pléiades Neo 3 satellite image from 17th April 2023, pixel size 0.3 m). LPIS2023-SK-12 covers parts of Pezinok and Senec districts in west part of Slovakia (EC provided Pléiades

Neo 3 satellite image from 12nd April 2023, pixel size 0.3 m). LPIS2023-SK-13 covers parts of Veľký Krtíš and Levice districts in south part of Slovakia (EC provided Pléiades Neo 3 satellite image from 23rd May 2023, pixel size 0.3 m).

The satellite images were georeferenced by SSCRI staff. Measured and archive control and check points were used. For all zones the Quality checks of georeference were carried out and control protocol were elaborated.
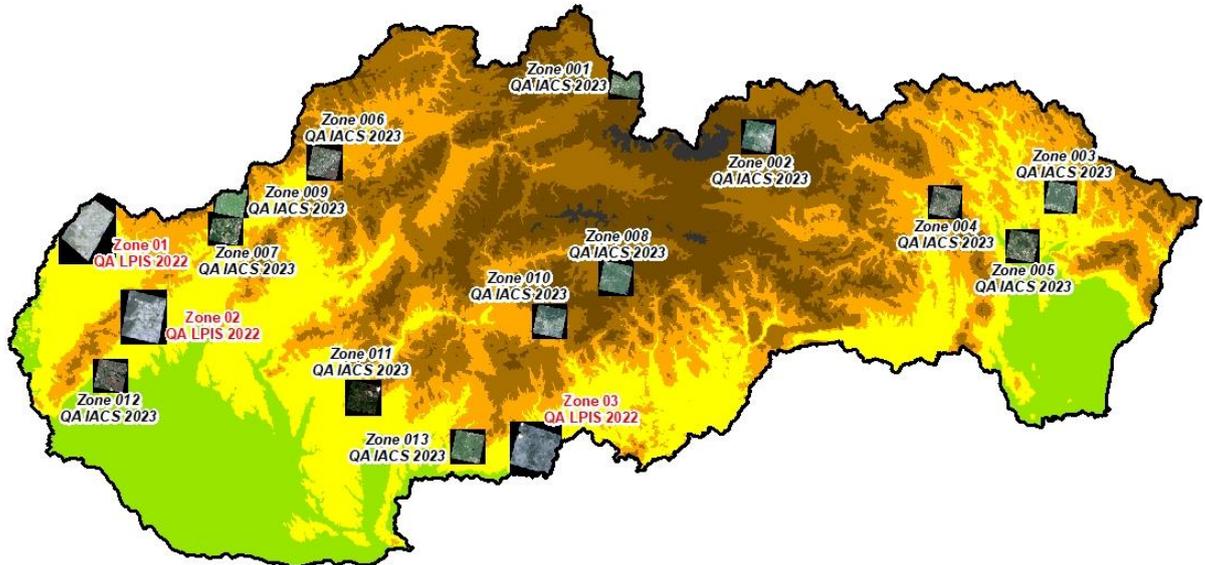
Figure 5.20. *Localization of the controlled sites in QA LPIS 2022 and QA IACS 2023.*

Figure 5.21. *Example of case with identified critical defect – Total absence of eligible features caused by update – changes of the underlying land were not applied (the cyclical update of LPIS was in 2019. The land use change occurred after it).*

Figure 5.22. *Example of the classification error with cause "Erroneous processing "- a mistake of LPIS operator (part of the LPIS parcel with permanent grassland is used as arable land).*

Figure 5.23. *Example of the occurrence of non-agricultural land cover features (artificial sealed surface and associated areas) on the reference parcels caused by update.*

3. Remote sensing within crop yield and crop production forecasting (2022; 2023)

Monitoring of Crop Conditions and Crop Monitoring

Regional monitoring of natural crop conditions aims to study the influence of weather (coupled with soil) on crop growth and crop development during current vegetation season.

NDVI (Normalized Difference Vegetation Index) is derived from NOAA's AVHRR sensor. The NDVI characterizes the total biomass state (volume and vitality), the higher the NDVI value, the more biomass is developed (characterized by a higher content of chlorophyll in plants and hence a more potent photosynthesis).

Development of the NDVI in 2023 and its comparison with the situation in 2022 and long-term average is documented on Fig. 5.24.
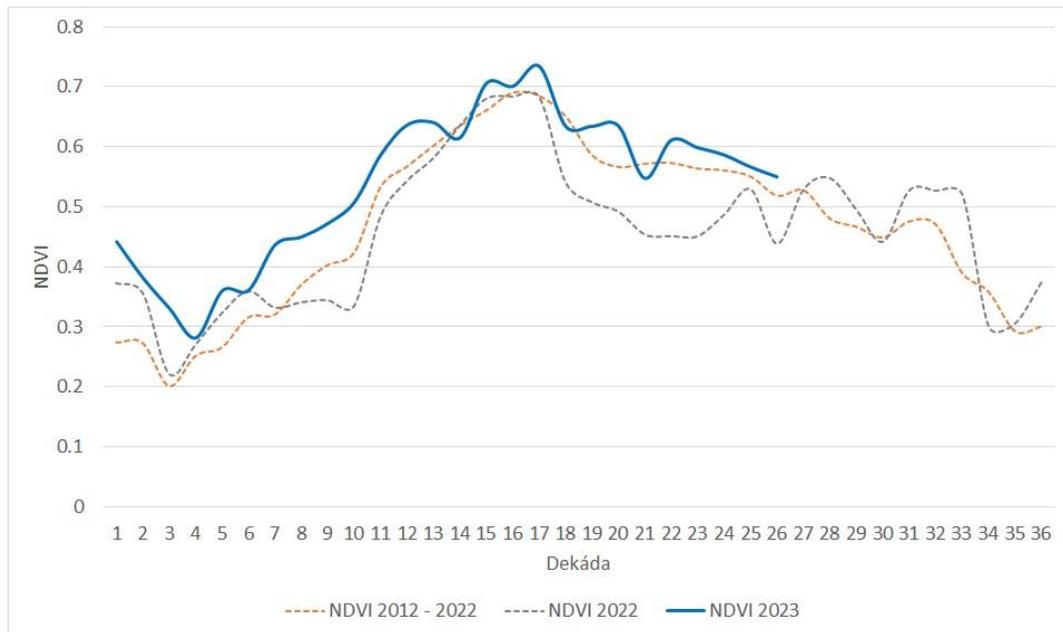
Figure 5.24. *Development of the NDVI vegetation index in 2023 and its comparison with the situation in 2022 and long-term average, data source: NPPC-VÚPOP.*

Crop yield forecasting

The aim of the crop yield and crop production forecasting is to provide the most likely, scientific, and as precise as possible independent forecast for main agricultural crop yields for Ministry of Agriculture and Rural Development of the Slovak Republic and for the public.

National Crop Yield and Crop Production Forecasting System has been created on SSCRI and is based on three different principles which are applied to specify vegetation indexes as biomass development stage and biomass development:

- Remote sensing method – method of interpretation of vegetation indicators (as NDVI or DMP- Dry Matter Development) from satellite images (mainly from low resolution satellite sensors as NOAA AVHRR and SPOT Vegetation satellite system);
- Bio-physical modeling (WOFOST model) and simulation of vegetation indexes (mainly TWSO – Total Dry Weight of Storage Organs and TAGP – Total Above Ground Production). In WOFOST, weather and phenological data, soil hydro-physical data and crop physiological data are utilized as model key inputs;
- Integrated assessment method, which means the implementation of specific meteorological and vegetation indicators in the statistical analysis, assesses the impact of weather on the projected harvest. Integrated estimate summarizes a wider range of disparate indicators and indices that are currently for the purposes of forecasting yields and consequently the production of crops used.

The crop yield and crop production forecasting is carried out for main agricultural crops – winter wheat, spring barley, oil seed rape, grain maize, sugar beet, sunflower and potatoes. The forecasts are reported six times per year – in the half of May, June and July for "winter and spring crops" and in the end of July, August and September for "summer crops". The forecast results are interpreted at national level as well as at NUTS3 and NUTS4 level. The example of crop yield forecasting in 2023 can be seen in the Fig. 5.25.

55
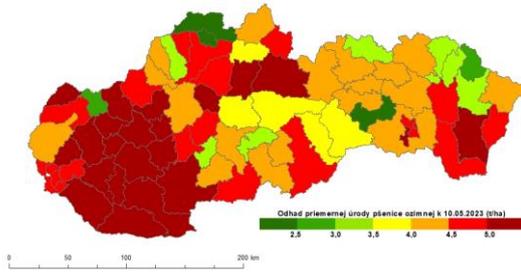
6a   6b
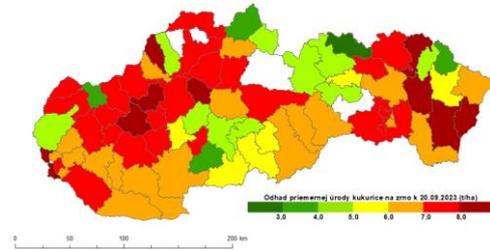
Figure 5.25. Example of crop yield forecasting with remote sensing in first decade of May in 2023 for winter wheat (a) and in the second decade of September for maize (b).

4. URANOS (Data and knowledge support for decision-making and strategic planning systems in the field of agricultural landscape adaptation to climate change and minimization of agricultural soil degradation – URANOS 2022; 2023)

The activity was focused on creating a library of representative values of monitored parameters at different spatial resolution levels (agriculture parcel, district). District level example is documented on Figs. 5.26 and 5.27. From the satellite image records for all periods of the monitored period since 2011, only those that had reliable records were selected.
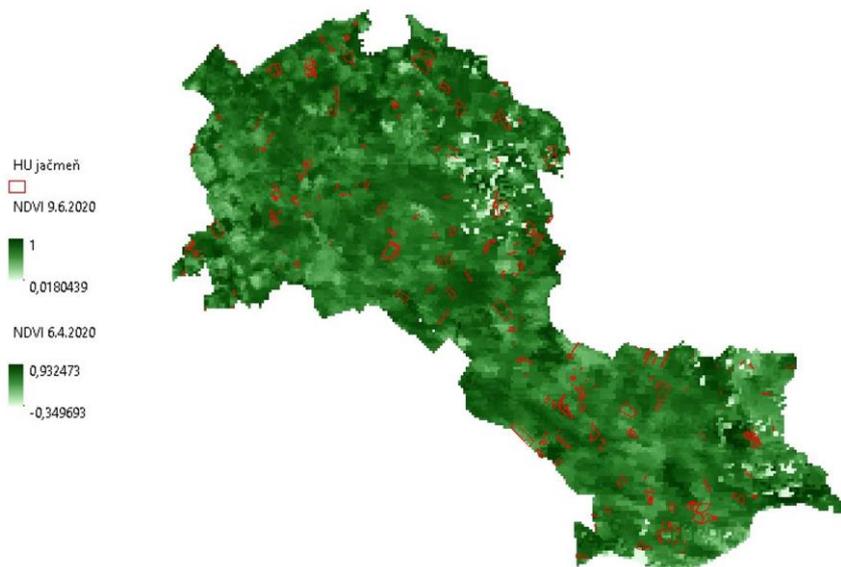
Figure 5.26. Creation of a library of NDVI index values specifically crop-oriented at the level of parcels and districts since 2011 Nové Zámky district.
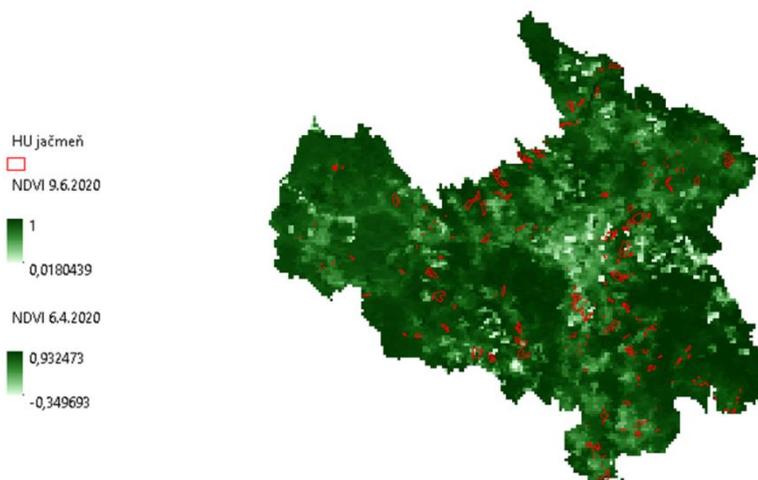
Figure 5.27. Creation of a library of NDVI index values specifically crop-oriented at the level of parcels and districts since 2011 Prešov district.

We selected, on the basis of information from the second channel of satellites, all images that had unreliable records for various reasons, images with other codes 4305; 7425; 7633; 7683, these are not further included in the calculations as they would distort the outputs and their plausibility, and only images with code 4096 were left for the calculation. Subsequently, a library of NDVI index values (and subsequently their weighted averages) was created at the level of parcels by crops (wheat; barley; canola; corn; sunflower; sugar beet; potatoes; soybeans and permanent grasslands) and districts for all periods (8 days NDVI averages) and years.

Multitemporal crop classification approaches have demonstrated high performance in a given seasons. However, inter-seasonal and inter-regional crop classification presents a unique portability challenge. This study addresses this challenge by adopting a domain generalization approach, e.g. by training models over multiple seasons to improve generalization to new, following target years.

With this approach, we are trying to improve the quality and precision of agricultural crop yield estimates. We do this by selecting specific agricultural parcels within the borders of Slovakian districts sown with one main crop and then calculating the NDVI indexes during the vegetation period, followed by statistical evaluation within the framework of the estimation of the yields of the main agricultural crops. The results will need to be checked and verified in the following years, but the logical conclusion is that they already show correlations with the official estimates of the statistical office and JRC EC. As an example of the different development of NDVI values during the growing season, we present two instances of areas with different conditions – Nové Zámky district Fig. 5.28 and Prešov district Fig. 5.29.

Rapeseed, grassland and sugar beet consistently show stable transmissibility across seasons. We observe that all periods play a key role in the classification process, with July being the most important and August the least important. Acceptable performance can be achieved as early as June, with only slight improvements towards the end of the season. Finally, the use of a multi-classifier approach allows the determination of reliability at the plot level, thereby increasing the reliability of crop distribution maps.
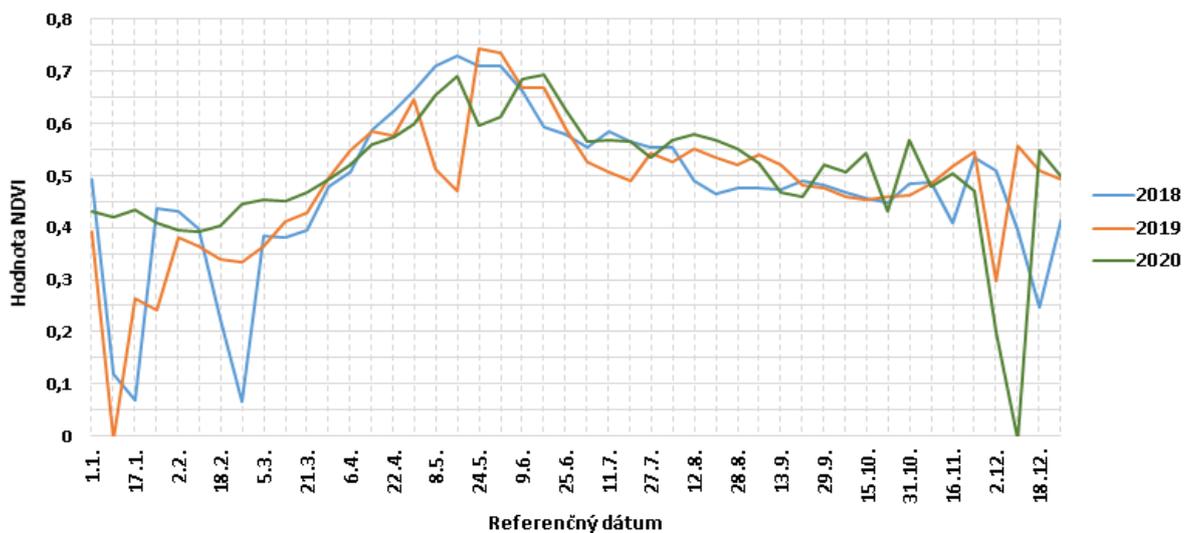
Figure 5.28. *NDVI of barley development in the Nové Zámky district in 2018-2020.*
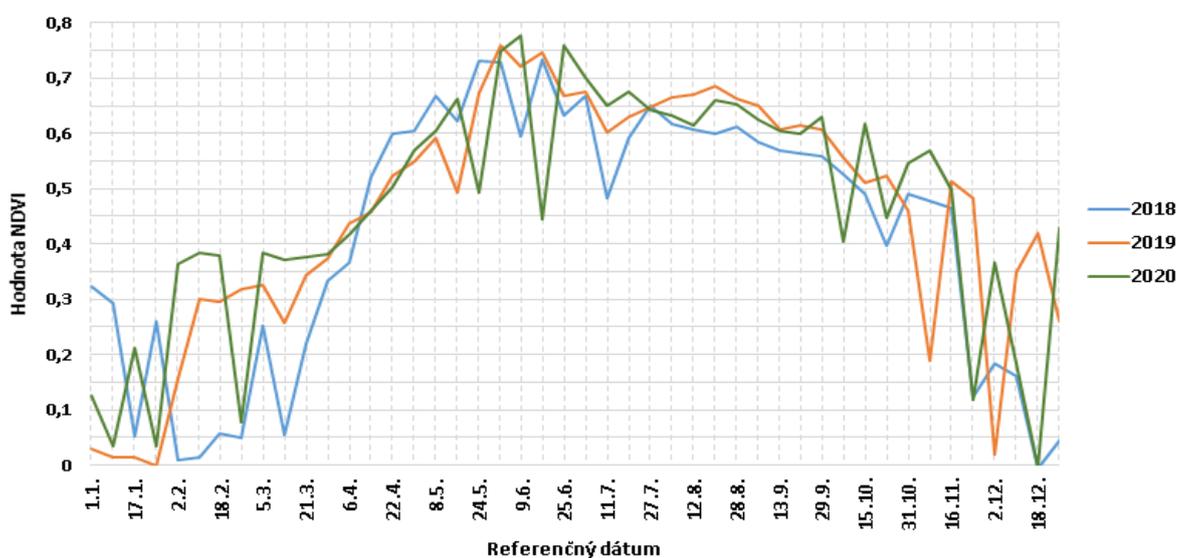
Figure 5.29. *NDVI of barley development in the Prešov district in 2018-2020.*

58

Institute of Landscape Ecology, Slovak Academy of Sciences in Bratislava

During the reporting periods of 2022-2023, two distinctive activities, partly funded by European Space Agency (ESA) projects, were undertaken to enhance our understanding and management of agricultural and environmental resources through advanced satellite technology. The first project, titled "Towards Quantification of Non-Photosynthetic Vegetation from Copernicus Hyperspectral Imaging Mission for the Environment" (Acronym: CHIME_NPV), was launched as a two-year preparatory study in March 2022. This initiative is dedicated to the critical examination of non-photosynthetic vegetation (NPV), which includes dead plants, litter, and crop residue, crucial for ecosystem dynamics and agricultural management. The project underscores the significance of the shortwave infrared (SWIR) spectral range (1300-2500 nm) for mapping NPV, aiming to overcome the limitations of existing space-borne sensors. Through the integration of radiative transfer models and machine learning, CHIME_NPV seeks to advance the quantification of NPV. Initial efforts involved conducting spectral measurements to create datasets for model realistic parametrization and undertaking an extensive literature review (Verrelst et al., 2023) to set the stage for future satellite mission requirements. Further advancements were made in data collection and 3D radiative transfer modeling, significantly improving simulation capabilities.

The second activity expanded on the earlier ESA-funded "Satellite-based Delineation of Yield Productivity Zones for Slovak Crop Fields" (SatZones) by continuing the development of the "SK_CROP-net: Satellite Based Crop Classification Model" initiative. This effort concentrated on developing and testing machine learning algorithms for crop classification at a regional scale, using Sentinel-2 satellite data (Rusňák et al., 2023). This research was a component of the ESA PECS (Plan for European Cooperating States) initiative, marking a crucial step in preparing and enhancing the capacity of Slovak research and development institutions for full ESA membership. These endeavours culminated in Slovakia's attainment of Associate Membership in 2022, significantly broadening the opportunities for the Slovak space sector to participate in European projects.

References:

[1] BUCHA, T. – SITKOVÁ, Z. – PAVLENDOVÁ, H. – SNOPKOVÁ, Z. (2022). Spring phenology of oak stands in the Western Carpathians: validation of satellite metrics from MODIS using ground-based observations. *Central European Forestry Journal*, 68(4), 191-202.

[2] BUCHA, T. – GERGEĽ, T. – BARKA, I. – SEDLIAK, M. – TOMAŠTÍK, J. – CHUDÁ, J, – SUROVÝ, P. (2022). Využitie satelitných snímok pri identifikácii prejavov sucha na zdravotnom stave lesov v roku 2022 [The use of satellite images in identifying the effects of drought on the forests health condition in 2022]. APOL: Aktuálne problémy v ochrane lesa: Výskyt škodlivých činiteľov v lesoch Slovenska v roku 2021 a prognóza na rok 2022: *Časopis Lesníckej ochranárskej služby*, 3(3), 386-394.

[3] BUCHA, T. – KOREN, M. – SITKOVÁ, Z. – PAVLENDOVÁ, H. – SNOPKOVÁ, Z. (2023). Trends and driving forces of spring phenology of oak and beech stands in the Western Carpathians from MODIS times series 2000-2021. *iForest*, 16, 334-344.

[4] FULMEKOVÁ, Z. – ZVERKOVÁ, A. – SKALSKÝ, R. – SVIČEK, M. – KUSÝ, D. (2022). The yield forecast of winter crops in the first decade of May 2022. *Naše pole*, 26, 8, 40-42.

[5] FULMEKOVÁ, Z. – ZVERKOVÁ, A. – SKALSKÝ, R. – SVIČEK, M. – KUSÝ, D. (2022). The yield forecast of winter crops in the first decade of June 2022. *Naše pole*, 26, 9, 42-45.

[6] FULMEKOVÁ, Z. – ZVERKOVÁ, A. – SKALSKÝ, R. – SVIČEK, M.– KUSÝ, D. (2022). The yield forecast of summer crops in the second decade of September 2022. *Naše pole*, 26, 11, 41-43.

[7] FULMEKOVÁ, Z. – ZVERKOVÁ, A. – SVIČEK, M. – KUSÝ, D. (2023). Application and updating of the national agro-meteorological modeling system to estimate crop production and crop yield (SK_CGMS). Final report to solving tasks under the contract with MPRV for the year 2023. SSCRI, Bratislava.

[8] FULMEKOVÁ, Z. – ZVERKOVÁ, A. – SVIČEK, M. – KUSÝ, D. (2023). The yield forecast of winter crops in the first decade of May 2023. *Naše pole*, 27, 8, 18-21.

[9] FULMEKOVÁ, Z. – ZVERKOVÁ, A. – SVIČEK, M. – KUSÝ, D. (2023). The yield forecast of summer crops in the second decade of September 2023. *Naše pole*, 27, 11, 46-49.

[10] GALLAY, M. – KAŇUK, J. – ZGRAGGEN, C. – IMBACH, B. – ŠAŠAK, J. – ŠUPINSKÝ, J. –HOLLAUS, M. (2023). Unpiloted airborne laser scanning of a mixed forest. A case study from the Alps, Austria, pp. 1-13. In: Meneely, J. (Ed.). *3D Imaging of the Environment: Mapping and Monitoring*. Boca Raton: CRC Press. https://doi.org/10.1201/9780429327575

[11] RUSŇÁK, T. – KASANICKÝ, T. – MALÍK, P. – MOJŽIŠ, J. – ZELENKA, J. – SVIČEK, M. – ABRAHÁM, D. – HALABUK, A. (2023). Crop mapping without labels: Investigating temporal and spatial transferability of crop classification models using a 5-year Sentinel-2 series and machine learning. *Remote sensing*, 15, 3414, 1-35. https://doi.org/10.3390/rs15133414

[12] SAČKOV, I. (2022). Forest Inventory Based on Canopy Height Model Derived from Airborne Laser Scanning Data. *Central European Forestry Journal*, 68(4), 224-231.

[13] SAČKOV, I. – BARKA I. (2023). A Geoprocessing Tool for the Calculation of Primary Wood Transportation Distance. *Forests*, 14, 907.

[14] SZATMÁRI, D. – KOPECKÁ, M. – FERANEC, J. (2022). Accuracy assessment of the building height Copernicus data layer: A case study of Bratislava, Slovakia. *Land*, 11, art. no. 590, 3-14.

[15] SZATMÁRI, D. – KOPECKÁ, M. – FERANEC, J. – GOGA, T. – OPRAVIL, Š. – SVIČEK, M. – FENCÍK, R. – PAPČO, J. (2023). Environmental data and satellite images: information sources for the identification of illegal activities in the landscape on the example of Slovakia. *Abstracts of the International Cartographic Association*, 6, 253. 31st International Cartographic Conference (ICC 2023), 13–18 August 2023, Cape Town, South Africa. https://doi.org/10.5194/ica-abs-6-253-2023

[16] VERRELST, J. – HALABUK, A. – ATZBERGER, C. – HANK, T. – STEINHAUSER, S. –BERGER, K. (2023). A comprehensive survey on quantifying non-photosynthetic vegetation cover and biomass from imaging spectroscopy. *Ecological Indicators*, 155, p. 110911. https://doi.org/10.1016/j.ecolind.2023.110911

6. SPACE METEOROLOGY

J. Kaňák, Ľ. Okon, L. Méri, M. Jurašek, P. Kaňák

6.1. Estimation of dry/wet regions over Slovakia and central Europe based on 10 years reference period of H SAF satellite precipitation products

In the frame of EUMETSAT H SAF project, in validation working group the evaluation of precipitation products is very important task. Validation is based on comparison of satellite data against ground truth (rain gauge or radar measurements). Mainly statistical comparisons of instantaneous precipitation or 24 hours accumulations we performed until nowadays to evaluate HSAF precipitation products quality and performance. Aim of this study is to use long-term accumulated precipitation data on monthly basis. Maximum 10 years of H05A/B H SAF products is available for this kind of work – operationally generated and archived data are covering the period from July 2012 until nowadays. For estimation of DRY/NORMAL/WET periods in terms of precipitation over Slovak territory, we worked in following way:

- Created monthly accumulated precipitation (monthly totals) in mm per month (120 months)
- Generation of monthly long-term normals from 10-years averages of accumulated precipitation for each month of the year
- Calculations of monthly anomalies (difference between monthly accumulated precipitation and monthly long-term normals)
- Final evaluation of monthly anomalies according DRY/NORMAL/WET classification table

Our satellite database contains 120 evaluated months, which we classified according to the above scheme and compared with the same classification of data from the rain gauge network. In the comparison of monthly precipitation totals from satellite products with the Slovak network of rain gauges for the period July 2012 to June 2022, we achieved agreement in 78% of cases.

The aim of this study was to use appropriately processed rainfall data on a monthly basis and for a sufficiently long period. As satellite observations are still evolving, obtaining a consistent time series of measurements from them is not easy. In the case of H-SAF precipitation detection, we have now reached the point where we have at our disposal a 10-year continuous series of areal precipitation estimates, used as a reference period. In climatology, standard reference periods mostly tied to decades are used, in this study, due to the availability of a consistent set of satellite precipitation observations, this is not yet possible. Specifically, we have available the product H-SAF H05A/B - operationally generated and available from the EUMETSAT archive for registered users from July 2012 until today. Product type A covers the territory of Europe, product type B covers the entire adjacent hemisphere, which is scanned by Meteosat from the position (0˚, 0˚) of latitude and longitude (Fig. 6.1). Algorithms of products A and B are physically identical, they differ only in the availability of supporting data from different regions - global or regional numerical models, different in the area of Europe, different in the area of Africa, etc. However, in principle, products of type A and B are consistent for the entire processed period 2012-2022.

The task was to estimate from satellite or rain gauge data on a monthly basis whether, in terms of the nature of precipitation, it is a dry, normal, or wet period, using the following procedure:

1. Preparation of monthly accumulated precipitation (monthly totals) in mm from the satellite and from the rain gauge network for 120 months from July 2012 to June 2022.

2. Preparation of monthly long-term normals, i.e. 10-year averages of accumulated precipitation for each month of the year - January to December.

3. Calculation of monthly deviations (anomalies), i.e. the difference between monthly accumulated precipitation and monthly long-term normals.

4. Evaluation of monthly anomalies for the entire territory of Slovakia according to the classification table of precipitation characteristics (DRY/NORMAL/WET). The software prepared for this purpose can be reconfigured for the evaluation of differently defined areas, such as regions, river basins, and the like.

5. We applied the procedure according to points 1 to 5 both to the data from the satellite product H05A/B and from the data of the SHMÚ rain gauge network.
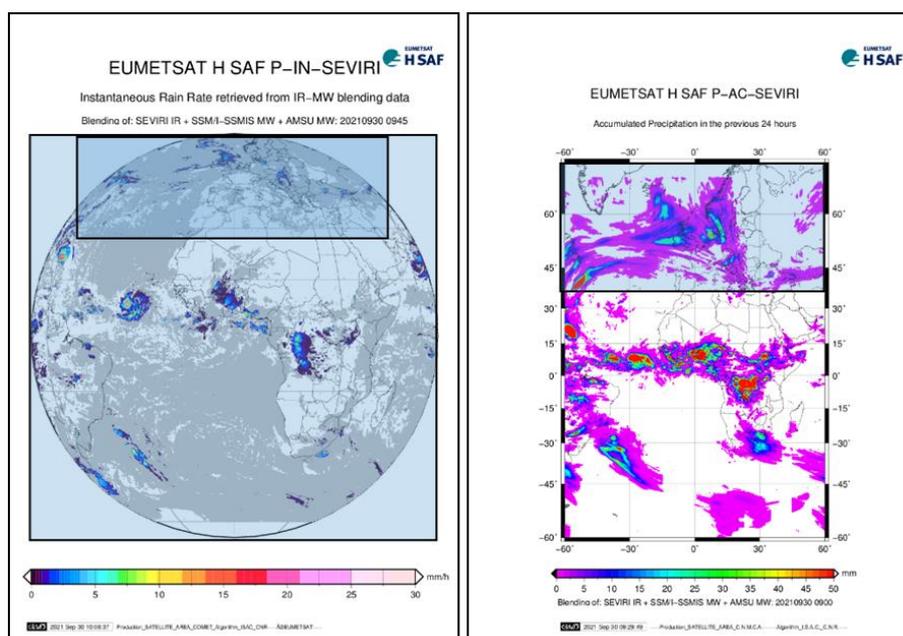
Figure 6.1. *Examples of the satellite precipitation products: H03A/B (P-IN-SEVIRI) (left) and H05A/B (P-AC-SEVIRI) P-AC-SEVIRI (right) product. Region B is full Earth disk, smaller region A covers only northern hemisphere (European countries) – highlighted by upper blue boxes.*

Classification of the nature of the rainy season:

Due to the variability of precipitation and its occurrence in time and space, it is necessary to adapt the boundaries of the intervals of different classes to the length of the period. Therefore, for periods of one month, wider intervals between the boundaries are used than for annual seasons, or for longer lasting periods. For example, a dry season lasting more than 3 months with even narrower intervals. The definitions of the characteristics used by us, as defined by the experts of the climatological service of the SHMÚ, are shown in Tab. 6.1.

Definition	*For monthly period*	*For year seasons*
Extremely dry	< 10 %	< 60 %
Very dry	10 - 49 %	60 - 79 %
Dry	50 - 79 %	80 - 89 %
Normal	80 - 120 %	90 - 110 %
Wet	121 - 150 %	111 - 120 %
Very wet	151 - 190 %	121 - 140 %
Extremely wet	> 190 %	> 140 %

***Table 6.1**. Definition of characteristics of precipitation periods for months and seasons.*

For our purposes in the final evaluation, we reduced the number of classes (Tab. 6.2) to make the results easier for interpretation and practical usage.

(1) DRY	Extremely and very dry	less than 50%
(2) NORMAL	Dry, normal and wet	From 50% to 150%
(3) WET	Extremely and very wet	More than 50%

***Table 6.2**. Simplified classification of characteristics of precipitation periods.*

In this study, we evaluate rainfall characteristics on a monthly basis. We plan to prepare more general software for data processing in future to evaluate seasons or other periods lasting weeks to months according user needs.

The first step in data processing was the preparation of monthly rainfall totals according to the satellite and according to the SHMÚ rain gauge network. The images are not presented here due to their extreme size in full resolution. For experts and our users, they are available in full quality on the SHMÚ intranet. In Fig. 6.2 we present the long-term normals of monthly rainfall totals obtained from the satellite (left) and from the SHMÚ rain gauge network (right). We have arranged them in 3x4 matrices so that the first row contains winter season, the second spring, the third summer months and the fourth autumn season. The winter months, the first two spring months and the last autumn month are characterized by lower totals than the last spring and all summer months with a prevailing meteorological events with convective precipitation. We observe this in both satellite and rain gauge data. On the maps from the rain gauges, thanks to the three-dimensional regularized spline algorithm used, the totals are clearly distributed according to the altitude - the higher the altitude, the higher the totals. For satellite data, this characteristic is missing, since the H05A/B (or newer H61B) product algorithm does not use any effect of orography. However, the advantage of satellite data is its area coverage. Thanks to it, we can work with total values at every point of the displayed map both within the territory of the Slovak Republic and outside it. The homogeneity of the quality of satellite data is algorithmically partially disturbed by dividing the entire matrix of the satellite product into smaller blocks with a step of 5° in latitude and longitude, within which the supporting parameters of the algorithm are used, which is described in the product documentation (ATBD H02B, 2019). Algorithm for H61B product was improved in 2022 and the latest data does not more reflect this kind of inhomogeneity. The effect is particularly noticeable in months with low monthly precipitation totals (winter months). The relative error of determining low precipitation totals with the satellite product is much larger than for high totals.
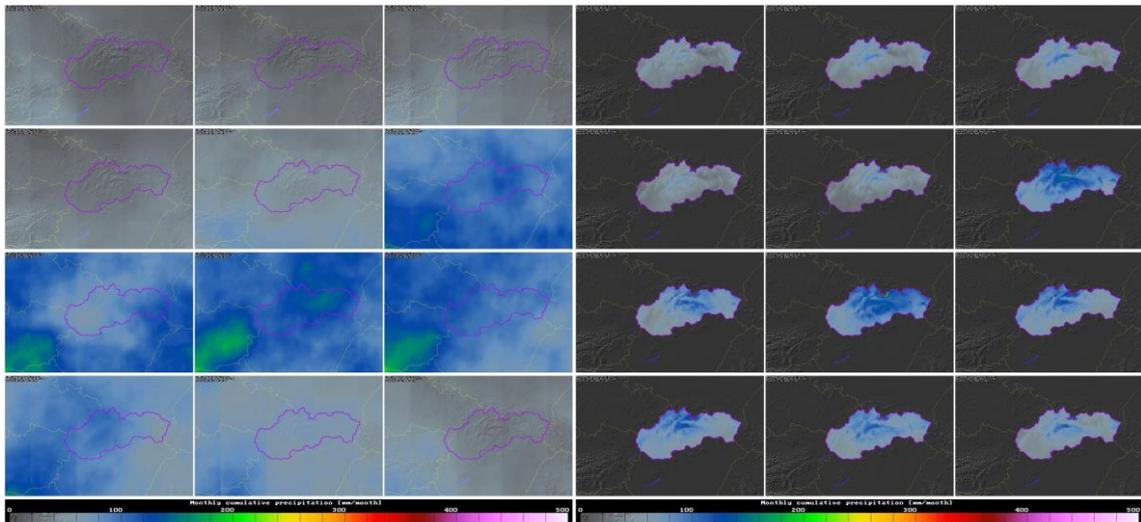
Figure 6.2. *10-year long-term normals of monthly precipitation totals 2012-2021 (July-December), or 2013-2022 (January-June). On the left – from the H05A/B satellite product, on the right – from the SHMÚ rain gauge network. In the mosaic, from left to right, first row – December, January, February, second row – March, April, May, third row – June, July, August, fourth row – September, October, November.*

After obtaining long-term monthly averages, we proceeded to calculate monthly anomalies for both sources of precipitation data. We thus obtained two sets of 120 image matrices, which are shown in Fig. 6.3 (anomalies by satellite) and Fig. 6.4 (anomalies according to the SHMÚ rain gauge network). Full-resolution images are available again to SHMÚ users via the intranet local applications.
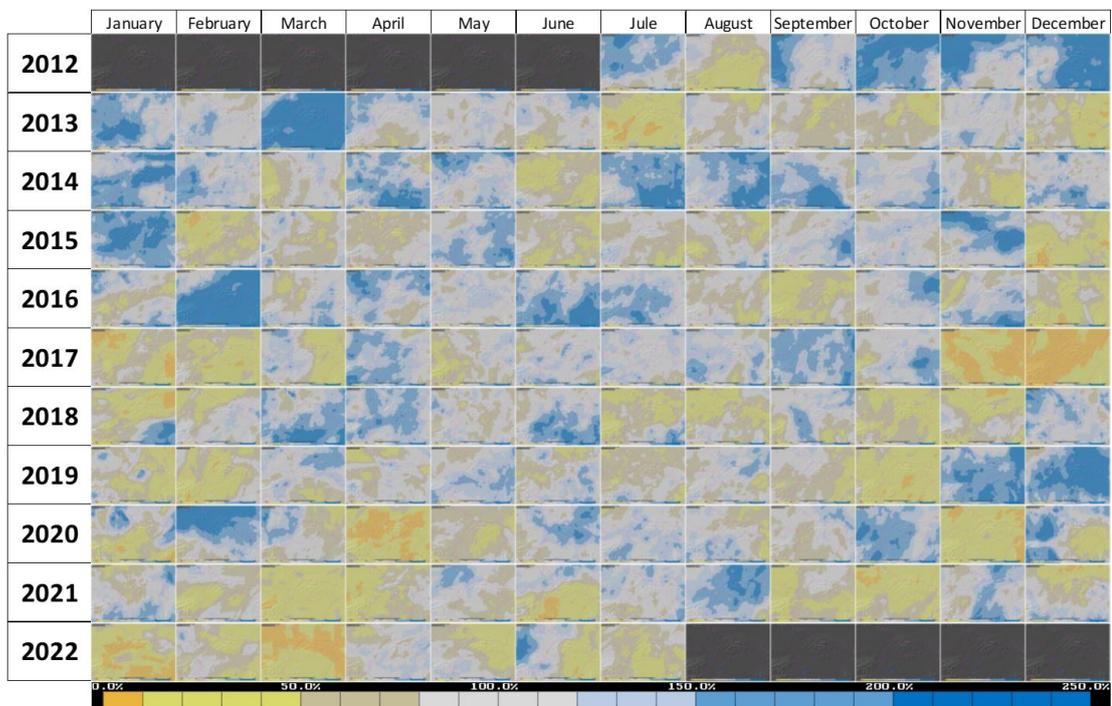
Figure 6.3. *Monthly precipitation anomalies according H05 product. Relative differences in [%] from 0 to 250% of monthly sums for each month in the period of years 2012-2022. 100% corresponds to the long-term average.*

64

	January	February	March	April	May	June	Jule	August	September	October	November	December
2012												
2013												
2014												
2015												
2016												
2017												
2018												
2019												
2020												
2021												
2022												
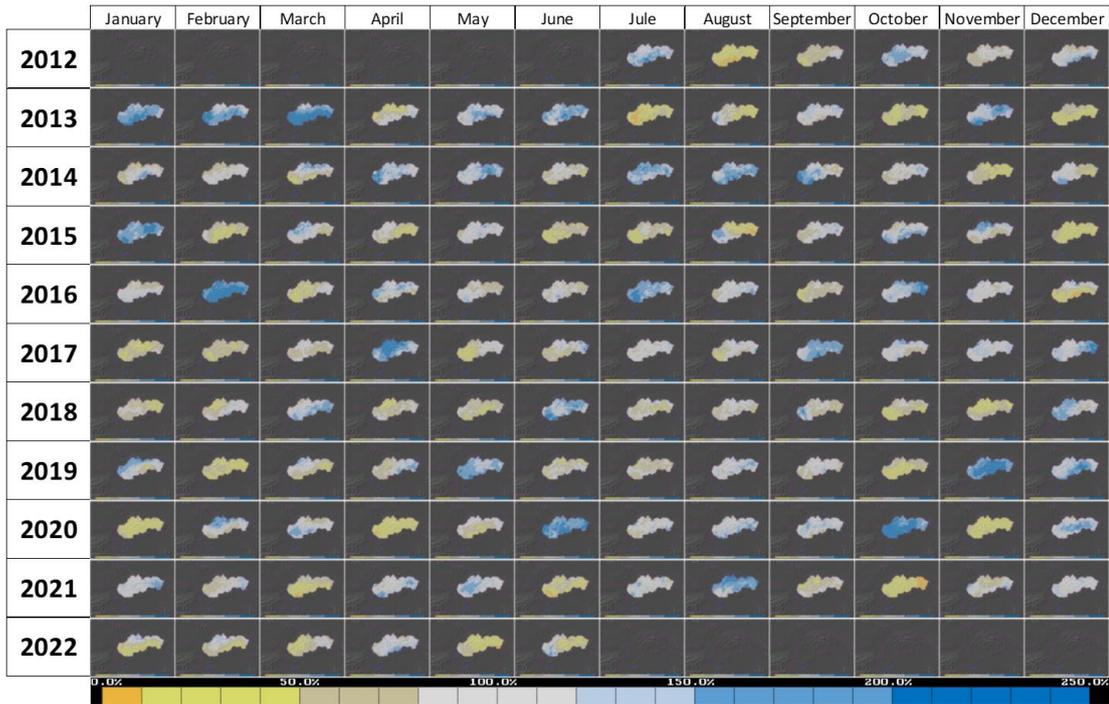
Figure 6.4. Monthly precipitation anomalies according SHMÚ rain gauge network in [%] from 0 to 250% of monthly sums for each month in the period of years 2012-2022. 100% corresponds to the long-term average.

To illustrate, in this report we will give three examples out of many, how we can use satellite observations to evaluate selected months according to dry, normal or rainy weather prevailed:
These are the sample cases: February 2016 (Fig. 6.5), July 2019 (Fig. 6.6) and June 2022 (Fig. 6.7).
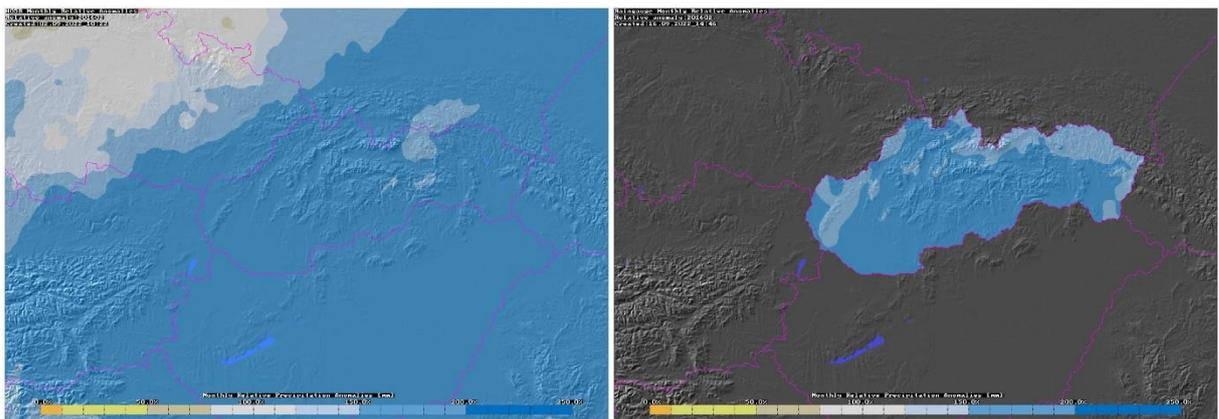
Figure 6.5. Comparison of the monthly anomaly for February 2016. Example of a wet month. On the left - according to the satellite, on the right - according to the rain gauge network.

65
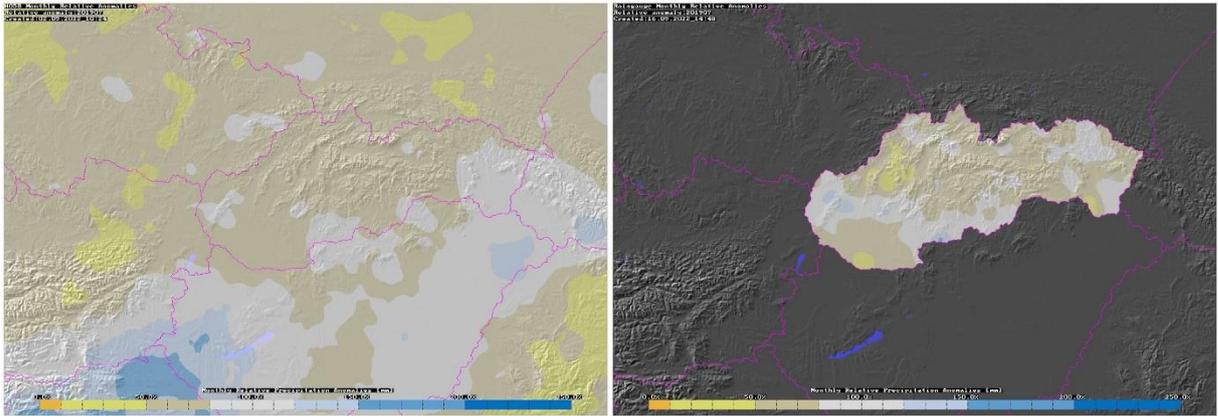
Figure 6.6. *Comparison of the monthly anomaly for July 2019. Example of a normal to dry month. On the left - according to the satellite, on the right - according to the rain gauge network.*
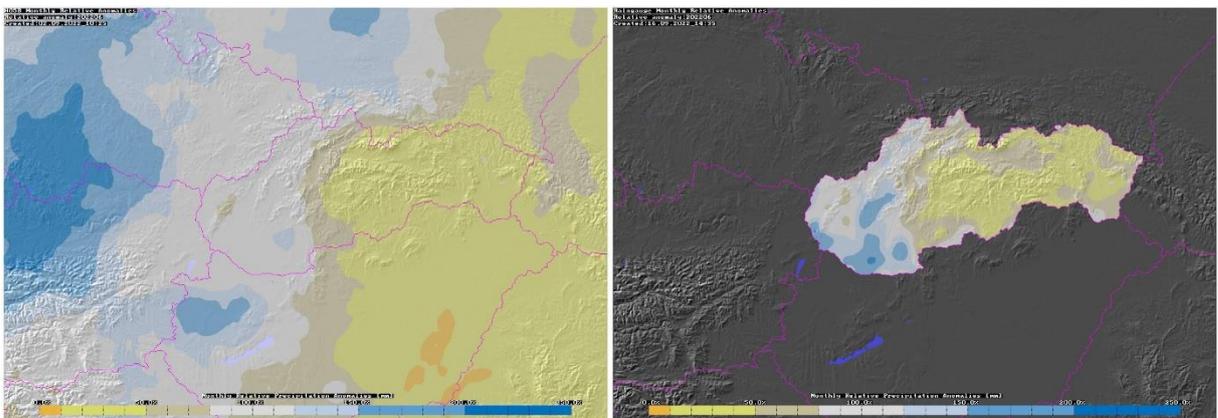
Figure 6.7. *Comparison of the monthly anomaly for June 2022. Example of month normal in west, dry in east part of Slovakia. On the left - according to the satellite, on the right - according to the rain gauge network.*

In this study, we have shown that, in the long term, satellite products have a sufficiently high predictive value in the classification of dry and wet periods on a monthly basis in comparison of monthly rainfall totals from satellite products with the Slovak network of rain gauges. Their usefulness will be proven in the short future, or based on new experience, we will adapt the satellite data processing methodology.

6.2. Atmospheric waves induced by Hunga Tonga eruption we observed in Meteosat satellite WV imagery

The underwater volcano Hunga Tonga-Hunga Ha'apai has erupted twice this month, causing major gravity and shockwaves to reverberate around the world.

Experts in and outside of EUMETSAT have taken an in-depth look at a wide variety of satellite and meteorological data from the major eruptions (and in particular the shockwaves).

In Slovak Hydrometeorological Institute we made our own processing of satellite data with interesting results, which shows that the inflection point (turning point) of the pressure wave from the eruption of the Hunga Tonga volcano was observed on images from the METEOSAT satellite in the Sahara. The exact location should be 5E, 20S, somewhere over southern Algeria. Of course, the wave after passing half of the planet becomes inhomogeneous, but its overall shape holds well. We made a video from 53 consecutive images of the MSG satellite, channel 6.3um (water vapor absorption band), more precisely difference images from two consecutive dates from 15.1.2022 13:30 to 16.1.2022 02:30UTC. One MSG term (15:45UTC) is missing in the EUMETSAT archive. That's why we lost two difference images, which causes a bigger jump to be recognized right at the beginning of the animation. In an ideal case, the circular wave traveling around the entire planet shrinks to a single point, from which it expands again in the opposite sequence. Therefore, for example, in Bratislava, a primary wave coming directly from the volcano should be detected first, which, given the distance, must take significantly longer than the arrival of the secondary wave to Bratislava from the inflection point in the Sahara. From a graphical point of view, it is interesting that we cannot recognize the wave in the static image due to the large noise of the difference images on the water vapor channel, or it is just very difficult to observe. This is the reason we provide below the link to the video uploaded in the internet resources. The wave becomes visible to the human eye precisely through animation, because the eye is then more sensitive to rapid small changes in brightness in the image. The images are in the projection of a regular longitude-latitude grid, which makes the circular image of the Earth oval, which of course also distorts the shape of the wave, which is actually also circular. We observed such a phenomenon at SHMÚ thanks to the correct procedure for processing satellite images for the first time. Link to video of the event:

https://www.facebook.com/watch/?v=425125242683496

EUMETSAT case study, for which we provided our materials, contains following materials prepared at SHMÚ from Meteosat data:

Video from Meteosat 11: (15 minutes interval from 15 Jan 22 13:30 to 16 Jan 22 2:30 UTC)

Video from Meteosat-8: (15 minutes interval from 15 Jan 22 12:00 to 16 Jan 22 11:30 UTC)

Video from Meteosat-9: (5 minutes interval from 15 Jan 22 16:00 UTC to 16 Jan 4:25 UTC)

Algorithm used to calculate the images uses SEVIRI WV 6.2μm data. Instrument counts were converted to calibrated radiances and radiances were converted to brightness temperatures. Then the image differences were calculated from two consecutive images in time. Changes resulting to the signal from wave movement are quite low but they are amplified by the increased contrast of images. Shockwaves are highly visible over cloud-free areas and when the displacement of the wave per time step is equal to half the wavelength.

First stage of eruption was observed at the location of Volcano itself in Pacific Ocean. Satellite imagery from showed huge dust and volcanic ash cloud seen in light brown colour in Fig. 6.8.

In the animation of Himawari Ash RGB images which were created at SHMÚ, SO_2 plume was observed more than 24 hours from 15 January 06:30 UTC to 17 January 04:30 UTC (Fig. 6.9.), the spread of SO_2 cloud from the volcano can be followed all the way to the Australian continent (bright green or blue-green shades).

The Meteosat-11 captured from the animation (Fig. 6.10) shows the movement of shockwaves from 15 January 13:30 UTC to 16 January 02:30 UTC, in 15-minutes time-steps. Image is centered to 0˚ longitude. It shows how the circular shaped wave was oscillating between the volcano located in Pacific Ocean and a North Africa inflexion point. Direct link to this video is: https://user.eumetsat.int/s3/eup-strapi-media/Meteosat_11_Shockwave_video_3226fe9421.mp4
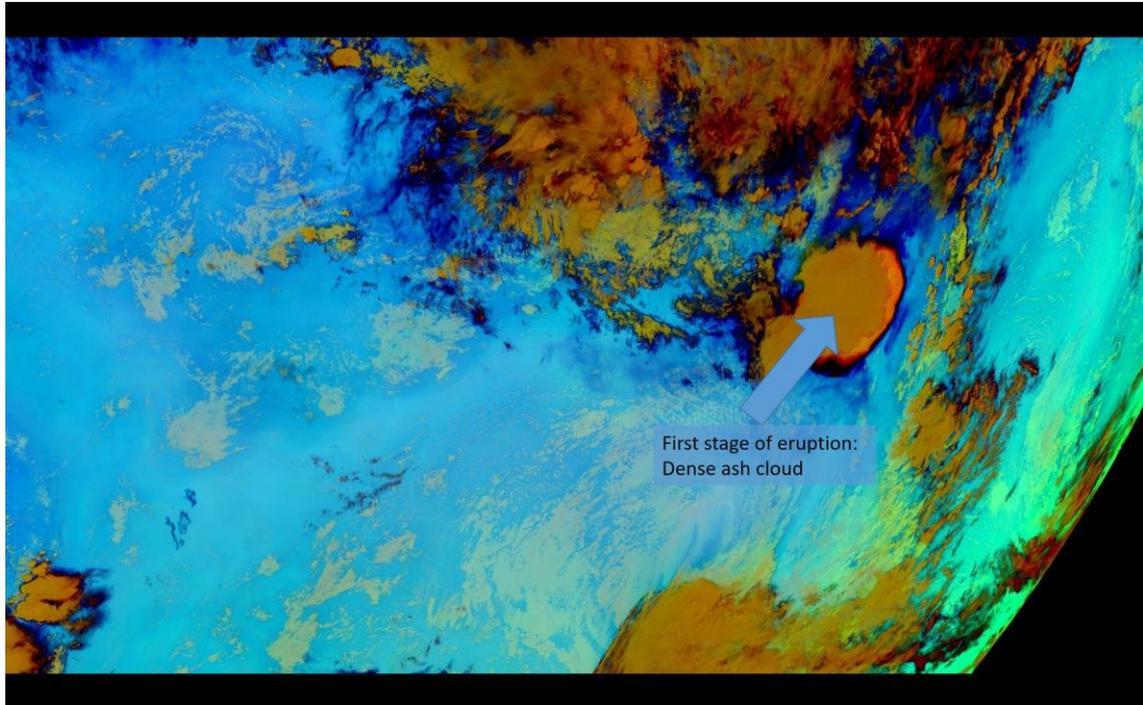
Figure 6.8. *Himawari ASH RGB, 15 January 2022 07:30 UTC, ash plume in brown colours over Pacific ocean.*
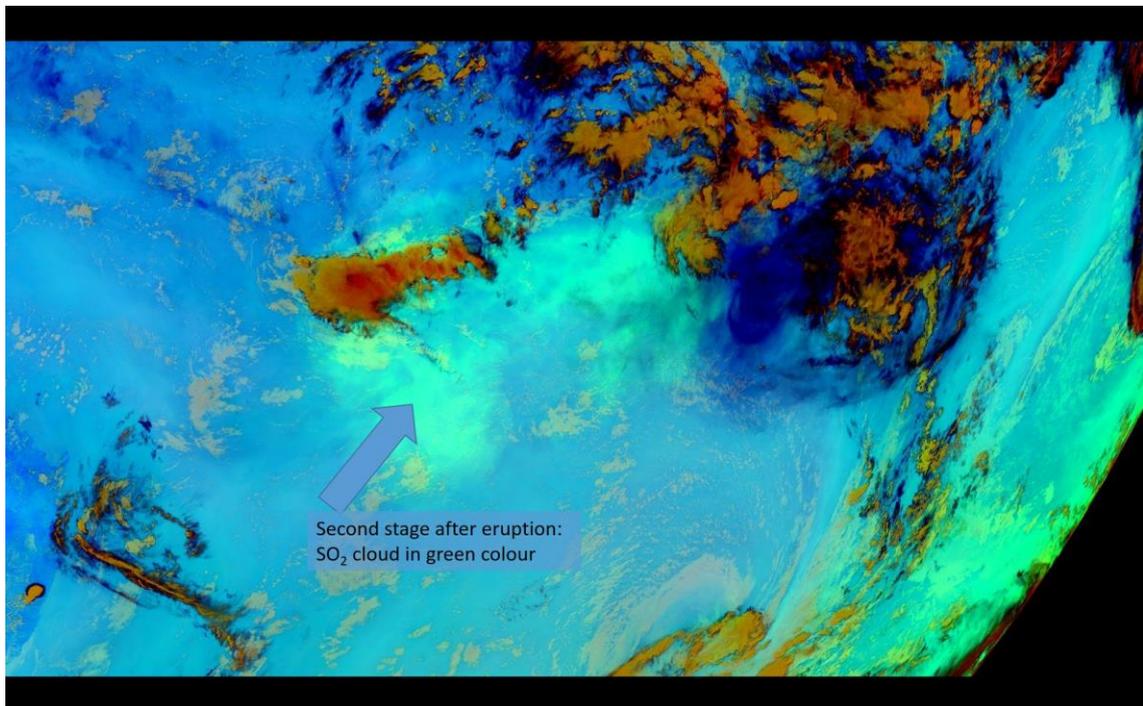
Figure 6.9. *Himawari ASH RGB, 16 January 2022 02:30 UTC, SO2 cloud in green colours approaching Australia.*
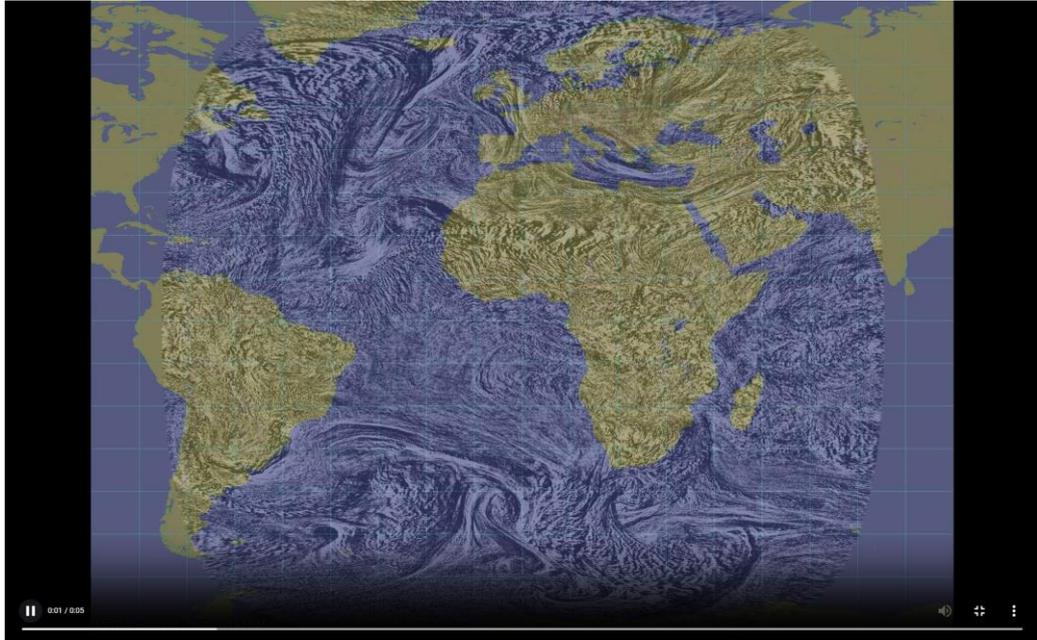
Figure 6.10. *Meteosat-11 IR6.2 brightness temperature differences between successive images*, 15 January 13:30 UTC to 16 January 2022 02:30 UTC.*

In the Meteosat-8 animation, from 15 January 12:00 UTC to 16 January 11:30 UTC (15-minutes time-steps) (Fig. 6.11), thanks to the eastern satellite position, the wave can be very clearly seen travelling from west Australia over the Indian Ocean and from the south after passing over Antarctica. To see the waves use direct link to this video:
https://user.eumetsat.int/s3/eup-strapi-media/Meteosat_8_IODC_Shockwave_video_1680w_web_4f076f3173.mp4
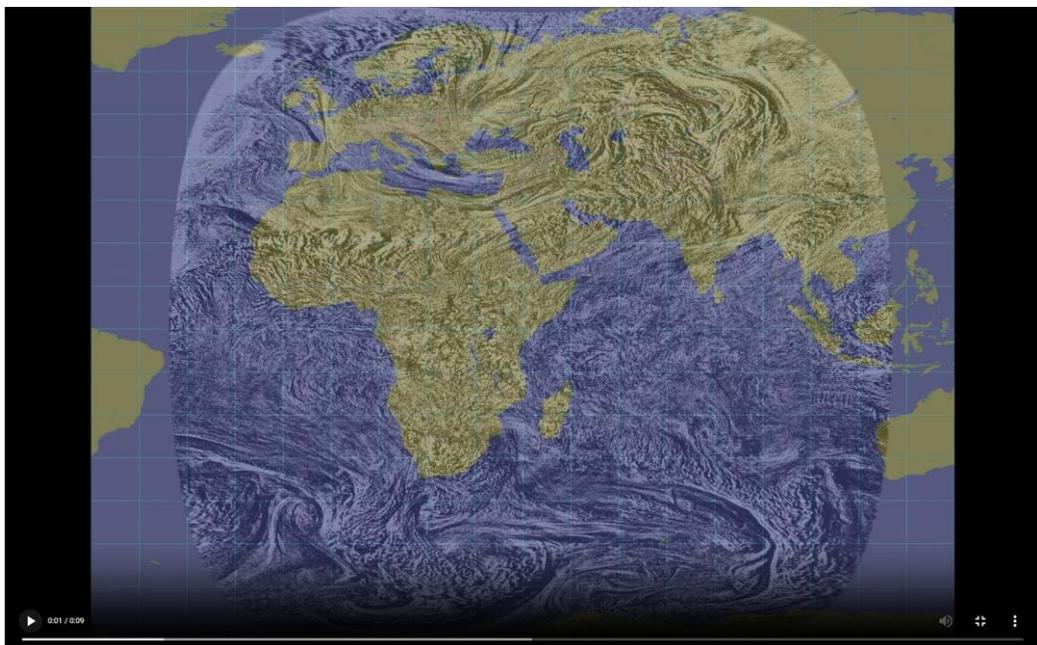
Figure 6.11. *Meteosat-8 IODC (centered to 41.5˚ E), IR6.2 brightness temperature differences between successive images*, 15 January 12:00 UTC to 16 January 2022 11:30 UTC.*

6.3. Arctica-M N1 satellite: Study on sample data.

Link to orbital data and mission description:
https://database.eohandbook.com/database/missionsummary.aspx?missionID=713

The era of geostationary meteorological satellites dates back to the late 1970s. Meteosat-1 has been available since 1977. However, the position of the satellite in a circular orbit at an altitude of 36,000 above the equator brings great limits when monitoring the areas around the Arctic Circles and the Earth's polar regions in general.

Therefore, in parallel with the development of geostationary meteorological space missions, all known world space agencies also brought the so-called polar satellites. They orbit the Earth in a direction perpendicular to the equator at a significantly lower altitude, from 800 to 1000 km. Thanks to this, they fly periodically with a frequency of 90 to 110 minutes over the Polar Regions and thus supplement the meteorological information necessary for complete monitoring and weather forecasts.

There has long been an idea of how to provide monitoring of the Polar Regions from space in a similar way as geostationary satellites do. Such an idea is the extremely eccentric elliptical orbit of the Molniya type (https://en.wikipedia.org/wiki/Molniya_orbit). It is a highly elliptical orbit with an inclination of 63.4 degrees, an argument of perigee of 270 degrees, and an orbital period of approximately half a sidereal day.

In 2022, EUMETSAT had data from a satellite of this type with the designation Arctica M-N1 (Fig. 6.12). At SHMÚ, we had available test data from part of the orbit of this satellite, precisely from the time when the satellite flies over the northern hemisphere and scan them in a similar mode as Meteosat satellites but from geostationary orbit.

This study was focused on the comparison of the spectral channels of the Arctica and Meteosat satellites, on the comparison of spatial resolution and regional coverage. We documented these comparisons in the form of data processing and preparation of RGB image products.
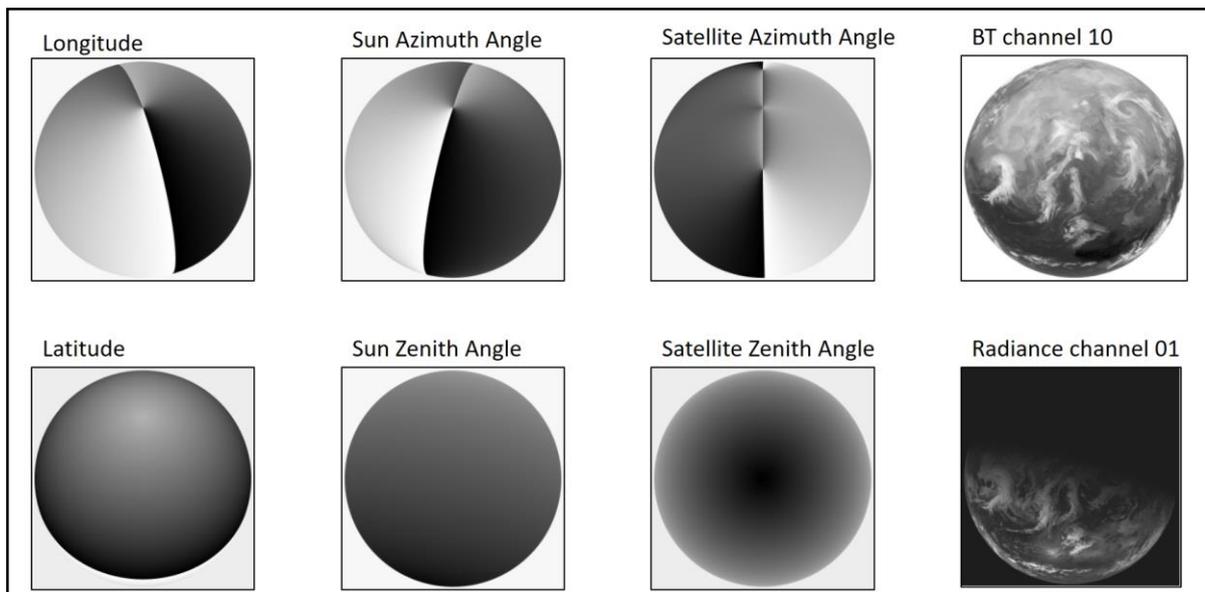
Figure 6.12. *Visual interpretation of parameters encoded in test data files necessary for proper geo-reference. Longitudes of west hemisphere are in white, in east in black colours. Sun azimuth and Sun zenith angles are important for proper calibration of visible channels of the imager.*

In general, we can state that coverage of Polar Regions is excellent, can be very good supplement of both – geo and polar orbiting satellites concerning Earth imaging perfect for large synoptic scales analyses.

Satellite Arctica M-N1 measures in 10 spectral channels: three visible channels, one near infrared 4.0 µm, water absorption band channel at 6.0µm and five infrared channels can provide resources for creation of the most known RGB image composites (Fig. 6.13).
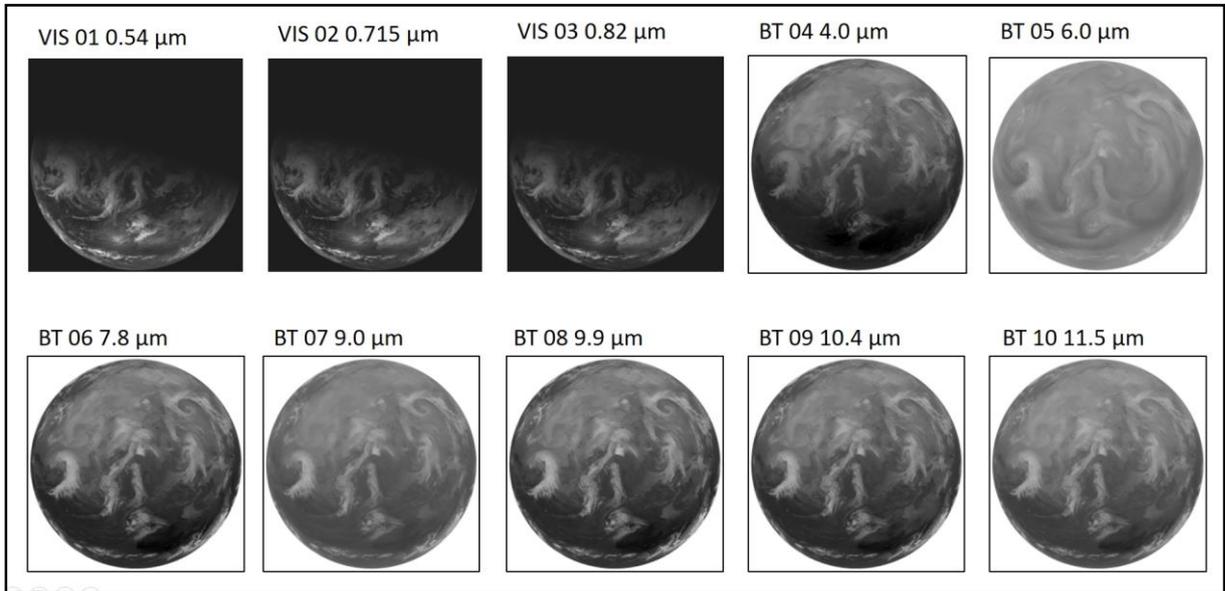
Figure 6.13. *Full set of spectral channels from satellite Arctica M.N1.*

Comparing IR images from Meteosat 11 and from the Arctica M-N1 satellite we can say that in the case of Meteosat, coverage of the northern regions is very limited, while Arctica allows us to monitor the weather in the entire area around the North Pole (Fig. 6.14). Note that spectral characteristics of different instruments are similar but usually not exactly the same.
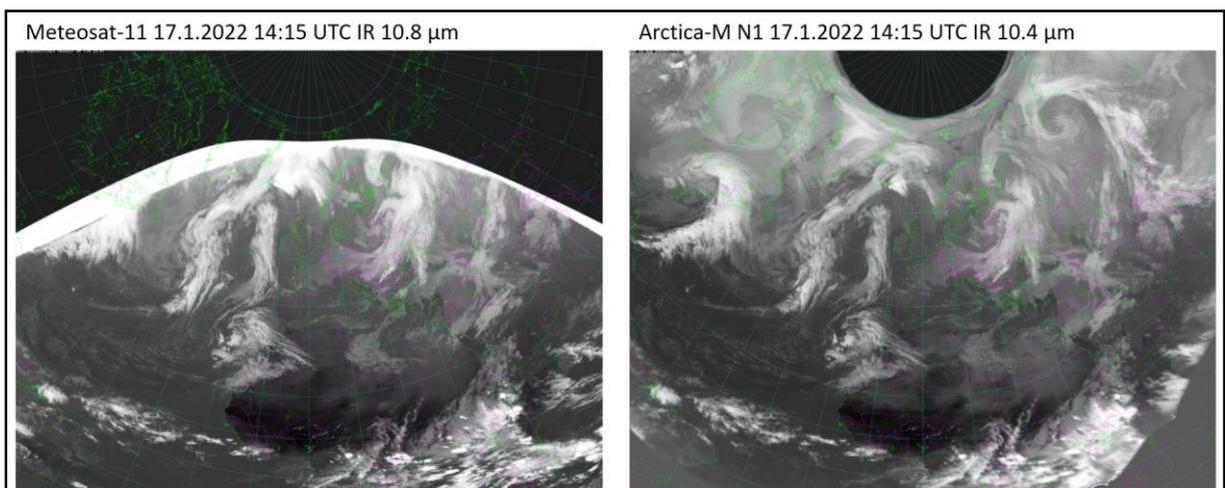
Figure 6.14. *Comparison of coverage – Meteosat-11 versus Arctica-M N1 for mid-latitudes and Polar Regions in infrared bands 10.8 and 10.4 µm.*

Next comparison is devoted to WV images from Meteosat 11 and from the Arctica M-N1 satellite. In the case of Meteosat, coverage in the north is also very limited, while Arctica allows users to monitor the weather in the entire area near the North Pole. It is also evident that anisotropy of the atmosphere is observed for high satellite zenith angles. In case of Meteosat anisotropy affects northern part of image, in case of Arctica southern part (Fig. 6.15 left and middle). Merging southern part of Meteosat image with northern part of Arctica we can obtain full coverage of defined domain (Fig. 6.15 left). This can be very helpful for analyses of synoptic features over the whole big region.
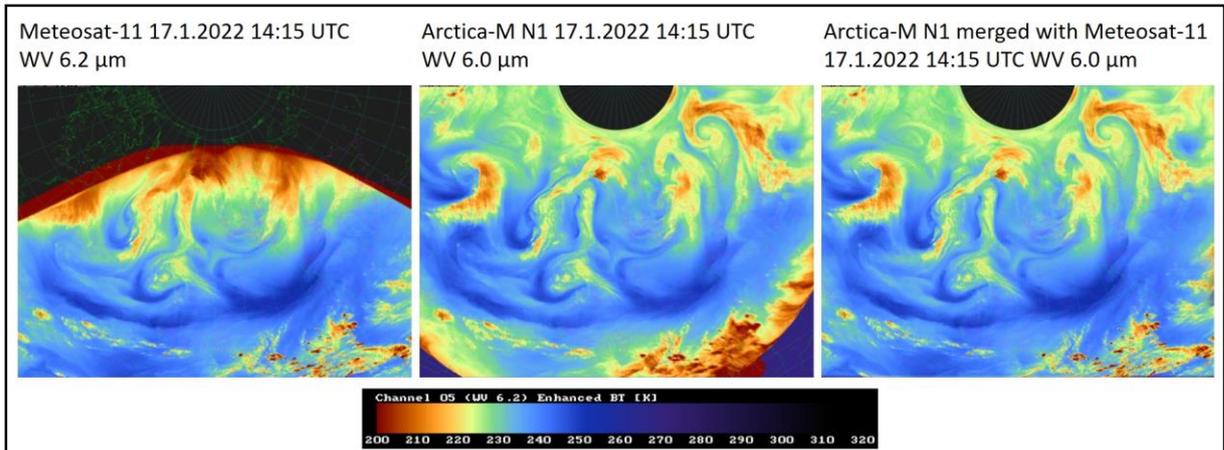
Figure 6.15. Comparison of coverage – Meteosat-11 versus Arctica-M N1 for mid-latitudes and Polar Regions in water vapor absorption band 6.2 or 6.0 μm. Region displayed in background map is domain operationally used in SHMÚ weather forecasting office.
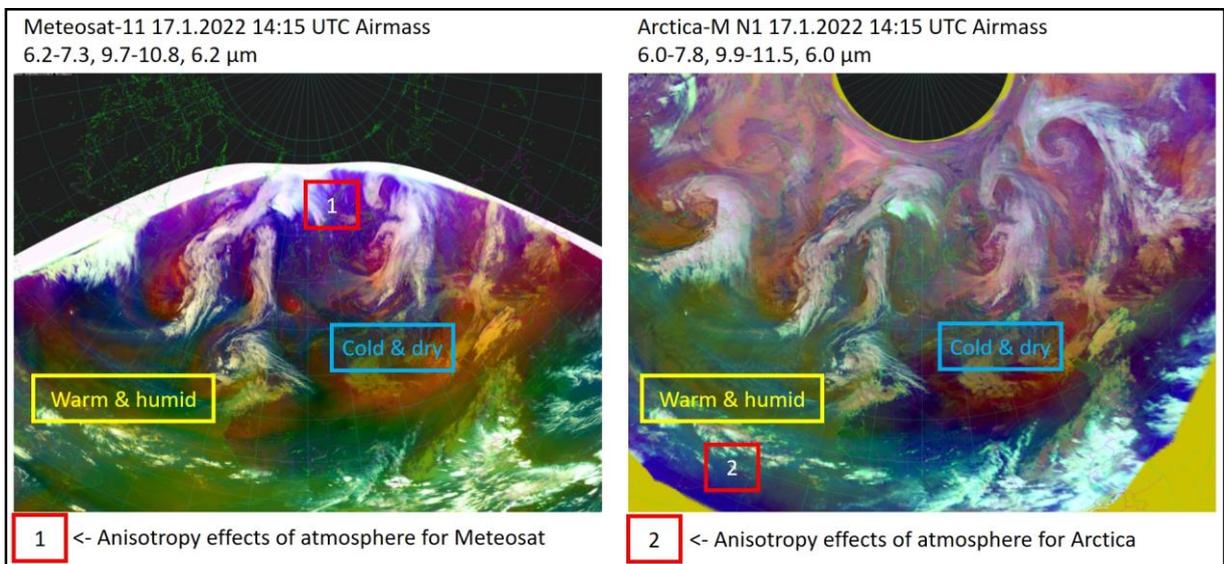
Figure 6.16. Comparison of coverage – Meteosat-11 versus Arctica-M N1 for mid-latitudes and Polar Regions as Airmass RGB composite image. This product is used mainly for monitoring of warm, cold, humid and dry air masses.

In conclusion, we can conclude that by combining satellites with geostationary and Molnyia orbits, it will be possible to obtain very complete information about the state of the atmosphere on the entire Earth in the future. However, polar satellites will certainly not lose their importance, but all types of satellites and devices on them will complement each other.

6.4. Satellite measurements of solar radiation falling on the earth's surface and their use in evaluating the efficiency of photovoltaic power plants.

The amount of solar energy coming from the Sun through the atmosphere to the Earth's surface depends on many astronomical and meteorological factors. Using satellite measurements, we obtain continuous information about the state and processes in the atmosphere for the entire globe, based on which we can use physical and mathematical calculations to determine the intensity of solar energy falling on any point on the earth's surface. The aim of our work is to map the average intensity of solar energy incident on the territory of Slovakia and surrounding countries, and to point out the monthly and annual variability of incident solar radiation to different localities using satellite data. Secondly, we compare the average values of solar radiation falling on the earth's surface measured using satellites and conventional meteorological devices for measuring solar radiation intensity, pyranometers, for selected SHMÚ meteorological stations, purposefully distributed to cover the largest possible territory of Slovakia. The last step is to compare the output of the photovoltaic power plant with the measured satellite data and to evaluate numerically its efficiency. We processed maps of average monthly values of solar radiation based on Meteosat satellite measurements for the period 2012 – 2021 (Fig. 6.17). On regular monthly bases we continue with production estimations of the amounts of solar energy and calculate anomalies (monthly differences) of solar energy from 10-year averages (Fig. 6.18 and Fig. 6.19). For validation purposes we compared the satellite data with pyranometers as reference measurements. We obtained a good agreement, especially for meteorological stations located in lowland areas. Significant deviations in mountainous areas are related to the orography of the terrain, the frequent occurrence of snow cover in winter and the occurrence of convective clouds in summer. The average efficiency of a selected photovoltaic power plant for the examined years 2020 and 2021 we estimated to 14.7%. The efficiency in the summer months was a few percent lower than in
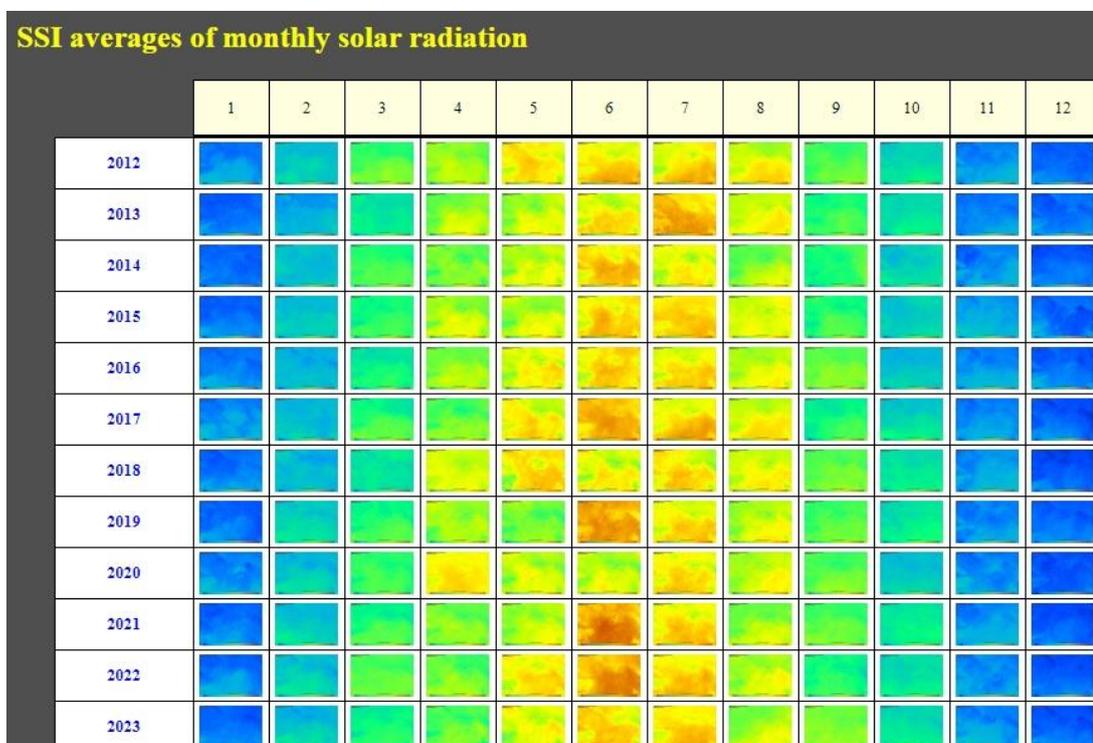
Figure 6.17. *Averaged surface solar irradiance in W/m² per day for each month from 2012 to 2023.*
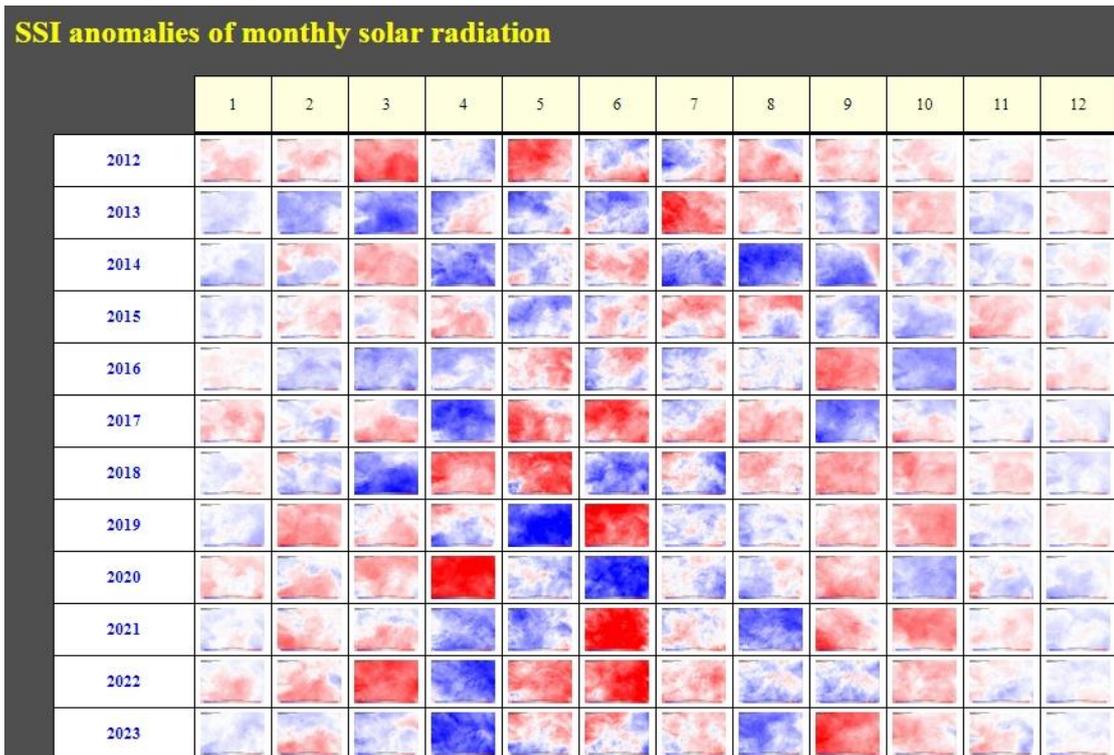
Figure 6.18. *Monthly surface solar irradiance anomalies for each month from 2012 to 2023.*
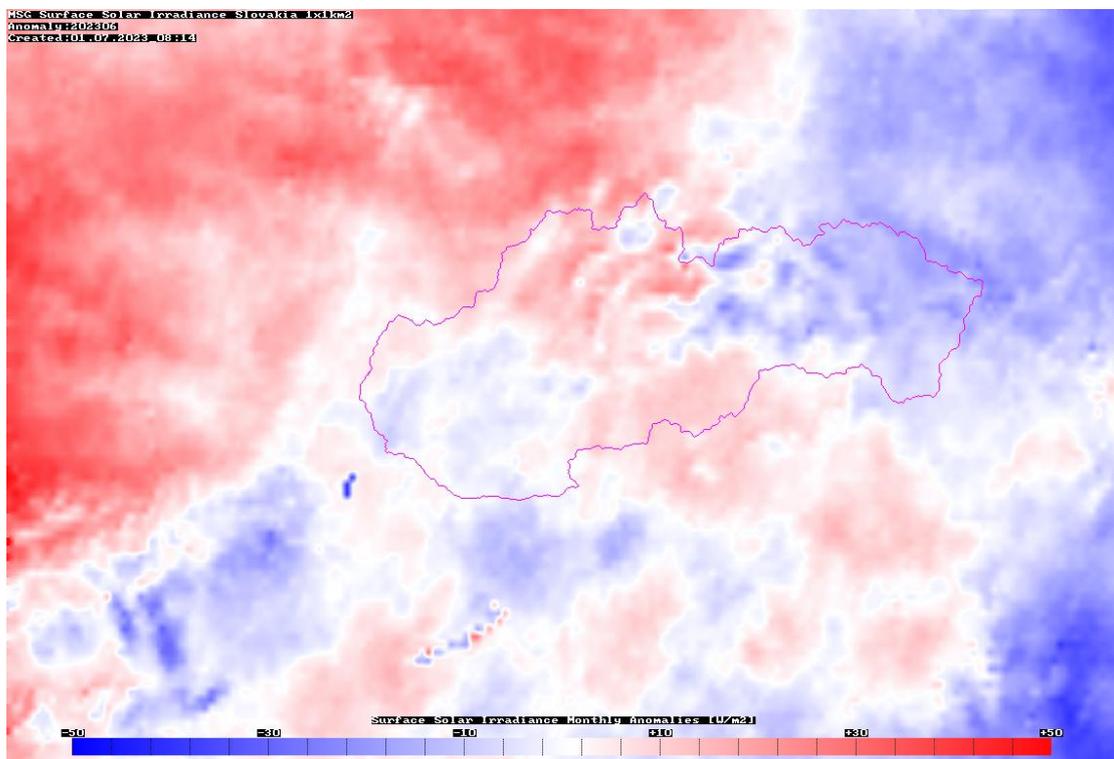
Figure 6.19. *Example of monthly surface solar irradiance anomaly for June 2023. Zero anomalies are in white, negative in blue and positive in red shades.*

winter. Using the satellite data we also determined the highest possible efficiency of the power plant at 19.4% in case the photovoltaic panels could rotate perpendicular to the sun's rays, but such kind of installation for photovoltaic panels is not used very often in practice.

In addition to long-term monitoring of changes in solar radiation, we also monitored short-term variations in sunshine caused by variable cloud cover. Especially in the summer, convective situations prevail in Central Europe. Rapid changes in solar radiation caused by the passage of clouds in front of the Sun cause large fluctuations in the performance of photovoltaic panels, and sudden changes in their temperature also change their immediate efficiency (Fig. 6.21). These fluctuations are not favorable for the efficient use of solar power plants. When voltage fluctuations in the external power grid are added to this, unnecessary interruptions in electricity production can occur.
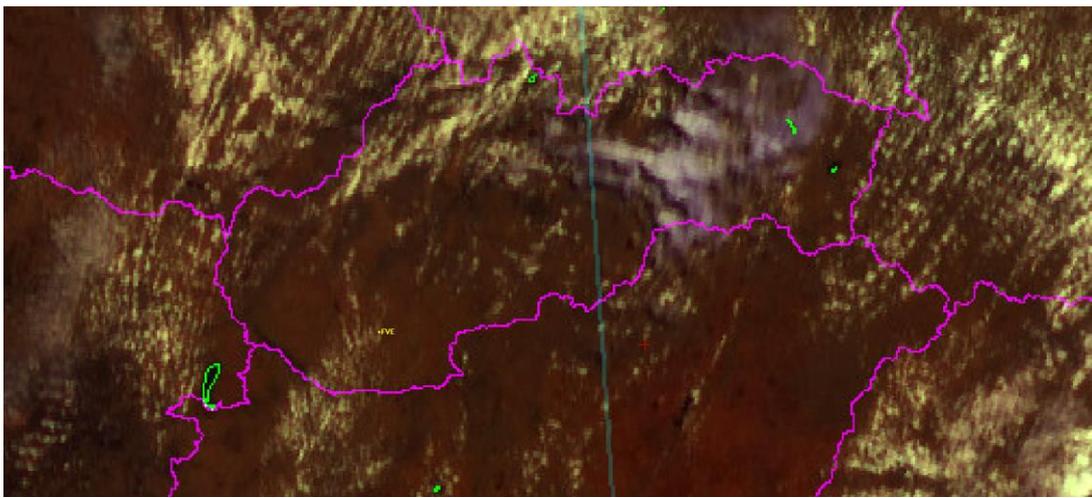
Figure 6.20. *Meteosat Rapid-scan image (RGB HRV Near Natural in 5/minutes time intervals) from 9th of September 2023 11:05UTC. Position of monitored photovoltaic power plant is assigned by yellow text „FVE" located in south-west part of Slovakia.*
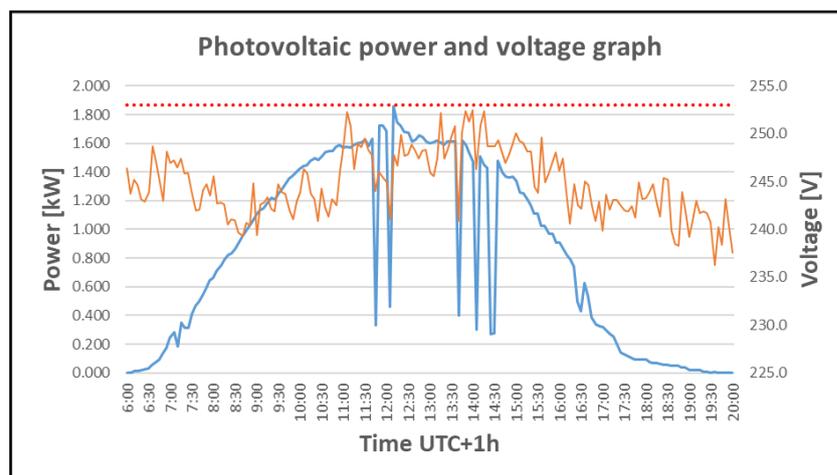
Figure 6.21. *Time changes of power and grid voltage of photovoltaic power plants monitored by means of Meteosat satellite imagery.*

Satellite images from the Meteosat satellite in a 5-minute step help us understand the behavior of the photovoltaic device in variable weather, because the monitoring step of the power plant is also in the same time step. When processing images, it is necessary to determine

whether the sun was covered by a cloud or not in a given 5-minute interval. For this we use graphs of the albedo course in the visible band 0.6 μm and the radiation temperature course in the infrared band 10.8 μm (Fig. 6.22).
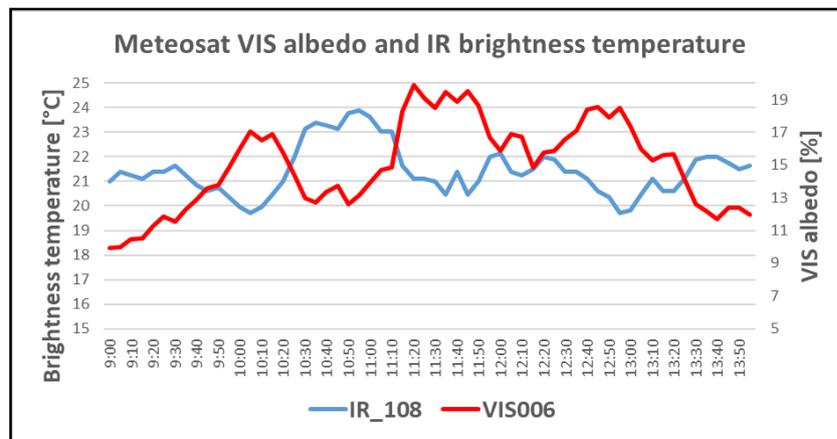
Figure 6.22. *Meteosat 4 September 2023 albedo in VIS 0.6μm channel and brightness temperature in IR 10.8 μm channel. The graph shows the inverse relationship of these two quantities, which affect the instantaneous performance of the photovoltaic power plant.*

Results achieved in this study can be helpful in increasing the share of electricity production from large as well as small photovoltaic power plants in Slovakia. They provide detailed data on the distribution of solar energy falling on individual locations in our territory in the long term, which is significant considering the time return on investment in renewable energy sources. Satellite observations of incident solar radiation thus find their significance not only in meteorology, but also in practical life. More and more people are interested in the installation of small photovoltaic power plants in Slovakia, and our study can help in choosing the optimal assembly in terms of price ratio and performance, but also in terms of location and local climatological conditions (Fig. 6.23).
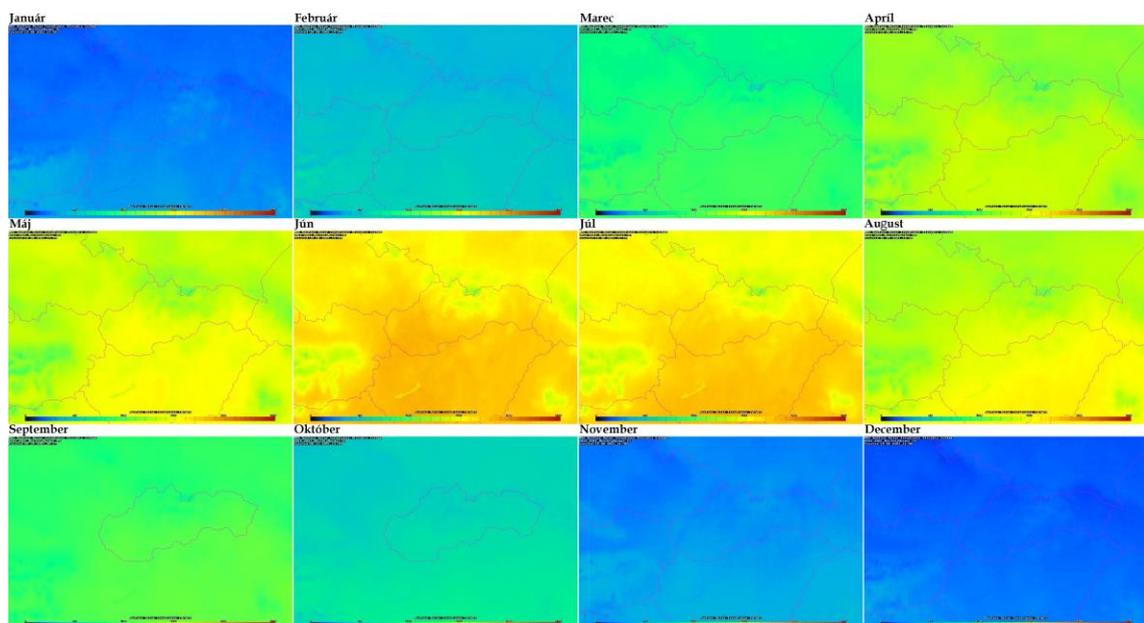
Figure 6.23. *10-year's average (2012-2021) of solar irradiation for each month of year over central Europe estimated from measurements of Meteosat geostationary satellite.*

6.5. Processing software for data from new generation of geostationary meteorological satellites developed by SHMÚ and operated at EWC (European Weather Cloud) in EUMETSAT.

Working with the first image data from FCI (Flexible Combined Imager) on-board MTG-I1 (Meteosat Third Generation Imager) using GEOProc/MTGProc training environment developed for EWC (European Weather Cloud), we found obvious shifts of the different channels relative to each other, in terms of pixel position, or of the entire image matrix (up-down, left-right). It turns out that when translating channels with different native resolutions (2km, 1km, 0.5km), especially when we do other arithmetic operations, for example, we calculate the difference of a pair of images, these image matrices are mutually shifted by several pixels. This causes big differences in the resulting RGB imagery – strange colours, especially at the edges of clouds.

Furthermore, in the study, we are interested in the geometry of the images throughout the image, i.e. whether the found pixel displacement is the same in every location of the image, or whether it changes, for example, in the north-south direction or in the east-west direction. We are trying to find out the answers to these questions from the time sequence of images coming shortly after each other, but also from different days, as long as the MTG-I1 satellite produces images in operational mode.

Mastering the preparation of high-quality RGB products in high resolution will bring much more detailed physical information about clouds compared to the existing RGB products known from the MSG satellite, as indicated by the tests of the generated RGB products performed in this study. We believe that with the correct geo referencing and projection of data from channels in three different resolutions (2 km, 1 km and 0.5 km) into the common grid, both new and already known RGB products will bring a lot of new information about dangerous phenomena, such as the initiation of convection, developed storms with through their overshooting tops, or in winter the formation and dissolution of valley fogs, the formation and development of wave clouds and other similar small scale meteorological phenomena.

A significant extension of this EWC solution is a simple but practical web interface (Fig. 6.24), in which the user can view sets of RGB products generated in defined regions (domains) in real time for several geostationary satellites GOES-16, GOES-18, MTG-I1 and HIMAWARI -9.

Developed training environment will mainly be used for the following activities:

- Generation of MTG-FCI and MTG-LI imagery for data familiarization and for training and case study activities
- Generation of GOES-ABI and HIMAWARI-AHI imagery for training and case study activities
- Creation of NRT and archive imagery from above instruments for training activities
- Image generation for specific case study activities

The target audience is EUMETSAT trainers and internal users. However, an extensive usage is also foreseen for EUMETSAT organized trainings events. The EWC is providing NRT data access via EUMETCast Terrestrial feed that was provided to tenants in it. The development status as of December 2023 is as follows:

Operational processing of image NETCDF data from GOES-16, GOES-18 and MTG-I1 satellites. There are 17 RGB products predefined for the ABI and AHI instruments (Fig. 6.24), 28 RGB products for the FCI instrument. All image products can be generated in predefined geographic projections and over defined regions. Detailed Cloud Types (Fig. 6.26), Cloud

Phase (Fig. 6.27) and other new RGB products in 0.5 km per pixel can provide high quality information for meteorological services. Detection of fog, low level moisture, high semi-transparent clouds, severe storms and other features will be available.

Figure 6.24. *Set of RGB products from GOES-16 ABI instrument generated by GEOProc software at EWC.*
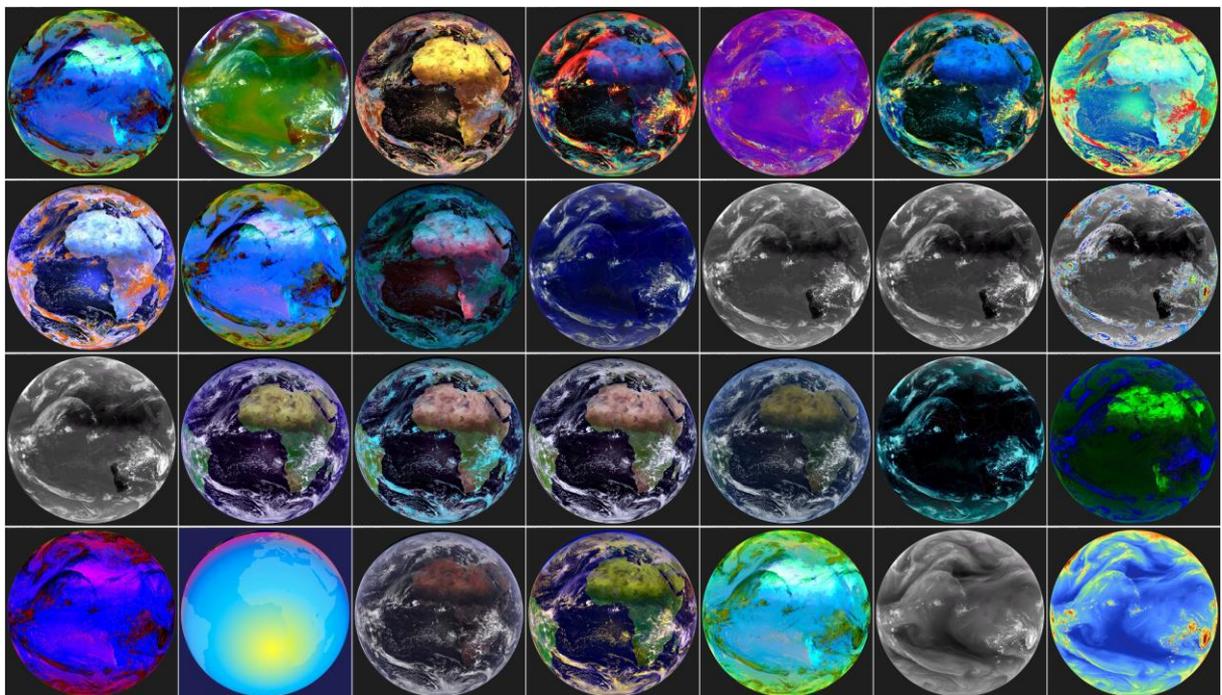
Figure 6.25. *Set of RGB products from MTG-I1 FCI instrument generated by GEOProc software at EWC.*
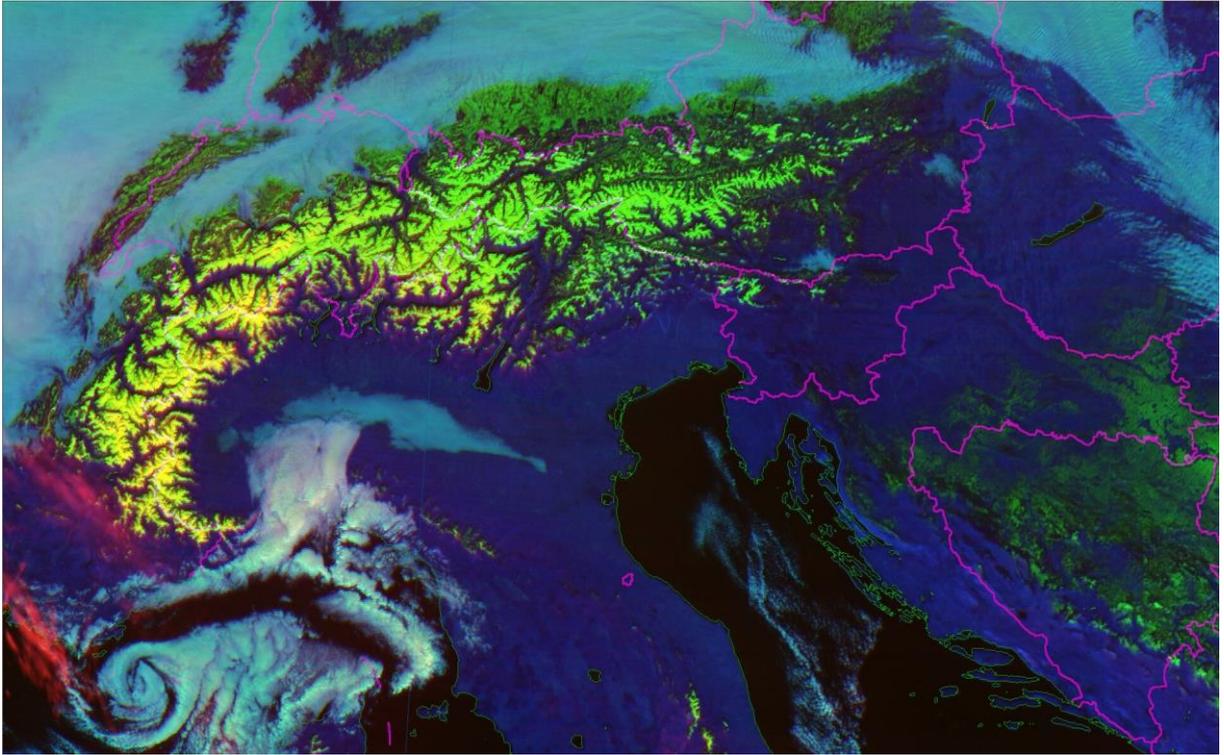
Figure 6.26. *Detail of Cloud Types RGB product from MTG-I1 FCI instrument, 13 January 2024 11:50 UTC.*
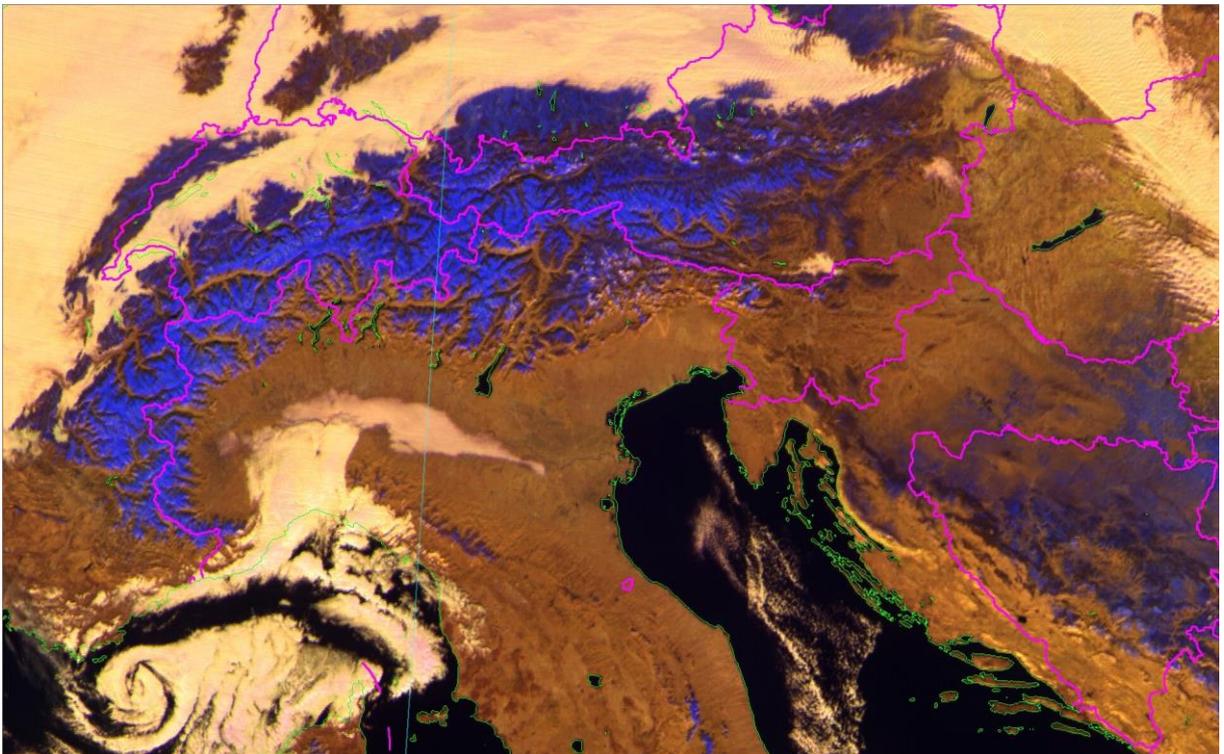
Figure 6.27. *Detail of Cloud phase RGB product from MTG-I1 FCI instrument, 13 January 2024 11:50 UTC.*

References:

[1] KAŇÁK, J. – OKON, Ľ. – MÉRI, L. – HRUŠKOVÁ, K. – ZVOLENSKÝ, M. – MADARA, M.: Satellite products at SHMÚ and their potential in monitoring precipitation and drought conditions. Fifth H SAF User Workshop, 24-28 January 2022. Online.

[2] SETVÁK, M. – KAŇÁK, J. – SPURNÝ, P. – BOROVIČKA, J.: Waves generated by Hunga Tonga eruption. EUMETSAT CWG and MTG-3T workshop, 16 – 20 May 2022, Budapest. https://doi.org/10.13140/RG.2.2.13655.55204/1

[3] KAŇÁK, J., H05 - Rain gauge 10-years precipitation normals for estimation dry/wet periods over Slovakia and central European region (July 2012 - June 2022). HSAF EUMETSAT Case Study at:
https://hsaf.meteoam.it/CaseStudy/GetDocument?fileName=2012-2022_H05-RG_Slovakia_case_study_JK_LO_PK_20221115.pdf

[4] KAŇÁK, J.: Arctica-M N1 Sample Data – Feedback from Slovakia. 52nd STG Operations Working Group Meeting, 8-9 September 2022, EUMETSAT, Darmstadt, doc No. EUM/STG-OPSWG/52/22/VWG/15, v1A, 17 August 2022

[5] KAŇÁK, P. – OKON, Ľ.: Satelitné merania slnečného žiarenia dopadajúceho na zemský povrch a ich využitie pri hodnotení účinnosti fotovoltických elektrární. Meteorologický časopis/Meteorological Journal, Slovenský hydrometeorologický ústav, Bratislava, 2022. Ročník 25 – číslo 2/Volume 25 – Number 2. Jeséniova 17, P.O. Box 15, 833 15 Bratislava 37, IČO 00 156 884, R. č. MK SR: 3268/09, ISSN 1335-339X.
https://www.shmu.sk/File/ExtraFiles/MET_CASOPIS/1674803629_MC_2022_2.pdf

[6] KAŇÁK, J. – OKON, Ľ. – KAJABA, P. – MÉRI, L. – JURAŠEK, M.: 10-ročné dlhodobé priemery zrážok zo satelitov a zrážkomerov pre určenie suchých a vlhkých období na území Slovenska (JÚL 2012 – JÚN 2022). Meteorologický časopis/Meteorological Journal, Slovenský hydrometeorologický ústav, Bratislava, 2023. Ročník 26 – číslo 1/Volume 26 – Number 1. Jeséniova 17, P.O. Box 15, 833 15 Bratislava 37, IČO 00 156 884, R. č. MK SR: 3268/09, ISSN 1335-339X.
https://www.shmu.sk/dynamic/shmu_apps/meteocasopis/download.php?opendocument=12

[7] KAŇÁK, J. – OKON, Ľ. – KAJABA, P. – MÉRI, L. – JURAŠEK, M.: Estimation of dry/wet regions over Slovakia and central Europe based on 10 years reference period of H SAF precipitation products. EUMETSAT 2023 - Meteorological Satellite Conference, 11 - 15 September 2023, Malmö, Sweden. Poster.
https://imagine.eumetsat.int/smartViews/view?view=EMSC

7. INSTITUTIONS INVOLVED IN SPACE RESEARCH

Members of the National Committee of COSPAR with e-mail addresses.

The website of NC is http://nccospar.saske.sk.

Astronomical Institute (AI)
Slovak Academy of Sciences (SAS)
Stará Lesná
059 60 Tatranská Lomnica
contact: J. Rybák (choc@ta3.sk, NC member)

Faculty of Mathematics, Physics and Informatics (FMPI)
Comenius University
Mlynská dolina
842 15 Bratislava
contact: J. Masarik (Jozef.Masarik@fmph.uniba.sk, NC member)

National Forest Centre
T.G. Masaryka 22
960 92 Zvolen
contact: T. Bucha (bucha@nlcsk.org)

Earth Science Institute (ESI)
Slovak Academy of Sciences (SAS)
Dúbravská cesta 9
840 05 Bratislava
contact: M. Revallo (milos.revallo@savba.sk, Secretary of NC)

Institute of Animal Biochemistry and Genetics CBs
Slovak Academy of Sciences (SAS)
Dúbravská cesta 9
840 05 Bratislava

Biomedical Research Center of the Slovak Academy of Sciences (SAS)
Institute of Experimental Endocrinology (IEE)
Dúbravská cesta 9
845 05 Bratislava

Institute of Experimental Physics (IEP)
Slovak Academy of Sciences (SAS)
Watsonova 47
040 01 Košice
contact: P. Bobík (bobik@saske.sk, NC member)

Institute of Geography (IG)
Slovak Academy of Sciences (SAS)
Štefánikova 49
814 73 Bratislava
contact: J. Feranec (feranec@savba.sk, Vice-Chair of NC)
Institute of Materials and Machine Mechanics

Slovak Academy of Sciences (SAS)
Dúbravská cesta 9/6319
840 05 Bratislava
contact: M. Gebura (ummsgebu@savba.sk, NC member)
Note: J. Lapin died on 22 May 2023

Institute of Measurement Science (IMS)
Slovak Academy of Sciences (SAS)
Dúbravská 9
842 19 Bratislava
contact: I. Frollo (frollo@savba.sk)

Institute of Normal and Pathological Physiology (INPP)
Slovak Academy of Sciences (SAS)
Sienkiewiczova 1
813 71 Bratislava

Slovak Central Observatory (SCO)
Komárňanská 137
947 01 Hurbanovo
I. Dorotovič (ivan.dorotovic@suh.sk, Chair of NC, Representative
of Slovak NC to COSPAR)

Ministry of Environment of the Slovak Republic
Tajovského 28
975 90 Banská Bystrica
contact: J. Nováček (jozef.novacek@enviro.gov.sk)

Slovak Hydrometeorological Institute
Jeséniova 17
833 15 Bratislava
contact: J. Kaňák (jan.kanak@shmu.sk, NC member)

Michaela Musilová, o. z.
Hroboňova 7
81104 Bratislava
contact: M. Musilová (michaela@michaelamusilova.com, NC member)

National Agricultural and Food Centre
Soil Science and Conservation Research Institute
Trenčianska 55
821 09 Bratislava
contact: M. Sviček (michal.svicek@nppc.sk)